Forward programmed neurons as a tool for human neuronal network analysis and disease modeling

Doctoral thesis

to obtain a doctorate (PhD)

from the Faculty of Medicine

of the University of Bonn

Jianbin Wen

Henan, China

2022

Written with authorization of

the Faculty of Medicine of the University of Bonn

First reviewer: Prof. Dr. Oliver Brüstle

Second reviewer: Prof. Dr. Walter Witke

Day of oral examination: 01.02.2022

For the institute of Reconstructive Neurobiology

Director: Prof. Dr. Oliver Brüstle

Table of contents

List of abbreviations

This table summarizes abbreviations and acronyms used in this thesis. Note the list does not include abbreviations or acronyms used only once or within the same page.

Abbreviation	Explanation
AED	antiepileptic drugs
AMPA	α-amino-3-hydroxy-5-methyl-4-isoxazolepropionic acid
ASD	autism spectrum disorders
ATG	autophagy-related gene
BDNF	brain-derived neurotrophic factor
cAMP	cyclic adenosine monophosphate
CBZ	carbamazepine
CC	coiled-coil
CNV	copy number variations
CRISPR	clustered regularly interspaced short palindromic repeats
CTD	C-terminal domain
CytoD	cytochalasin D
DCX	Doublecortin
DISC1	Disrupted-in-schizophrenia 1
EPSP	excitatory postsynaptic potential
FAK	focal adhesion kinase
FIP200	FAK family kinase-interacting protein of 200 kDa
FRP	fast-recovery component of readily releasable pool
GABA	gamma-aminobutyric acid
GFAP	glial fibrillary acidic protein
hiPSC	human induced pluripotent stem cell
hrGFP	humanized renilla reniformis green fluorescent protein
IBI	inter-sub-burst intervals in network super burst
iGABAN	induced GABAergic neurons by forward-programming
iGlutN	induced glutamatergic neurons by forward-programming
LC3	microtubule-associated proteins 1A/1B light chain 3
LEV	levetiracetam
LTP	long-term potentiation
MEA	micro-electrode array
MRT	MRT68921
mTOR	mechanistic target of rapamycin
MUNC13	mammalian uncoordinated-13

continued to the next page

NB	network burst
NGN2	Neurogenin 2
NMDA	N-methyl-D-aspartic acid
NPC	neural progenitor cell
NSB	network super-burst
NTD	N-terminal domain
PCR	polymerase chain reaction
PDBu	phorbol 12, 13-Dibutyrate
PKC	protein kinase C
Pyk	proline-rich tyrosine kinase
r-, TMS	repetitive, transcranial magnetic stimulation
RB1CC1	retinoblastoma1-inducible coiled-coil 1
RCP	presynaptic recycling vesicle pool
ROS	reactive oxygen species
RRP	readily releasable pool
SHANK	SH3 and multiple ankyrin repeat domains protein
SRP	slow-recovery component of readily releasable pool
STD	short-term depression
SV2A	synaptic vesicle protein 2A
TNF	tumor necrosis factor
TSC	tuberous sclerosis
ULK	UNC-51–like kinase

1. Introduction

The human brain is arguably the most complex biological system ever described. It is responsible for receiving and processing information from both the internal and external environments, and sending commands to the body to avoid hazards or meet physiological needs. It is also where higher functions like sympathy, reasoning, abstraction, and language reside, which collectively give rise to human societies, cultures, religions, arts, and sciences. An adult male human brain is estimated to contain 86 $x10^9$ neurons and a roughly equal number of non-neuronal cells (Azevedo, 2009). Such a large number matters here because, unlike in other organs where cells of the same type are identical in function and thus interchangeable, each neuron in the brain is presumably functionally unique and irreplaceable. For example, the neocortex, the outermost layer of the brain, appears structurally homogeneous at the microanatomical level. Functionally, however, it can be divided into distinct regions, i.e., soma sensory, motor, auditory, vision, language, working memory, etc. All parts of the brain are interconnected and functioning highly coordinately, so any disturbance to it risks leading to the development of neurological and psychiatric disorders. Because of a lack of fundamental understanding of the functionality of the human brain, these disorders present significant challenges for clinical researchers and practitioners.

Studies into the mechanisms of brain functionality have been hindered by both technical and ethical limitations. Brain activity has been observed in healthy individuals with minimal to non-invasive methods, such as electroencephalogram (EEG), positron emission tomography (PET), functional magnetic resonance imaging (fMRI), and functional near-infrared spectroscopy (fNIRS). Combined with predefined behavioral paradigms, these techniques provide abundant information about the principles of brain function. Yet they have limitations in sampling scope and both spatial and temporal resolution, and a finer level of observation of the human brain activity is only briefly available on patients undergoing invasive neurosurgery. Resected brain tissues can be cultured for further investigation, yet they are of limited availability and their normal function has been compromised by pathological effects. While postmortem materials can be studied with much more details, they lose biophysiological properties.

The nervous system of other animals shares similarities with that of humans at various

levels, from molecular and cellular to the circuit and behavioral patterns. It is therefore helpful to use animals as models to investigate the principle of neurobiology, whose findings can then also be applied to humans. For example, a variety of behavioral assays have been established to assess executive, emotional, and social competence of rodents (Koob and Zimmer, 2012). These have helped to identify potential mechanisms linking genetic variants, molecular and cellular pathways, and micro-and macro-circuit functions to behavioral deficiencies (Seong et al., 2002). Likewise, due to their evolutionary closeness, non-human primates can not only help to study basic principles of brain functionality (Klink et al., 2021), but also contribute to research on neural prosthetics (Scherberger, 2009) and neurological diseases (Capitanio and Emborg, 2008). However, accessible human neural models are still needed to address species-specific questions. In this regard, techniques to derive human neurons *in vitro* can be a complementary approach to the aforementioned methods.

The following sections of this introductory chapter will first summarize methods to generate human neurons and neural cultures *in vitro*, then discuss how to assess the electrophysiological properties of these cultures and how computational neural network simulation could help to better interpret the obtained data, and finally explore the utilization of *in vitro* human neuronal cultures in the study of a gene that implicates in psychiatric disorders.

1.1 Generating human neurons *in vitro*

1.1.1 Obtaining neuronal cells from somatic tissues

Neurons can be derived from neuroblastoma obtained from surgery. Initially cultured and studied for diagnostic purposes (Murray and Stout, 1947), these tissues are capable of unlimited proliferation, and thus have been used to establish cell lines to study cancer biology (Schlesinger et al., 1976). Because these cells bear some neuronal properties, they can also be used for neurotoxicity testing (Selkoe et al., 1978) and studying neurotransmitter synthesis (Biedler and Schachner, 1978). Additionally, neuroblastoma cell lines can differentiate into different neuronal types given proper conditions, and thus have been used as a model for neuronal differentiation (Prasad, 1991). Neurite outgrowth and electrophysiological properties can also be assessed in neuroblastoma and its derivatives (Arcangeli et al., 1993). Neuroblastoma cell lines are relatively easy to obtain and handle, but these cells lack the authenticity and purity of defined types of neurons, and their tumor origin further limits their potential for clinical application (Kovalevich and Langford, 2013).

There are possibilities to obtain tissue that can give rise to neural progenitors and neurons from healthy individuals with minimally invasive methods. One example is the olfactory epithelium, which can be obtained with a simple brush swap in the nasal cavity (Benítez-King et al., 2011). Stem cells in the olfactory epithelium can form neurospheres, which produce neurons, glia, and other non-neural cell types (Murrell et al., 2005; Zhang et al., 2006). It is proposed that neurons derived from olfactory epithelium could reflect certain aspects of the central nervous system (Borgmann-Winter et al., 2015), and thus could be used to study psychiatric disorders, neurodegenerative, and neurodevelopmental disorders (Talamo et al., 1989; Matigian et al., 2010). In addition, neural progenitors derived from olfactory epithelium can produce neurotrophic factors that ameliorate motor neuron degeneration and spinal cord injury in animal models, and thus have been explored as a potential autologous source for cell-based treatment for Parkinson's disease (Wang et al., 2012). However, olfactory epithelium cells lack central nervous system identity, and therefore cannot fully represent neurobiological properties of the brain.

1.1.2 From hESCs to hiPSCs, reviving embryonic neurogenesis

An ideal way to obtain brain neurons *in vitro* is to reproduce the neurogenesis that occurs during embryonic development. Embryonic stem cells (ESCs) are derived from the inner cell mass of blastocyst-stage embryos. They can differentiate into all three germ layers: ectoderm, endoderm, and mesoderm, and are thus pluripotent. The first human ESC lines were established in 1998 (Thomson et al., 1998). Before long, methods to derive neural progenitors and neural cells from them were developed. The critical step involved the manual isolation of neuroectodermal progenitors from the embryoid body-like aggregates. These progenitors then organized into structures resembling the neural tube and could be expanded in the presence of fibroblast growth factor (FGF) and epidermal growth factor (EGF). Withdrawal of growth factors promoted their differentiation into neurons, astrocytes, and oligodendrocytes *in vitro*. These progenitors could then also be implanted into a host mouse brain for differentiation, which gave rise to functionally integrated neurons and glia (Reubinoff et al., 2001; Zhang et al., 2001).

Since then, better knowledge of embryonic neurodevelopment has helped achieve substantial progress in producing more defined neural subtypes from hESCs in less laborious manners. Noteworthily, chemical inhibition of SMAD-dependent transforming growth factor (TGF)-ß and bone morphogenetic protein (BMP) signaling pathways (dual-SMAD inhibition) with small molecules can prevent the development of extraembryonic and meso-endoderm at the early embryonic stage, which bypasses the formation of embryoid bodies and manual isolation of neural stem cells and thus reduces batch-to-batch variation (Chambers et al., 2009). After the formation of the neural tube in embryo development, further specification of the proto central nervous system is temporally and spatially coordinated by morphogen gradients along the anterior-posterior and dorsal-ventral axes, including FGFs, WNTs, retinoic acid, BMPs, and Sonic hedgehog (SHH) (Tao and Zhang, 2016). For example, two major groups of neurons composing the cerebral cortex, i.e., the excitatory, glutamatergic projection neurons and the inhibitory, gamma-aminobutyric acid (GABA)-ergic interneurons. During development, the glutamatergic neurons are generated in the dorsal part of the anterior neural tube (the forebrain), while the GABAergic neurons are originally generated in the ventral part of the forebrain, the ganglionic eminence (GE), and migrate in only afterward (Wonders and

Anderson, 2006). Dual-SMAD inhibition results in anterior identity by default, then by adjusting SHH for ventralization and the antagonizing activity of WNT canonical pathway and BMP pathway for dorsalization, it is possible to generate highly pure glutamatergic (Shi et al., 2012) and GABAergic cortical neurons (Kim et al., 2014), respectively.

However, many ethical obstacles regarding hESC-based studies remained. In this regard, the breakthrough of induced pluripotent stem cells (iPSCs) has revolutionized stem cell-based biomedical studies (Takahashi and Yamanaka, 2006; Yu et al., 2007). By overexpressing four transcription factors, OCT4, KLF4, SOX2, and C-MYC in fibroblasts, Yamanaka et al. successfully 'reprogrammed' human somatic cells back to the pluripotent state – similar to that of hESCs. This method makes it possible to produce a virtually unlimited number of neurons from any individual and therefore is of great help for *in vitro* research of the human neural system, especially regarding the study of neurological diseases. Early studies first reported the utilization of iPSC-derived motor neurons from patients to study the pathological mechanism of diseases affecting the spinal cord (Dimos et al., 2008; Ebert et al., 2009). HiPSCs were then employed to model a variety of brain disorders, including but not limited to: Alzheimer's disease (Israel et al., 2012), Parkinson's disease (Soldner et al., 2011; Jiang et al., 2012), schizophrenia (Brennand and Gage, 2011; Brennand et al., 2011), autism spectrum disorders (Marchetto et al., 2010), bipolar disorder (Mertens et al., 2015a). A comprehensive review on this subject was recently published (Vadodaria et al., 2020). For these reasons, hiPSCs are a unique tool that can be used to uncover the enigma of the human brain.

1.1.3 Forward programmed and transdifferentiated neurons

There is still space for improvement. First, protocols to reprogram somatic cells into iPSCs and induce neuronal cells from iPSCs not only vary from group to group, but they also result in considerable batch-to-batch difference due to the often lengthy procedures (Falk et al., 2016). Second, human cortical neurogenesis *in vivo* lasts over two months (Caviness et al., 1995), whereas *in vitro* the differentiation usually takes 4-8 weeks; and the subsequent functional maturation may take several months depending on cell types (Tao and Zhang, 2016). These time-consuming processes can also inevitably introduce large variability. In addition, the combinations of signaling molecules may not guarantee homogenous populations, making them suboptimal for clinical research and applications

(Oh and Jang, 2019). Recently, researchers inspired by the “reprogramming” of somatic cells to pluripotent stem cells by manipulating the expression of transcription factors have uncovered transcription factors that can ‘forward-program’ hPSCs into neurons, e.g., NGN2 can promote hPSC into glutamatergic neurons (Zhang et al., 2013), and that the combination of ASCL1 and DLX2 can induce the generation of GABAergic neurons from hPSCs (Yang et al., 2017). Forward programming can not only significantly shorten the differentiation and maturation time, but can also yield a very high purity of specified subtype of neurons (Flitsch et al., 2020). Therefore, this method is advantageous for high-throughput research and clinical applications. Forward programmed neurons from hPSCs have proven to be robust platforms for characterization in terms of neuromorphology, electrophysiology, and synaptic transmission and plasticity and, therefore, have been widely employed to model brain diseases (Pak et al., 2015; Muratore et al., 2017; Frega et al., 2019; Shao et al., 2019; Mossink et al., 2021a). Moreover, our group and our collaborators have systematically characterized the glutamatergic and GABAergic neurons from both small molecule-based methods and the forward programming approach with an autaptic system (Meijer et al., 2019; Rhee et al., 2019a).

It was once a common belief that the differentiation of stem cells into postmitotic somatic cells was an irreversible process in higher mammals including humans. And this partly explained their relatively poor regenerative ability, especially in neural tissues (Iismaa et al., 2018). The development of ‘reprogramming’ and ‘forward-programming’ techniques have since challenged this notion and provided an alternative view that cell fate can be manipulated (Ladewig et al., 2013). It has been shown that somatic cells of one type could be converted to another type without going through the pluripotent state, a process called transdifferentiation (Vierbuchen et al., 2010; Du et al., 2014). Much has been learned about the transcriptional regulatory network, and it is now possible to predict which factors would be needed to convert one cell type to another (Rackham et al., 2016). In the case of the brain, neurons could be converted directly from glia (Pang et al., 2011; Tanabe et al., 2018). This approach can be advantageous in several aspects. First, it further shortens the time needed to generate neurons *in vitro*. Second, directly converted neurons retain age-associated epigenetic signatures that would have been lost if reprogrammed through iPSC, which is valuable for the study of neurodegenerative diseases (Mertens et al., 2015b). And third, transdifferentiation of neurons provided a promising tool for in situ

neural repairment (Torper et al., 2015; Chen et al., 2020).

It is worth mentioning that transcription factors are not the only route to achieve fate conversion. Small molecules can also promote iPSC induction (Hou et al., 2013) and direct neuronal conversion (Ladewig et al., 2012). Recently, two studies reported that direct *in situ* glia-to-neuron conversion could be achieved by RNA-mediated knock-down of a single protein PTBP1, and the lost neuronal function in disease models could thus be restored, presenting a promising tool for brain repairment (Qian et al., 2020; Zhou et al., 2020).

1.1.4 From 2D to 3D, brains in a vat?

Conventional *in vitro* neuronal cultures are maintained in an attached monolayer form, i.e., two-dimensionally. While easier to handle and retaining key biophysiological properties, they lack the structural organization that is critical for brain functionalities. In this regard, a three-dimensional neural culture system termed ‘organoid’ was firstly reported by Eiraku et. al, in 2008 (Eiraku et al., 2008). Here, neuroectoderm derived from hPSCs was embedded in scaffold droplets and maintained in a floating three-dimensional form, while a spinning bioreactor was needed to enhance substance exchange. The resulting organoid developed a ventricular-like cavity where the neural stem cells could give rise to cortical-like laminar structure — strikingly similar to the *in vivo* neural developing processes. Many forms of human brain organoids have since been developed and they have proved to be uniquely helpful for studying human brain development and neurodevelopmental diseases (Di Lullo and Kriegstein, 2017).

Caution needs to be taken at this point, however. A recent study compared electrophysiological activities recorded from brain organoids with the electroencephalograms of developing embryos, claiming that they shared substantial similarities (Trujillo et al., 2019). Preliminary as it is, this study represents a closer step towards the substantiation of the philosophical thought experiment: ‘brains in a vat’ (Putnam, 1981). This thought experiment is concerned with the ongoing discussions about the ethical challenges and uncertainties of brain organoid studies, with the most pressing question being: ‘could some form of subjective consciousness arise from a brain organoid that needs to be taken into moral (and legal) consideration’ (Koplin and Savulescu, 2019; Sawai et al., 2019)? Most researchers believe we are yet to reach the point. However,

because the definition of consciousness itself is still unsettled in many regards, the question becomes ‘how do we know when we reach the point?’ and even ‘how do we know we have not already reached the point’? While these questions deserve broader and more throughout discussions, the crux of the matter is how to obtain a deeper understanding of the functional capability of this system. This will be discussed partly in the following sections.

1.2 Functional characterization of human *in vitro* neuronal networks

The fundamental functions of neurons manifest in their ability to collect and transmit information via chemical or electrical connections with each other, i.e., in circuits or networks. It is the delicate organization of these single units, occurring in astronomical numbers, that gives rise to brain functionalities (Barbey, 2018). Therefore, it is important to understand how single neurons *in vitro* could develop and organize into networks, and what functional properties could emerge during this process in healthy and disease-prone conditions. For this, it is necessary to observe or measure, and preferably manipulate, the electrophysiological activity of large ensembles of neurons simultaneously and over longer periods of time. One technique that could meet these needs is the microelectrode array (or multi-electrode array, both could be shortened as the MEA). The MEA differs from the intracellular electrophysiological patch-clamp technique in that it allows non-invasive, long-term extracellular recording at fine spatial and temporal resolution and scale (Obien et al., 2015). It also allows manipulation of the neuronal network by delivering electrical stimuli. This makes the MEA an important tool for *in vitro* neurobiological studies.

1.2.1 A brief introduction to the MEA technique

Thomas et al. firstly developed an MEA system to record electrical activities from *in vitro* cell cultures of dissociated chick cardiomyocytes (Thomas et al., 1972). The array is composed of 30 platinized gold electrodes measured ~ 50 μm^2 and arranged in the center of a coverslip and linked by radial and insulated wires to the surrounding metal patches that connect to the amplifier, a classic design that is still being used nowadays (Figure 1-1). This device was able to successfully record rhythmic potentials from contracting cardiomyocyte assemblies. Later, similar MEA systems were used to record activity from neuronal cultures, i.e., ganglion neurons from snail (Gross et al., 1977) and rats (Pine, 1980).

MEAs have since also been used to monitor the activities in cortical neuronal cultures, mostly from neonatal or embryonic rodent brain, which has revealed a common functional development pattern of *in vitro* neural networks (Kamioka et al., 1996; Pelt et al., 2004; Chiappalone et al., 2006). During the first 1 to 2 weeks, the cultures usually show uncorrelated and sparse spikes which are believed to arise from individual spontaneously firing neurons. This simple activity can then develop into more correlated activities and

eventually synchronized network-level burst, indicating the establishment of a substantial number of functional synaptic connections. The emergence of network bursts depends on the density of the cultures (Ito et al., 2010a). Both glutamatergic and GABAergic synaptic transmissions are believed to be implicated in this process since it can been modulated by α-amino-3-hydroxy-5-methyl-4-isoxazolepropionic acid (AMPA), NMDA, and GABA-A receptor antagonists (Opitz et al., 2002). The termination of network bursts is believed to be due to synaptic short-term depression mediated by depletion of presynaptic vesicle pools (Cohen and Segal, 2011). Less consistently, some researchers have also reported more complex patterns of activities arising from cortical neuronal networks cultured on the MEA, indicating further potential of the *in vitro* system (Wagenaar et al., 2006a, 2006b; Stephens et al., 2012).

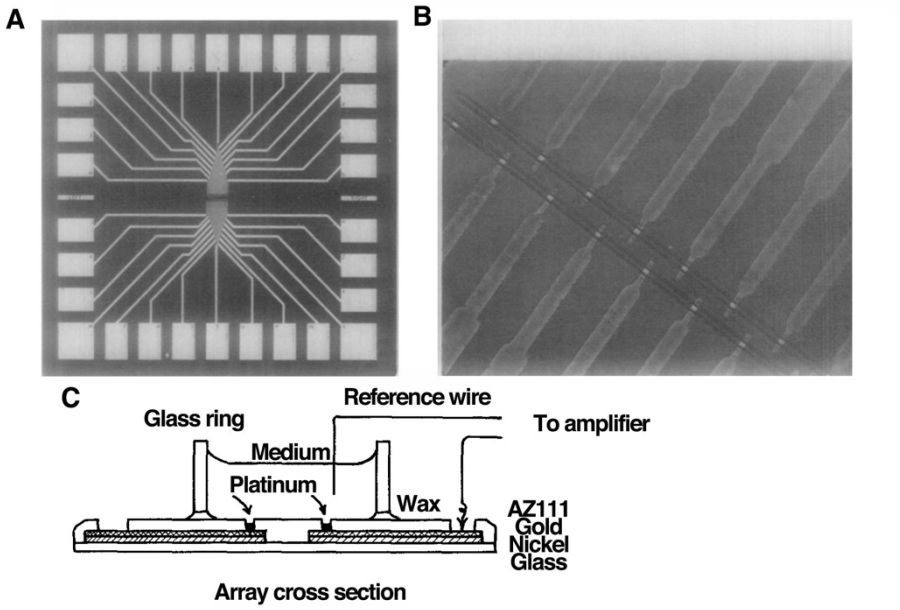

Figure 1-1 The MEA developed by Thomas et al., 1972. (A) The plan view of the MEA. (B) Enlarged view of the electrodes. (C) Diagrammatic illustration of the design of the MEA.

Neurons form circuits and networks to implement functionality, i.e., processing information or computation. To achieve this, neural circuits and networks have to continuously evolve according to external feedbacks, for example by changing the synaptic strength. This basic idea has inspired a whole new field, namely the “artificial neural network” or “machine learning”, which has yet to fully flourish but is already transforming virtually all branches of applied and natural sciences (Krogh, 2008). It is no wonder that researchers

have asked if a biologically based *in vitro* neural network could be constructed and adapted to perform computations similar to those of artificial neural networks *in silico*. In this regard, the MEA has been used to 'train' *in vitro* neural networks to perform a variety of tasks: controlling a robot (Tessadori and Chiappalone, 2015), pattern classification (Ruaro et al., 2005; Isomura et al., 2015), and storing information (Le Feber et al., 2015; Kim et al., 2019). However, acquiring functionality relies on the neural plasticity being modulated towards predefined goals, and it is still unresolved how to induce plasticity in cultured neural networks efficiently (Wagenaar et al., 2006c). Research along this direction is, therefore, not yet well-developed.

Nevertheless, the MEA as a technique itself has been continuously improved. One goal is to monitor as much of the network as possible and with as high of a resolution as possible. In this regard, the introduction of complementary metal-oxide-semiconductor (CMOS) techniques to the MEA system now makes it possible to record electric activities from nearly all neurons in a culture spanning several square millimeters at a sub-cellular resolution (Frey et al., 2010; Ballini et al., 2014). With such a high resolution, researchers can now trace the propagation of action potentials along the axon of single neurons, providing a unique opportunity for electrophysiological studies (Bakkum et al., 2013). Meanwhile, recently developed MEAs with electrodes arranged three-dimensionally are able to monitor activity from the aforementioned 3D *in vitro* neural cultures, facilitating their further utilization in neurobiological studies (Spanu et al., 2020; Shin et al., 2021).

It is worth mentioning that, although beyond the scope of this thesis, the MEA is also being used to record neural signals *in vivo* for both scientific and clinical purposes (Hong and Lieber, 2019; Musk, 2019). The author of this thesis has also previously worked on using *in vivo* MEAs for preoperational cortical functional mapping and anatomical linguistics studies (Wen et al., 2017b, 2017a, 2018).

1.2.2 Using MEAs to record hPSC-derived neuronal networks

With the aforementioned advantages, MEAs have also been used to characterize hPSC-derived neuronal networks since 2009 (Heikkilä et al., 2009). Human neural cultures *in vitro* show similar patterns of activity to that of rodents, i.e., from single spikes to network bursts, but require significantly longer time to mature (Napoli and Obeid, 2016; Odawara et al., 2016; Hyvärinen et al., 2019). Network features of hPSC-derived neural cultures

are consistent among different cell lines from different laboratories, making the MEA a robust and reliable platform for human-specific neurobiology research and neurotoxicity testing *in vitro* (Novellino et al., 2011; Odawara et al., 2018; Mossink et al., 2021b). The MEA has helped to uncover genotype-phenotype correlations of brain diseases in many studies (Martens et al., 2016; Amin et al., 2017; Wang et al., 2021).

Excitatory-to-inhibitory imbalance is believed to be part of the pathophysiological mechanisms of brain diseases including epilepsy (Thijs et al., 2019), autism spectrum disorders (Nelson and Valakh, 2015), schizophrenia (Gao and Penzes, 2015), and Alzheimer's disease (Vico Varela et al., 2019). The development of the forward-programming technique made it possible to establish *in vitro* human neuronal cultures with defined excitatory-to-inhibitory ratios, which has provided a unique opportunity to study the functional balance of human neural networks. The MEA is thus a necessary tool for this purpose. A few studies have explored this direction and obtained preliminary results. For example, it was found that more inhibitory neurons in the network led to shorter network bursts, lower total firing rate, and a higher percentage of random spikes (Sasaki et al., 2019; Mossink et al., 2021a). However, there is still no consensus regarding which parameters constitute the criteria of a 'balanced' neural network *in vitro*, and further work is needed to address this question.

1.3 Neuronal dynamics and computational simulation

1.3.1 Mathematization of neural systems

Mathematic theorization and computational simulation of neural networks can not only validate experimental findings but can also help to form and test new hypotheses in advance, guiding the direction of further experiments. Yet due to their complexity, establishing mathematical models to quantitively describe biological processes and predict their behaviors have been more difficult to develop than in other natural sciences, e.g., chemistry and physics. The ground-breaking work of Hodgkin and Huxley in revealing the mechanism of action potentials, i.e., the H-H model, was generally regarded as the landmark of computational neuroscience (Hodgkin and Huxley, 1952). Based on data collected from the giant squid axon, the H-H model abstracts segments of axon as electrical circuits: the cell membrane as a capacitor, ion channels (Na^+, K^+, and Cl^-) as conductance, the electrochemical gradients across the cell membranes as voltage sources, ion pumps and leak channels as constants. The breakthrough of their work was a precise description of how the conductance of each ion channel changes as a function of time and the membrane potential, i.e., the ‘voltage-gating’ phenomenon. This basic model could be extended spatially to a model of whole axons that can convey action potentials and, with other modifications, models of synapses, the soma, and the dendritic tree. By linking these models together one can form a model of a complete neuron, which is called a compartmentalized model (Carnevale and Hines, 2006; Bower and Beeman, 2012).

For a neuronal network of considerable scale, modeling every ion channel of every compartment of every neuron is computationally unrealistic, and, therefore, further abstraction and simplification are need. One of the most widely used neuronal models for network analysis is the integrate-and-fire model (Burkitt, 2006). In this model, neurons are deduced to point processes with no spatial extensity and are represented by a single variable: the voltage potential. The voltage potential could be modulated by post-synaptic effects from upstream neurons, and an artificial action potential ‘event’ would be triggered when the potential crosses a predefined threshold, leading downstream neurons to be excited or inhibited accordingly. With some modifications, this type of model could faithfully recapitulate experimental data when given defined current input (Badel et al.,

2008). If necessary, further simplification could be employed so that a group of neurons are represented collectively in a single process (Knight, 1972). This is useful when studying the interaction of distinct neuronal populations during sophisticated tasks (Gerstner et al., 2014). For example, population models have helped to explore the neural basis of perception, memory and decision making (Romo and Salinas, 2003).

1.3.2 Simulating *in vitro* neuronal networks

In silico modelling can also be helpful for understanding the functional properties of *in vitro* neural networks. Some researchers have tried to establish a framework to explain how the functional and morphological changes of single neurons can drive network-level functional development (Van Ooyen et al., 1995; Gritsun et al., 2012; Kawasaki and Stiber, 2014; Okujeni and Egert, 2019). Others have focused on mimicking the mechanism of network bursts in neural cultures through the use of computational modeling (Gritsun et al., 2011, 2012; Huang et al., 2017; Pasquale et al., 2017). Of note, Zhan et al. assess the effects of glia in shaping network bursts through a numerical model, highlighting the importance of glial cells and extra-synaptic receptors in neural network activity (Zhan et al., 2011). The first computational model of a hESC-derived neuronal network was reported by Lenk et al. Based on data recorded with MEAs, their model provides a theoretical blueprint of human *in vitro* neural network development (Lenk et al., 2016). Yet so far, there is no model specifically for forward programmed neuronal networks with defined compositions.

1.4 Application of forward programmed neurons in studying high-risk variants for psychiatric disorders

One of the applications of hPSC-derived *in vitro* neuronal cultures is to study psychiatric disorders. Psychiatric disorders, or mental illness, are a group of conditions characterized by cognitive, emotional, behavioral, and social impairments and cause substantial disturbance to personal functioning. These disorders are a leading cause of disability, which can result in drastic consequences for both affected individuals and their families. The health care burden of psychiatric illnesses is greater than that of chronic somatic diseases such as cancer or diabetes (World Health Organization, 2008; Whiteford et al., 2013; Patel et al., 2016; Trautmann et al., 2016). The modest to high heritability of psychiatric disorders has been consistently demonstrated through early twin and adoption studies (Kendler, 1993, 2001; Plomin et al., 1994). Later studies, however, employing large cohorts and genome-wide linkage and association empowered by high-throughput sequencing techniques have only identified genes that are accountable for <2% of heritability (Crow, 2011). This has led to the conclusion that psychiatric disorders are very rarely related to highly penetrant monogenic variants, while polygenic variation (of up to thousands of genes) is believed to contribute jointly to the development of psychiatric disorders (Purcell et al., 2009). It has also been observed that copy number variations (CNV) of large genomic regions are associated with a higher risk of psychiatric disorders (Sebat et al., 2007; Stone et al., 2008).

Neurons can be generated from iPSCs derived from psychiatric patients of known or unknown genetic causes to uncover possible pathogenesis mechanisms (Marchetto et al., 2010; Brennand et al., 2011; Cheung et al., 2011; Chiang et al., 2011; Wen et al., 2014; Hartley et al., 2015; Xu et al., 2016; Harrison et al., 2016; Lu et al., 2016; Vadodaria et al., 2016; Ni et al., 2020). Yet this approach is faced with drawbacks. As aforementioned, psychiatric disorders are mostly polygenic, and donors recruited have different genetic backgrounds. It is estimated from a large cohort in a post-mortem schizophrenia study that ~28500 subjects would be needed to detect with adequate power the difference from a single gene's expression (Fromer et al., 2016). This number is believed to be comparable in hPSC-based studies, if not higher (Hoffman et al., 2019). Even with known common mutations, different genetic and epigenetic landscapes could still contribute to

reduced homogeneity in produced neurons. This heterogeneity could be addressed with tight control of the genetic background, for example, by creating isogenic control cell lines with corrected mutants, or isogenic mutated cell lines from healthy controls. Thanks to the recently developed clustered regularly interspaced short palindromic repeats (CRISPR)/CRISPR associated protein (Cas) 9 system (Jinek et al., 2012; Cong et al., 2013; Ran et al., 2013) highly accurate and efficient genome editing is now widely available for hPSCs (Hockemeyer and Jaenisch, 2016). CRISPR, coupled with RNA-guided Cas9 nuclease, was originally discovered to function as a part of the microbial adaptive immune system. By modifying a 20-nt sequence in the guide RNA, Cas9 can be led to the targeted genome to create a double-strand break, which then, depending on the design, can result in either nonhomologous end joining or in homology-directed repair. CRISPR/Cas9 has been successfully used in hPSC-based research of psychiatric disorders (Powell et al., 2017). The combination of CRISPR/Cas9-mediated genome editing on hPSCs and forward programming technique to derive neurons provides a valuable opportunity to study psychiatric diseases *in vitro*. The following paragraphs will focus on one candidate gene that has been associated with psychiatric disorders, RB1-inducible coiled-coil 1 (RB1CC1).

1.4.1 Mutations of RB1CC1 are associated with psychiatric disorders

A study conducted locally in the Bonn-Mannheim region, with 1627 schizophrenia patients and 1637 controls, found that duplications affecting RB1CC1 occurred in five patients and one control. Combined with additional follow-up data, duplications of RB1CC1 were revealed to be significantly over-represented in 9 out of 8461 (~ 0.1%) patients, compared to 14 out of 112871 (~ 0.012%) in control individuals (Degenhardt et al., 2013). Independently, duplications affecting RB1CC1 were also reported in developmentally delayed (Cooper et al., 2011) and autism patients (Marshall et al., 2008), and a *de novo* mutation causing a frameshift of RB1CC1 was reported in a schizophrenia patient (Xu et al., 2011). Recently, Errichiello et al. reported a schizophrenia patient with suicidality and obesity who carried a *de novo* complete duplication of RB1CC1, which led to over-expression of this gene in peripheral blood lymphocytes (Errichiello et al., 2020). In summary, there is a strong link between mutations of RB1CC1 and psychiatric disorders, especially schizophrenia. Therefore, understanding basal functions of RB1CC1 in

neuronal cells may help to uncover potential etiological and pathogenic mechanisms of schizophrenia.

1.4.2 Identification, function and structure of RB1CC1

The human *RB1CC1* gene is localized on chromosome 8q11. It has 24 exons and encodes a protein with 1594 amino acid residues and a molecular weight of 183 kDa. RB1CC1 was discovered by Ueda et, al. in a yeast two-hybrid screen while searching for potential proteins interacting with proline-rich tyrosine kinase (Pyk2) (Ueda et al., 2000). It was found to bind to the kinase domain of Pyk2 and inhibits its kinase activity. Considering structural similarities of Pyk2 and focal adhesion kinase (FAK), in following studies the same group found this protein also binds to the kinase domain of FAK and inhibits its kinase activity and autophosphorylation *in vivo*, and thus dubbed it as FAK family kinase-interacting protein of 200 kDa (FIP200). Additionally, overexpression of RB1CC1 was found to inhibit cell spreading and migration and cell cycle progression, which was correlated with its inhibition of FAK activity *in vivo* (Abbi et al., 2002). RB1CC1 also interacts with the tuberous sclerosis (TSC) 1–TSC2 complex and regulates cell size, which led to the finding that it acts in autophagy signaling pathways (Gan et al., 2005). They also found deletion of RB1CC1 in mice led to embryonic lethality (embryonic day 16.5). In RB1CC1$^{-/-}$ mouse embryos, fibroblasts and liver cells showed increased apoptosis and reduced c-Jun N-terminal kinase phosphorylation in response to tumor necrosis factor (TNF) α stimulation (Gan et al., 2006). Independently, the same gene/protein was identified in a screening of multidrug resistance to anti-cancer agents, where Chano et al. noticed a gene of 6.6 kb that encoded for a 1594 aa protein (Chano et al., 2002a). Its expression level was found to be highly correlated with that of retinoblastoma 1 (RB1), and thus termed it as RB1-inducible Coiled-Coil 1 (RB1CC1). The same group soon reported that RB1CC1 is frequently mutated in breast cancer and showed characteristics of a classical tumor-suppressor gene (Chano et al., 2002b). They later characterized the expression of RB1CC1 in the development of murine and human embryos (Bamba et al., 2004). Due to the lack of direct evidence, however, the hypothesis that RB1CC1 acts as a tumor suppressor gene was not well-developed (Chano et al., 2010). Another study from this group has also indicated RB1CC1 regulates TSC-mTOR pathways in neuromuscular tissues (Chano et al., 2006) and may potentially have a role

in how Alzheimer's disease affects the brain (Chano et al., 2007). It was not until 2008 that Hara et, al. found RB1CC1 binds to UNC-51–like kinase (ULK) 1 to initiate the formation of autophagosomes (Hara et al., 2008). Independently, Ganley et, al. also found that RB1CC1 forms a protein complex with ATG13 and ULK1, which is essential for the localization and stabilization of ULK1 in autophagosome formation (Ganley et al., 2009). The important role of RB1CC1/FIP200 in autophagy initiation has since been regarded as its canonical function.

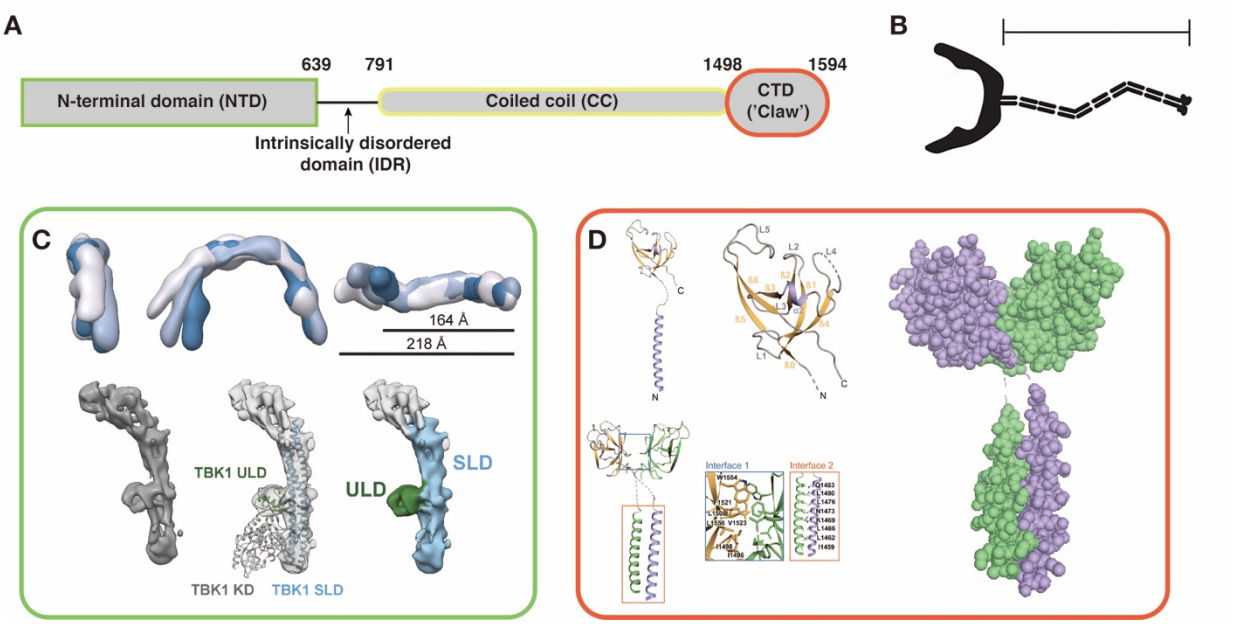

Figure 1-2 Known structure of RB1CC1, adapted from Turco et al., 2019 and Shi et al., 2020. (A) Schematic depiction of the RB1CC1 protein. (B) Cartoon depiction of the RB1CC1 dimer. Scale bar = 50 nm. (C) Visualization of RB1CC1 NTD dimer (upper) and monomer (lower). Robetta analysis indicates that TBK1 scaffold-like domain (SLD) and ubiquitin-like domain (ULD) fit well with the density map of RB1CC1 NTD. (D) The resolved structure of RB1CC1 CTD monomer and dimer.

In autophagy, RB1CC1 is arguably the functional homologue of yeast Atg17 (Hara and Mizushima, 2009). Yet the two protein are not evolutionarily related, therefore, the known structure of Atg17 (Ragusa et al., 2012) could not be used to help determine the structure of RB1CC1 through homology modeling. Early predictions indicated that RB1CC1 protein contains a nuclear localization signal, a leucine zipper motif, and a large coiled-coil structure (Chano et al., 2002a). It relies on domains near the N-terminal and/or the coiled-coil to interact with and inhibit FAK (Abbi et al., 2002). Nevertheless, it was not until very recently that we saw breakthroughs in the structure determination of RB1CC1, especially

in the context of autophagy (Turco et al., 2019; Shi et al., 2020b, 2020a). Although the high-resolution structural architecture of RB1CC1 has yet to be revealed, we now know that it forms dimers that are essential for autophagy (Figure 1-2).

Its N-terminal domain (NTD, 1-639) forms a C-shaped dimeric structure that presumably acts as an organizational hub for the ULK1 complex, with an asymmetric 1:2:1:1 ULK1:FIP200:ATG13:ATG101 stoichiometry. Within this locus, aa 443–450 mediates its binding with ATG13 (Shi et al., 2020b). These findings differ from those of a previous study where Chen et al. reported that residues 582-585 (LQFL) in RB1CC1 mediate its interaction with ATG13 and found that replacing these residues with AAAA abolished its canonical autophagy function (Chen et al., 2016). Shi et al. demonstrated that this locus might instead be critical for dimerization of RB1CC1 NTD, rather than being directly involved in the interaction between RB1CC1 and ATG13. Nevertheless, mutating aa 582-585 to AAAA led to neonatal death of mice similar to knock-out (KO) of other ATGs (Kuma et al., 2017) and also maintained a protective role in TNFα-induced apoptosis. The NTD is followed first by an intrinsically disordered domain and then by a long and presumably flexible coiled-coil domain of 710 amino acid residues which spans up to 107 nm. The coiled-coil is linked with a C-terminal domain (CTD), of which the crystal structure has been determined (Turco et al., 2019). Dimers of RB1CC1 CTD form a ‘claw’ or ‘pocket’ structure that binds with p62 and is mutually exclusive of p62’s binding to LC3B, which indicates that it mediates the translocation of to-be-degraded cargo from p62 to the autophagosome. This idea has been further strengthened by studies focused on selective autophagy. Autophagy had been regarded as non-selective bulk processes, yet new evidence indicates that there are multiple, tightly regulated subtypes of autophagy which first require for the cargo to be recognized, e.g., aggregated proteins (aggrephagy), mitochondria (mitophagy), peroxisomes (pexophagy), ribosomes (ribophagy), endoplasmic reticulum (reticulophagy) and pathogens (xenophagy) (Stolz et al., 2014). Cargo recognition is mediated by a group of cargo receptors such as p62, neighbor of BRCA1 (NBR1), nuclear dot protein 52 kDa (NDP52), and optineurin. Recently, NDP52 was shown to be able to bind to the C terminal of the coiled-coil region of RB1CC1 and thus recruit ULK1 complex to damaged pathogen-containing vacuoles and mitochondria (Ravenhill et al., 2019; Vargas et al., 2019; Turco et al., 2020). It has been shown that binding of NDP52 can increase the membrane affinity of the C-terminal of coiled-coil of

RB1CC1, effectively promoting its recruitment of membrane and downstream autophagy machinery (Shi et al., 2020a). This process could occur even without ATG7 and LC3 (Ohnstad et al., 2020). These findings lead to an interesting hypothesis that the binding of cargo receptors to RB1CC1 might act as a triggering event for selective autophagy, which could happen in a form that is vastly different from non-selective autophagy. In addition, RB1CC1 also directly interacts with ATG16L1, mediating the regulatory effect of the ULK1 complex to the ATG5-ATG12 complex (Gammoh et al., 2013). In summary, the NTD of RB1CC1 helps to assemble the ULK1 complex, the C-terminal of its coiled-coil domain at least promotes its binding to the membrane, the long coiled-coil domain acts as a tether of which the N-terminal domain and the 'claw' structure linked to it translocate receptor-labeled cargos to the autophagy machinery. All of this suggests RB1CC1 to be a core organizer of autophagy.

1.4.3 Neuronal specific function of RB1CC1 and its possible pathogenic implication in schizophrenia

Liang et al. described the effects within the nervous system of a neural-specific deletion of RB1CC1 using Nestin-Cre and FIP200$^{f/f}$ mouse lines (Liang et al., 2010). They found 45% of the mutant mice died within days after birth; afterwards the survival rate remained stable until post-natal day 14 and then sharply decreased to zero by post-natal day 60. Cerebellar degeneration with neuronal loss, spongiosis, and neurite degeneration was also observed**.** Using glial fibrillary acidic protein (GFAP)-Cre lines, they later reported that RB1CC1 deletion led to a deficiency of maintenance and differentiation of postnatal neural stem cells, which is related to intracellular reactive oxygen species (ROS) regulation by autophagy (Wang et al., 2013a). The same group later reported the activation of microglia to have mediated these NSC deficiencies (Wang et al., 2017). Using Best1-Cre mice, Yao et al. found RB1CC1 deletion led to the loss of photoreceptors and the degeneration of the retinal pigment epithelium, possibly due to disruption of autophagy (Yao et al., 2015). The combination of these findings suggests the role of RB1CC1 is critical to the nervous system.

Although schizophrenia is believed to be largely genetically predisposed, environmental stress emerging in gestation and early life, such as obstetric complications (Cannon et al., 2002), prenatal infection and malnutrition (Brown, 2006; Brown and Susser, 2008), and

socioeconomic disturbance (Cantor-Graae and Selten, 2005; Krabbendam, 2005) might also lead to a higher vulnerability of developing the disorder. Interestingly, stressful insults in adolescence seem to be relatively tolerable in terms of not increasing the risk for developing schizophrenia, suggesting there may be a critical window of pathogenesis (Giovanoli et al., 2013). Stress itself could lead to structural and functional impairment to the prefrontal cortex (Arnsten, 2009) and altered dopamine release (Howes et al., 2017). Additionally, physiological and psychological stressors are also associated with oxidative stress in the brain (Schiavone et al., 2013), indicating an potentially important intermediary from etiology to pathology. Specifically, oxidative stress could lead to multiple pathophysiological consequences related to schizophrenia, such as inflammation, mitochondrial dysfunction, hypoactive NMDA receptors, and the impairment of fast-spiking GABAergic interneurons (Bitanihirwe and Woo, 2011). Autophagy, which is dependent on RB1CC1, could alleviate these impairments by clearing damaged biomolecules like proteins, DNA, and lipids (Filomeni et al., 2015). RB1CC1 might also counteract proinflammatory TNF-α/NF-κB pathways independent of autophagy (Chen et al., 2016).

Schizophrenia has an average onset age between 16 to 30 years (Owen et al., 2016), overlapping with the critical neurodevelopmental window of synaptic pruning (Silbereis et al., 2016). Post-mortem studies and neuroimaging studies have consistently reported reduced grey matter in schizophrenia patients (Selemon et al., 2002; Hulshoff Pol and Kahn, 2007), which is likely due to the decrease of dendritic spines (Moyer et al., 2015; MacDonald et al., 2017). On the other hand, reduction of spine density might result from excessive spine pruning due to microglia-mediated inflammatory response (Paolicelli et al., 2011; Trépanier et al., 2016) or deficiency of dendritic arborization (Flores et al., 2016; Shao et al., 2019). RB1CC1 could act on these processes to moderate this abnormality: preventing inflammatory damage via autophagy-dependent and/or -independent pathways (Chen et al., 2016; Wang et al., 2017) or by promoting dendritic arborization by inhibiting the FAK/protein kinase C (PKC) signaling pathway (Garrett et al., 2012; Shao et al., 2019).

These possible implications could be assessed with forward programmed neurons derived from isogenic human pluripotent stem cell lines with RB1CC1 loss of function. This may

hopefully shed light on the mechanisms underlying the pathogenesis of RB1CC1-related psychiatric disorders.

1.5 Aims of the thesis

The first objective of this study is to establish and functionally characterize an *in vitro* platform based on forward programmed neuronal cultures derived from hPSCs. For this, excitatory and inhibitory human neurons were to be generated by forward programming human hPSCs carrying the inducible transcription factors NGN2 and ASCL1/DLX2 expression cassettes, respectively. These neurons then had to be cultured with defined compositions on MEAs for electrophysiological measurements on a network level. In parallel, *in silico* neuronal network models fed with neuronal parameters obtained from the *in vitro* cultures had to be developed to explore potential mechanisms underlying the experimental observations with MEAs. The key goal of the combined *in vitro* and *in silico* approach was to give a systematic functional representation of human forward programmed neuronal networks. Another goal to be pursued in this study was to utilize human forward programmed neurons in brain disease modelling. Specifically, as an exemplar, this study focuses on a gene that has been associated with psychiatric disorders: RB1CC1. For this, hPSC lines had to be subjected to CRISPR-Cas9 mediated genome editing to introduce loss-of-function mutations into the RB1CC1 gene. This study then had to focus on the phenotypic characteristics of neurons derived from the isogenic cell lines, including molecular, morphological, and electrophysiological alterations due to RB1CC1 loss of function, with an emphasis on autophagy and FAK related pathways. Ultimately, this could help to identify valid biological pathways that link genetic susceptibility to endophenotypes and help to understand how the deficiency in risk genes impacts neuronal responses to pharmacological treatments. In summary, this study aims to explore forward programmed neurons as a tool for human neuronal network analysis and disease modeling.

2. Materials and methods

2.1 Experimental materials

2.1.1 Antibodies, chemicals, peptides, and recombinant proteins

Antibodies

Antibody name	Supplier	Identifier	Dilution
Alexa Fluor 488 Goat anti-Mouse IgM	Thermo Fisher Scientific	A-21042	1:1500 (FC)
Alexa Fluor 488 Goat anti-Rabbit Igg	Thermo Fisher Scientific	A-11008	1:1000 (IF)
Alexa Fluor 647 Goat anti-mouse Igg	Thermo Fisher Scientific	A-21236	1:500 (IF)
Anti-FIP200	Sigma-Aldrich	SAB4200135	1:1000 (WB)
Anti-mouse IgG, HRP-linked Antibody	Cell signaling	7076	1:1000 (WB)
Anti-rabbit IgG, HRP-linked Antibody	Cell signaling	7074	1:1000 (WB)
GAPDH	Santa Cruz Biotechnology	sc-47724	1:1000 (WB)
OCT4	Santa Cruz	sc-9081	1:500 (IF)
PSD95	Thermo Fisher Scientific	MA1-046	1:1000 (WB)
SOX2	R&D Systems	MAB2018	1:1000 (IF)
Synapsin1	Synaptic Systems	106 103	1:1000 (WB)
TRA-1-60	Sigma-Aldrich	MAB4360	1:1000 (FC)

WB = Western blot, FC = Flow cytometry, IF = Immunofluorescence.

Chemicals and other substances

Name	Supplier	Identifier
2-Mercaptoethanol	Thermo Fisher Scientific	21985023
Ampuwa (sterile water)	Fresenius	40676000
Agar	Carl Roth	2266
Arc-C	Sigma-Aldrich	C1768
Bicuculline	Tocris	2503
CNQX	Tocris	0190
DAPT	Sigma-Aldrich	D5942
dATP	VWR Life Science	20-1011
dCTP	VWR Life Science	20-1020
dGTP	VWR Life Science	20-1030

Name	Supplier	Identifier
DMSO	Sigma-Aldrich	D4540
Doxycycline	Sigma-Aldrich	D9891
dTTP	VWR Life Science	20-1041
EDTA	Sigma-Aldrich	E6635
Ethanol	Carl Roth	9065
Ethidium bromide	Thermo Fisher Scientific	15585011
Halt ™ Protease and Phosphatase Inhibitor	Thermo Fisher Scientific	78442
Luminata Classico Western HRP substrate	Merck Millipore	WBLUC0100
Methanol	Carl Roth	8388
$MgCl_2$	Thermo Fisher Scientific	AM9530G
Milk powder (low fat)	Carl Roth	T145
MRT68921	Tocris	5780
NaCl	Carl Roth	P029
PF573228	Tocris	3239
Poly-ornithine	Sigma-Aldrich	P4957
ROCK Inhibitor	Cellagen Technology LLC	C9127-2
Trehalose	Sigma-Aldrich	T9531
Tryptone	Carl Roth	8952
Yeast extract	Carl Roth	2904

Peptides and recombinant proteins

Name	Supplier	Identifier
Accutase	Thermo Fisher Scientific	A11105-01
Alt-R® S.p. Cas9 Nuclease V3	Integrated DNA Technologies	1081059
Geltrex	Thermo Fisher Scientific	A1413201
GoTaq® DNA Polymerase	Promega GmbH	M3001
Laminin	Sigma Aldrich	L2020
Matrigel	Corning B.V. Life Sciences	354230
Recombinant human BDNF	Cell Guidance Systems	GFH1
Recombinant Human bFGF	Life Technologies	PHG0021
Recombinant Human EGF	R&D Systems GmbH	236-EG-01M

2.1.2 Media, supplements, and buffers

Name	Supplier	Identifier
B27 supplement	Thermo Fisher Scientific	17504044
DMEM/F12	Thermo Fisher Scientific	11320-074
DPBS	Thermo Fisher Scientific	14190-094
Fetal bovine serum	Thermo Fisher Scientific	10500064
GlutaMAX	Thermo Fisher Scientific	35050-38
Knockout Serum Replacement	Thermo Fisher Scientific	10828028
N2 supplement	Thermo Fisher Scientific	17502-048
Name	Supplier	Identifier
Neurobasal Medium	Thermo Fisher Scientific	21103-049
NuPAGE™ MOPS SDS Running Buffer (20X)	Thermo Fisher Scientific	NP0001
NuPAGE™ Tris-Acetate SDS Running Buffer (20X)	Thermo Fisher Scientific	LA0041
Pierce™ LDS Sample Buffer, Non-Reducing (4X)	Thermo Fisher Scientific	84788
RIPA buffer	Sigma Aldrich	R0278
StemMACS iPS-Brew	Miltenyi Biotec	130-107-087
StemMACS iPS-Brew 50x supplement	Miltenyi Biotec	130-107-086

2.1.3 Primers, recombinant RNA, and recombinant DNA

Primers

Internal identifier	Sequence	Supplier
RB1CC1_E4KO_for	5’TGGGGAAGGTTTTAGAGTGAAATT-3’	Integrated DNA Technologies
RB1CC1_E4KO_rev	5’-TGAGCGTGCACATTGCCTTC-3’	Integrated DNA Technologies

Recombinant DNA and RNA

Name	Supplier	Identifier
Alt-R® CRISPR-Cas9 tracrRNA	Integrated DNA Technologies	1072532
ptfLC3	Addgene	21074
RB1CC1E4KO crRNA	Integrated DNA Technologies	Hs.Cas9.RB1CC1.1.AB CAAGATTGCTATTCAACACC

2.1.4 Commercial assays and kits

Name	Supplier	Identifier
FuGENE® HD Transfection Reagent	Promega GmbH	E2311
Maxwell RSC DNA Blood Kit	Promega GmbH	AS1400
Plasmid Maxi Prep Kit	Zymo Research	D4205
P3 Primary Cell 4D Nucleofector kit	Lonza	V4XP-3012
Pierce ™ BCA Protein Assay Kit	Thermo Fisher Scientific	23225
Wizard SV Gel and PCR Clean up System	Promega GmbH	A9281

2.1.5 Plastics and other consumables

Name	Supplier	Identifier
6-well-plate	Corning	3736
96-well-plate	Ibidi	89626
Cell Strainer 40 µm	BD Biosciences	352340
NuPAGE 10 % Bis-Tris gel	Thermo Fisher Scientific	NP0315BOX
NuPAGE 3-8 % Tris-Acetate gel	Thermo Fisher Scientific	EA0378BOX
Freezing container	Thermo Fisher Scientific	5100-0001
PVDF membranes	BIO-RAD	1620177
Syringe filter 0.2 µm	PALL	4612
Syringes	BD Biosciences	309646, 309661

2.1.6 Devices, software and external services

Devices

Device	Product	Manufacturer
Autoclave	D-150	Systec
Balance	LA310S, BL610, BP2100S	Sartorius
Block heater	Thermomixer compact	Eppendorf
Centrifuge and rotor	Megafuge 1.0R Rotor #2704 Rotor BS4402/A	Heraeus
Centrifuge and rotor	RC 26 PLUS RC5B PLUS Rotor SS-34 Rotor SLA-3000	Sorvall
Chemiluminescence detection	Chemidoc XRS detection system	BIO-RAD

Device	Product	Manufacturer
Counting chamber	Fuchs-Rosenthal	Faust
Flow cytometry	BD Accuri™ flow cytometry	Becton, Dickinson and Company
Fluorescence microscope	EVOS FLoid Imaging System	Thermo Fisher Scientific
Freezer -150°C	MDF-C2156VAN-PE	Panasonic
Freezer -80°C	Hera freeze	Heraeus
Incubator	HERAcell 150	Heraeus
Inverse light microscope	Axiovert 40C	Carl Zeiss
Live cell imaging microscope	Axiovert 200M Camera: Prog Res C14 UV-lamp: Ebq 100	Zeiss Jenoptik Zeiss
Nucleic acid extraction device	Maxwell RSC instrument	Promega
Multi-electrode array recording system	Axion Maestro Edge	Axion BioSystems
Nucleofector	Amaxa 4D Nucleofector	Lonza
pH-meter	HI 9321	HANNA Instruments
Power supply SDS-PAGE	POWER PAC 200	BIO-RAD
Refrigerators/freezers 4°C, -20°C	G2013 Comfort HERAfreeze	Liebherr Heraeus
Sterile laminar flow hood	HERAsafe	Heraeus
Thermocycler	ProFlex PCR system Mastercycler X50a	Thermo Fisher Eppendorf
Western blot chamber	Mini-PROTEAN 3 Cell	BIO-RAD
IN Cell Analyzer 2200	-	GE Healthcare

Software

Software	Supplier	Version
Adobe Illustrator CC	Adobe	22.0.2
Adobe Photoshop CC	Adobe	19.1.1
Axion Navigator	Axion BioSystems	2.0.4.21
Brian2	open source	2.4.2
Genome Studio	Illumina Inc.	2.0.4
Image Lab	Bio-Rad	6.0.0 build 26
ImageJ (FIJI)	Open sourse	2.20.0-rc-72/1.53c
INCell Analyzer	GE Healthcare	6.2-15347

Software	Supplier	Version
FlowJo	BD Biosciences	10.2
Leica application suite X	Leica Microsystems	3.0.0.15697
Matlab	MathWorks	9.4.0.813654 (R2018a)
NanoDrop 2000	Thermo Fisher	1.6.198
Python	open source	2.7.16
R / RStudio	open source / R studio	3.6.1 / 1.1.447
Sholl analysis Plug-in	open source	3.2.13

External services

Service	Supplier
Sanger sequencing	Microsynth Seqlab GmbH
Amplicon sequencing	GENEWIZ, Inc.
SNP sequencing	Institute of Human Genetics, University of Bonn
Mass spectrometry	BayBioMS (Bayerisches Zentrum für Biomolekulare MassenSpektrometrie), Technical University of Munich

2.2 Experimental methods

2.2.1 Human pluripotent stem cell cultivation

Geltrex-coating solution

Component	Concentration
DMEM/F12	-
Geltrex	1:30 – 1:100

The Geltrex was thawed on ice and aliquoted in small portions. Aliquots of Geltrex were dissolved in ice-cold DMEM/F12 and used immediately. The coating takes 1 hour in room temperature or overnight at 4 °C.

DPBS-EDTA solution

Component	Concentration
DPBS	-
EDTA	0.5 mM

Stembrew medium

Component	Concentration
StemMACS iPS-Brew XF basal medium	-
StemMACS iPS-Brew XF 50x Supplement	1:50

hPSC freezing medium

Component	Concentration
Stembrew medium	90%
DMSO	10%

Human PSCs were maintained in Geltrex-coated (1:100) 6-well-plates with Stembrew medium. Full medium change was performed every day. Passaging at a ratio of 1:3 was performed when the confluency reaches ca. 80%, roughly twice per week.

To passage hPSCs, the cultures were washed with DPBS once, then immersed in DPBS-EDTA solution for 5 minutes to dissociate the colonies. After that the DPBS-EDTA was replaced with fresh Stembrew medium, vigorous pipetting was applied to resuspend the colonies. The colony suspension was then transferred to new plates.

For cryopreservation of hPSCs, ice-cold hPSC freezing medium was used for resuspension after the cultures were dissociated with DPBS-EDTA. The suspension was transferred instead into cryo tubes. Cells were then kept in Mr. Frosty™ freezing containers and frozen to -80 °C overnight, then transferred to -150 °C or liquid nitrogen for long-term preservation.

To establish hPSC cultures from cryopreserved stocks, the cryo tube was quickly put in 37 °C water bath for complete resuscitation. The cell suspension was diluted in 10 mL prewarmed Stembrew medium, centrifuged at 800 x g for 3 minutes. Then the supernatant was removed, and the cell pellet was resuspended in Stembrew supplemented with 10 µM ROCK inhibitor, and transferred to Geltrex-coated culturing plates. ROCK inhibitor was removed the second day.

2.2.2 CRISPR/Cas9 RNP nucleofection of hPSC

Genome editing on hPSC was performed according to a 4D Amaxa Cas9 protein nucleofection protocol provided by the manufacturer.

To prepare the cr::tracer RNA, 5 µL of RB1CC1E4KO crRNA and 5 µL of tracrRNA (both at 100 µM) were mixed in a PCR tube, heated in a PCR block for 5 minutes at 95 °C, and then cooled down at room temperature for 30 minutes. To prepare the cas9-cr::tracerRNA RNP, 1 µL annealed cr::tracrRNA was mixed with 1 µL cas9 and 3 µL of nuclease free duplex buffer. The mixture was then incubated at room temperature for 10 minutes.

To harvest cells for nucleofection, hPSCs of ~80% confluency were incubated in accutase supplemented with 10 µM ROCK for 10 minutes at 37°C, which dissociated the colonies to single cells. Stembrew was used to stop the reaction and resuspend the cells. After counting, calculated volume of cell suspension containing 30000 cells was transferred to a 15 mL falcon tube and centrifuged at 800 g for 4 minutes.

To prepare the electroporation solution, 16.4 µL P3 solution and 3.6 µL supplement 1 (both from the P3 Primary Cell 4D Nucleofector kit) were mixed in a microcentrifuge tube. 1 µL RNP solution was added and mixed. The electroporation solution was used to resuspend the hPSC pellet after carefully removing all remaining medium.

To perform the nucleofection, the mixture was transferred in to a nucleocuvette and loaded into the Amaxa 4D Nucleofector. The electroporation was then performed using the

program coded CM150. After the nucleofection pulse, 100 µL prewarmed Stembrew with 10 µM ROCK inhibitor was add into the microcuvette to resuspend and retrieve the cells. The cells were seeded in a Geltrex-coated 6-well-plate with Stembrew supplemented 10 µM ROCK inhibitor. ROCK inhibitor was removed after 24 hours.

To obtain single-cell derived clones, 7 days later one well of the cultures was dissociated with accutase, counted, and replated in a 6-well-plate at a density of 200 cells per well. Stembrew supplemented with 10 µM ROCK inhibitor was used until colonies formed. The cultures were then maintained for another week. Single colonies were picked with 100 µL pipettes under Evos FL microscope and transferred into 96-well-plates coated with Geltrex. Each clone was expanded onto a 24-well-plate and then onto a 6-well-plate for further use.

2.2.3 DNA extraction, PCR, and Sanger sequencing for genotyping

For each obtained single cell-derived clone, ca. 1 million cells were collected and pelleted at 5000 g for 2 min. Genome DNA was extracted with Maxwell RSC DNA Blood Kit using Maxwell RSC instrument according to the manufacturer's instructions. The DNA concentration was determined with Nanodrop 2000 spectrophotometer.

To obtain the genome sequence corresponding to RB1CC1E4KO crRNA, PCR was performed with primer pair RB1CC1_E4KO_for (5'-GGGGAAGGTTTTAGAGTGAAATT-3)' and RB1CC1_E4KO_rev (5'-GAAGGCAATGTGCACGCTCA -3') using GoTaq® DNA Polymerase according to the manufacturer's instructions.

PCR Mix

Component	Concentration
5X Reaction Buffer	20%
dNTP	0.2 mM each
Primers	1 µM each
DNA Polymerase	0.025 u/µL
template DNA	100 ng
Nuclease-Free water	add to final volume

PCR protocol

Step	Temperature	Time	Repeat
1	95 °C	2 minutes	
2	95 °C	30 seconds	
3	60 °C	30 seconds	
4	72 °C	30 seconds	go to step 2, 35 times
5	72 °C	5 minutes	
6	4 °C	hold	

PCR products were purified with a Wizard SV Gel and PCR Clean-up System according to the manufacturer's instructions and the concentration was determined with Nanodrop.

Sanger sequencing was performed by Microsynth Seqlab. The results were analyzed using online genome editing assessment tool TIDE (https://tide.nki.nl/). Samples with frameshift mutation on both alleles with high confidence were kept for further analysis.

Amplicon sequencing was performed on selected clones by GENEWIZ, Inc. The results were analyzed using the online tool Outknocker (http://www.outknocker.org/). Samples with high purity were used for further experiments.

Genome DNA from selected clones was sent to the Institute of Human Genetics, University of Bonn, to perform chip-based SNP analysis for karyotyping. The results were analyzed using Genome studio.

2.2.4 Immunofluorescence

HPSCs cultivated in 96-well-plates were expanded to ca. 50% confluency for immunofluorescence analysis. The medium was then removed and replaced with 4% PFA, incubated for 12 minutes, and replaced with DPBS. To block the cultures, DPBS was replaced with the blocking solution (90% DPBS + 10% FBS, supplemented with 0.1% triton) and incubated for 1 hour at room temperature. The solution was then replaced with the blocking solution containing primary antibodies and then incubated overnight at 4 °C. Afterwards, the cultures were washed with DPBS three times, 5 minutes each time, and incubated in the blocking solution containing secondary antibodies at room temperature for 1 hour. The solution was replaced with 1 µg/ml DAPI dissolved in DPBS for 3 minutes and after that washed with DPBS once. Immunofluorescence pictures were taken with INCELL Analyzer 2200 and analyzed with ImageJ.

2.2.5 Flow cytometry

To assess the expression of TRA-1-60 in hPSCs with flow cytometry, 80% confluent hPSCs were dissociated with accutase and harvested as previously described. The cell suspension was centrifuged at 800 g for 3 minutes and resuspended in ice-cold DPBS. Anti-Tra-1-60 antibody (1:1500) was then added into cell suspension and incubated on ice for 15 minutes. The cell suspension was centrifuged again and resuspended in DPBS containing secondary antibody (Alexa 488 goat anti-mouse IgM, 1:1500), then incubated at 4 °C for 30 minutes. After the final centrifugation, pellets were resuspended in DPBS and transferred into separate FACS-tubes. Flow cytometry was then performed in BD Accuri C6 Plus and the results were analyzed using FlowJo.

2.2.6 Protein extraction and western blot

Western transfer buffer (10x)

Component	Concentration
Tris-Base	0.25M
Glycine	1.92M
For 1x Western transfer buffer: dilute in ddH2O and add 10% [v/v] methanol.	

TBS-buffer (10x)

Component	Concentration
Tris-Base	0.25M (pH7.4)
NaCl	1.5M
For 1x TBST-buffer: dilute in ddH2O, then add 1:1000 Tween-20.	

Cultures were washed with ice-cold DPBS once before being scratched off in cold DPBS and centrifuged to obtain cell pellets, which were then resuspended in cold RIPA buffer supplemented with 1:100 HALT protease and phosphatase inhibitor. The suspensions were then placed on ice for 30 minutes while being vortexed every 5 minutes for lysis. The solution was then centrifuged at 16100 g in 4 °C for 30 minutes. After centrifugation, the supernatant was collected, and the protein concentration was measured with Pierce BCA Protein Assay kit according to the manufacturer's instructions using Nanodrop.

30 µg protein samples were loaded with LDS Sample Buffer into a 10% Bis-Tris gel for electrophoresis and transferred onto a methanol-activated PVDF membrane with electroblotting. The membrane was then blocked in TBS-T buffer containing 5% milk

powder for 1h at room temperature before being rotated in primary antibodies dissolved in the blocking solution overnight at 4 °C. The membranes were then washed 3 times with TBS-T buffer and rotated in HRP-conjugated secondary antibodies dissolved in blocking solution for 1 h at room temperature. Luminata™ Western HRP Substrates were used for chemiluminescent in a Chemidoc XRS detection system. Quantification of relative protein levels was performed with the Image Lab software.

2.2.7 Forward programming of iGlutN and iGABAN

Neural induction (N2) medium

Component	Concentration
DMEM/F12	-
N2 supplement	1:100
Doxycycline	2 µg/mL

Neural maintenance (NBB27) medium

Component	Concentration
Neural Basal medium	-
B27 supplement	1:50
Component	Concentration
GlutaMAX	1:100
Doxycycline	1-2 µg/mL
BDNF	10 ng/mL

Neural cryopreservation medium

Component	Concentration
Knockout serum replacement	70%
1M trehalose	20%
DMSO	10%

HPSCs carrying doxycycline-inducible NGN2 or ASCL1/DLX2 cassette were established as previously reported by Dr. Matthias Hebisch (Peitz et al., 2020). To produce iGlutN and iGABAN, 80% confluent hPSCs were dissociated with accutase and seeded on Geltrex-coated six-well plates at a density of 7500 cells/cm^2 in the hPSC medium. One day after seeding, the medium was switched to N2 medium (DMEM/F12, 1% N2 supplement) supplemented with 2 mg/mL doxycycline to induce NGN2 or ASCL1/DLX2 expression. On day 2, the cells were dissociated with accutase and plated on Geltrex-coated 6-well-plates

at a density of 50000 cells/cm^2. The medium was switched to NBB27 medium supplemented with doxycycline. From day 3 on, 10 mM DAPT was added to the medium. A full medium change was performed every two days. To exclude remaining proliferative cells, 5 mM AraC (Cytosine β-D-arabinofuranoside hydrochloride) was added on day 7 and removed on day 8.

On day 9, the medium was removed, and the cultures were washed with DPBS once and then incubated in accutase supplemented with 10 µM ROCK inhibitor at 37 °C for 60 minutes. Gentle shaking or taping was applied when necessary to fully dissociate the cultures. Fresh medium was then applied to stop the reaction. The suspension was collected and centrifuged at 1200 g for 3 minutes, after which the supernatant was discarded. The pellet was then resuspended in ice-cold freezing medium, aliquoted in vials of 2 million cells, and cryopreserved. Resuscitation of forward-programmed human neurons from cryopreserved stocks was similar to that of hPSCs.

2.2.8 Cultivation of hPSC derived neuronal cultures

For morphological analysis, iGlutNs were seeded on inactivated confluent mouse astrocytes in Geltrex-coated ibidi 96-well-plate with a density of 50000 per well. For western blot, iGlutNs were seeded in Geltrex-coated 6-well-plate, 1 million per well, and cultured with astrocyte-conditioned NBB27 medium supplemented with 1 mg/ml doxycycline. A half medium change was performed twice per week.

For the MEA recording, 24-well plates with MEAs (M384-tMEA-24W, Axion BioSystems, Atlanta, USA) were coated with Geltrex (1:30). 30000 or 15000 forward programmed neurons were then seeded in each well, resulting a density of ~1000/mm^2 or ~500/mm^2. Mouse astrocytes were added the day following seeding of neurons to reach a final density of 1000/mm^2. Neuronal medium supplemented with 0.5% FBS was used for astro-neuronal co-cultures. Half of the medium was changed twice per week.

The MEAs plates were reused after cleaning with 1% Tergazyme overnight at 37 °C, sterilization with 75% ethanol at room temperature for 1 hour and ultraviolet treatment for 1 hour.

2.2.9 Preparation of fluorescence labeling plasmids

LB medium

Component	Concentration
H_2O	-
Tryptone	10 g/L
Yeast extract	5 g/L
NaCl	5 g/L

LB Agar

Component	Concentration
H_2O	-
Tryptone	10 g/L
Yeast extract	5 g/L
NaCl	5 g/L
Agar	10 g/L
Autoclaved and stored at 4°C.	

Two plasmids were used for fluorescence labeling of neurons and live-cell imaging. The autophagy reporter plasmid, mRFP-GFP tandem fluorescent-tagged LC3 (ptfLC3), was a gift kindly provided by Tamotsu Yoshimori (Addgene plasmid#21074; http://n2t.net/addgene:21074; RRID: Addgene_21074) (Kimura et al., 2007). To label individual neurons in dense cultures, a Doublecortin (DCX)::humanized renilla reniformis green fluorescent protein (hrGFP) reporter cassette was amplified from a lentiviral construct that has been utilized to monitor DCX activity in hPSC-derived neurons (Ladewig et al., 2008). The introduction of SfiI restriction sites enabled cloning of the DCX::hrGFP cassette into a small backbone to optimize the transient transfection of single neurons. The construction was provided by Mohamad Hajo and Nils Braun.

To amplify the plasmids, NEB stable competent E.coli was used for the transformation according to the supplier's instruction. After resuscitation on ice, 50 µL cells were gently mixed with 5 ng DNA and incubated on ice for 30 minutes. The mixture was then heated at 42 °C for 30 seconds before 950 µL LB medium was added and mixed. 100 µL of suspension was spread on LB agar plates containing kanamycin or ampicillin. The plates were incubated overnight at 37 °C. Single colonies formed on the plates were picked and transferred to 15 mL falcon tubes containing 5 mL LB medium with kanamycin or ampicillin

and shaken at 37 °C. 6 hours later, 10 µL of the culture was transferred into a 250 mL flask containing 80 mL LB medium with kanamycin or ampicillin, shaken at 37 °C overnight. Plasmids were then purified from bacteria via the Maxi preparation kits according to the manufacturer's instructions. The concentration was determined with Nanodrop.

2.2.10 Live fluorescence labeling and imaging of forward programmed neurons

The plasmid transfection was performed two weeks after iGlutNs had been seeded on mouse astrocytes. For each well in a 96-well-plate, 100 ng plasmid and 0.3 µL Fugene reagent (Promega GmbH, Walldorf, Germany) were mixed in 10 µL NBB27 medium and incubated at room temperature for 10 minutes before being added into the wells. The plate was gently titled for 30 seconds to evenly distribute the plasmids. A medium change was performed on the second day.

Live fluorescence imaging was performed with a Leica live cell imaging system (Leica Microsystems GmbH, Wetzlar, Germany) 7-10 days after the plasmid transfection. The plate was kept in a chamber with a temperature at 37°C and CO_2 at 5%. For neurite complexity profiling (i.e., the Sholl analysis), pictures of individual neurons were taken with 20x magnification. Sholl analysis was performed using the Sholl Analysis plug-in in ImageJ (Ferreira et al., 2014). For the quantification of axonal outgrowth and axonal pathology assessment, pictures of individual axons were taken with 40x magnification. Axonal swellings were counted manually. To assess the autophagy reporter, pictures of individual neurons were taken with 40x magnification.

2.2.11 Micro-electrode array recording and stimulation

The MaestroEDGE system (Axion BioSystems) was used for signal recording and stimulation of MEA plates. The plate was loaded into a chamber with the temperature maintained at 37°C and CO_2 at 5%. Raw data was recorded with a sampling rate of 12.5 kHz and a bandpass filter set between 0.1-2000 Hz. Online spike detection was performed with a threshold of 6 times standard deviations. Spike data containing the timestamp and waveform of each spike was saved. For spontaneous activity recording, the plate was first loaded and equilibrated for 20-30 mins and then recorded for 10 mins. For pharmacological experiments, the compounds were added at a ratio of 1:20 to reach the working concentration. After recording under drug application, the cultures were washed with fresh medium 3 times and recorded again after 20-30 min equilibration.

To electrically stimulate the cultures, biphasic voltage pulses predefined in the software (Neural Stimulation, amplitude = 100 mV, duration = 400 µs) were delivered to the target electrodes. Repetitive stimulation patterns were defined offline and delivered upon a single trigger during the recording.

2.2.12 MEA data analysis

Recorded data was processed with the Navigator software (Axion BioSystems) and customized scripts in MATLAB (The MathWorks Inc., R2018b). Spike sorting was performed using the algorithm reported in (Quiroga et al., 2004). The algorithm performs fully automatic and unsupervised spike sorting using a superparamagnetic clustering method. Network burst detection was performed using an algorithm reported in (Bakkum et al., 2014). A single-channel burst is marked if 5 spikes occurred in less than 100 ms, and a network burst is marked when 50% of all channels showed burst activity. A network super-burst was defined when a second network burst occurred less than 1000 ms after a preceding network burst.

2.2.13 Membrane protein biotinylation and mass spectrometry

Astro-neuronal cocultures were washed three times with ice-cold PBS and biotinylated with 1 mg/ml sulfo-NHS-SS-biotin in cold PBS for 45 min. After washing three times with cold PBS and then 10 min incubation , cultures were washed 3 times with cold quench buffer (125 mM NaCl, 2.5 mM KCl, 1.2 mM NaH_2PO_4, 1.2 mM $MgCl_2$, 2.4 mM $CaCl_2$, 26 mM $NaHCO_3$, 11 mM glucose, and 100 mM glycine) and then incubated two times for 25 min. Cultures were washed again with cold PBS and lysed in ice-cold RIPA buffer supplemented with HALT protease and phosphatase inhibitors for 30 min on ice while vortexing every 5 minutes. Following a centrifugation step with 18,000 x g for 15 min at 4 °C the supernatant was used for streptavidin precipitation employing magnetic streptavidin beads. Beads were equilibrated in RIPA buffer three times and added to the lysates. Binding was performed by rotating the tubes (Protein LoBind Tubes 1.5 mL, Eppendorf) on microcentrifuge tube rotator at 10 rpm overnight at 4 °C. Beads were then washed with RIPA buffer three times and the final pellet was subjected to mass spectrometry. Identified proteins were quantified across samples using the label-free quantification algorithm in MaxQuant as label-free quantification (LFQ) intensities.

LFQ intensities of each mapped protein were first normalized by subtracting the median intensity, then compared between genotypes with Student's t-test and corrected with the false discovery rate (FDR) method. T-values from the t-test of each protein were also used for a gene set enrichment analysis (GSEA) using WebGestalt 2019 (Liao et al., 2019). The GSEA was performed using enrichment category 'geneontology Biological Process noRedundant' and the significance level was set to FDR < 0.05.

2.2.14 Statistical analysis and data fitting

Statistical analysis was performed using MATLAB. N-way analysis of variance was used in experiments with nested and repetitive designs, and paired comparisons were corrected using the Tukey-Kramer method. Linear regression was performed using the 'fitlm' function in MATLAB. Custom equation fitting was performed using the nonlinear least squares method provided in the Curve Fitting Toolbox of MATLAB.

2.2.15 Computational simulation of neuronal networks

Computational neuronal network simulation was implemented with Brian2 (Stimberg et al., 2019). An exponential leaky integrate-and-fire neuronal model with conductance-based synaptic mechanism and short-term depression (STD) was used as the basic model, which is defined as:

$$T_m \frac{dv}{dt} = -(v - V_{rest}) + w_e g_e (E_e - v) + w_i g_i (E_i - v) + D_T e^{\left(\frac{v - V_{th}}{D_T}\right)} + \xi(t) \qquad \text{(eq. 2-1)}$$

where T_m is the membrane time constant, v is the membrane potential, V_{rest} is the resting membrane potential. w_e and w_i are adjusting factors of the weight of synaptic input. g_e denotes the conductance of glutamate receptor-coupled sodium channel and has a form of:

$$\frac{dg_e}{dt} = -\frac{g_e}{\tau_e} + w_s \delta\left(t - t_{pre-spk}\right) \qquad \text{(eq. 2-2)}$$

where g_e increases upon each excitatory presynaptic spike at $t_{pre-spk}$ and decays with a time constant τ_e. E_e is sodium equilibrium potential, g_i denotes the conductance of GABA receptor-coupled channels and has a form of:

$$\frac{dg_i}{dt} = -\frac{g_i}{\tau_i} + w_s\delta\left(t - t_{pre-spk}\right) \quad \text{(eq. 2-3)}$$

where, likewise, g_i increases upon each inhibitory presynaptic spike at $t_{pre\text{-}spk}$, and decays with a time constant τ_i. E_i is chloride equilibrium potential. D_T and V_{th} define the exponential threshold. Spikes are defined as $v >= V_{th}+10$ mV, after which v would be reset to V_{reset}. $\xi(t)$ is the thermal noise and has a standard deviation of 0.5 mV. For the basic synapse, the presynaptic neuron has a readily release pool (RRP) of which the level L_{RRP} is in the form:

$$\frac{dL_{RRP}}{dt} = \frac{(1 - L_{RRP})}{\tau_{RRP}} - L_{RRP}P_r\delta(t - t_{spk}) \quad \text{(eq. 2-4)}$$

Where τ_{RRP} is the RRP replenishment time constant, P_r is the releasing probability. On the postsynaptic part, L_{RRP} will directly be w_s in eq. 2-2 and eq. 2-3.

To construct a network, 1000 neurons as described above were connected randomly with a probability of 0.01. Most single neuronal parameters in the models were obtained experimentally with the same cell lines in an autaptic system (Rhee et al., 2019a). These are virtual point processes without morphological or spatial parameters which are randomly and uniformly connected by only one virtual synapse between each pair. The strength and probability of synaptic connections between neurons are unknown and would be simulated recursively. The basal synaptic strength was set to elicit 10mV excitatory or inhibitory postsynaptic potential on a resting postsynaptic target. Such settings do not produce spontaneous activity; therefore, for the beginning, an external stimulator was implemented to evoke the network. Simulated pulse stimulation was realized by depolarizing targeted neurons by 20 mV. Timestamps of the spikes from 10% of the neurons of the network, which were randomly selected, were recorded and then processed using the same script for *in vitro* data. When necessary, other continuous neuronal state parameters were saved at a time step of 1 ms.

Table 2-1 Parameters used in computational models (Exp. = experimentally derived)

Symbol	Value	Source
T_m	38.5 ms	Exp.
V_{rest}	-50 mV	Exp.
w_e	3	
w_i	3	
E_e	0 mV	
E_i	-70 mV	
V_{th}	-25 mV	Exp.
τ_e	5 ms	
τ_i	5 ms	
τ_{RRP}	1500 ms	Exp.
P_r	0.25	Exp.
V_{reset}	-65 mV	

3. Results

3.1 A defined human-specific platform for modeling neuronal networks

Our group and collaborators have previously characterized the morphology and function of forward programmed human neurons at a single-cell level with an autaptic system, including dendrite structure, synapse number, membrane properties, synaptic transmission, and short-term plasticity (Rhee et al., 2019a). Based on these works, section 3.1 of this thesis describes the systematic characterization of network properties of developing forward programmed neuronal cultures derived from hPSCs. For this, forward programmed glutamatergic and GABAergic neurons were cultured on MEAs at different ratios and densities. Spontaneous and electrically evoked electrophysiological activities were recorded during the network development (Figure 3-1-1). In parallel, computational models were developed to recapitulate experimental observations and to obtain possible biological explanations of observed the phenomena.

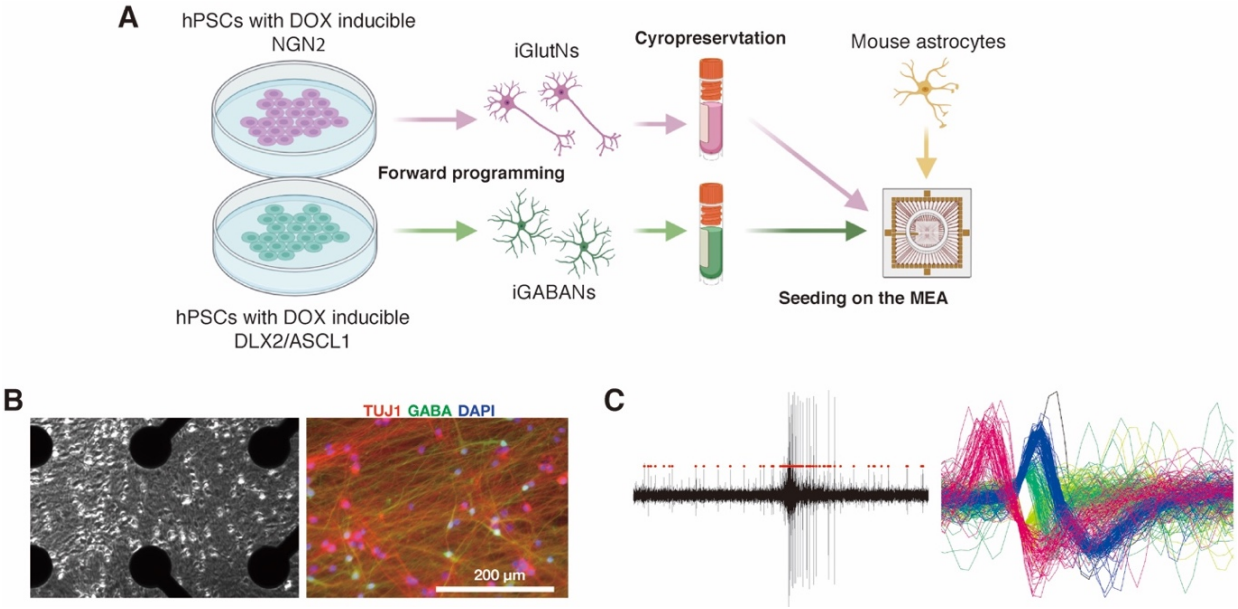

Figure 3-1-1 Schematic illustration of the experimental procedure and example results. (A) Schematic of the experimental procedure. (B) Left, an example live image of a 4-week-old forward programmed human neuronal culture, 1000/mm^2, 75% iGlutNs and 25% iGABANs. Right, immunofluorescent image of a human neuronal culture cultivated in parallel in a separate plate (sister plate) after 5 weeks, 1000/mm^2, 75% iGlutN and 25% iGABANs. (C) Left, 5s example recording from one electrode containing a burst event, detected spikes are indicated by red dots. Right, example results of spike sorting from one electrode, spikes were classified into 4 sources represented by different colors.

3.1.1 Functional characterization of developing forward-programmed human neuronal networks

Human cortical neurons forward programmed from hPSCs were seeded with two density conditions (500/mm^2 and 1000/mm^2) and at four different excitatory to inhibitory ratios (E/I ratio = 4:0, 3:1,1:3 and 0:4) in a 24-well plate with microelectrode arrays. During the first two weeks in culture, sparse single spikes emerged and then developed into synchronized network activity. On day 7 after seeding, all cultures showed spontaneous spikes, indicating a subpopulation of the culture had functionally matured. On day 10, synchronized activities could be observed, indicating the formation of functional synapses. On day 14, many cultures started to show synchronized network bursts (NBs) (Figure 3-1-2, A). Overall, the total frequency of spikes increased steadily during the first 6 weeks (multivariate linear regression, p<0.001), while seeding density had no statistically significant effect (p = 0.3221), increased levels of inhibitory neurons in the networks were found to lead to lower activity (p<0.001, Figure 3-1-2, B). Except for the 100% iGABAN cultures, synchronized NBs could be observed in all networks after 3 weeks with the number of NBs increasing along with maturation (p<0.001). And the average number of spikes per NB proved to be a distinctive parameter, i.e., denser, more excitatory, and more mature networks showed a higher number of spikes per NB (all p<0.001; Figure 3-1-2, C).

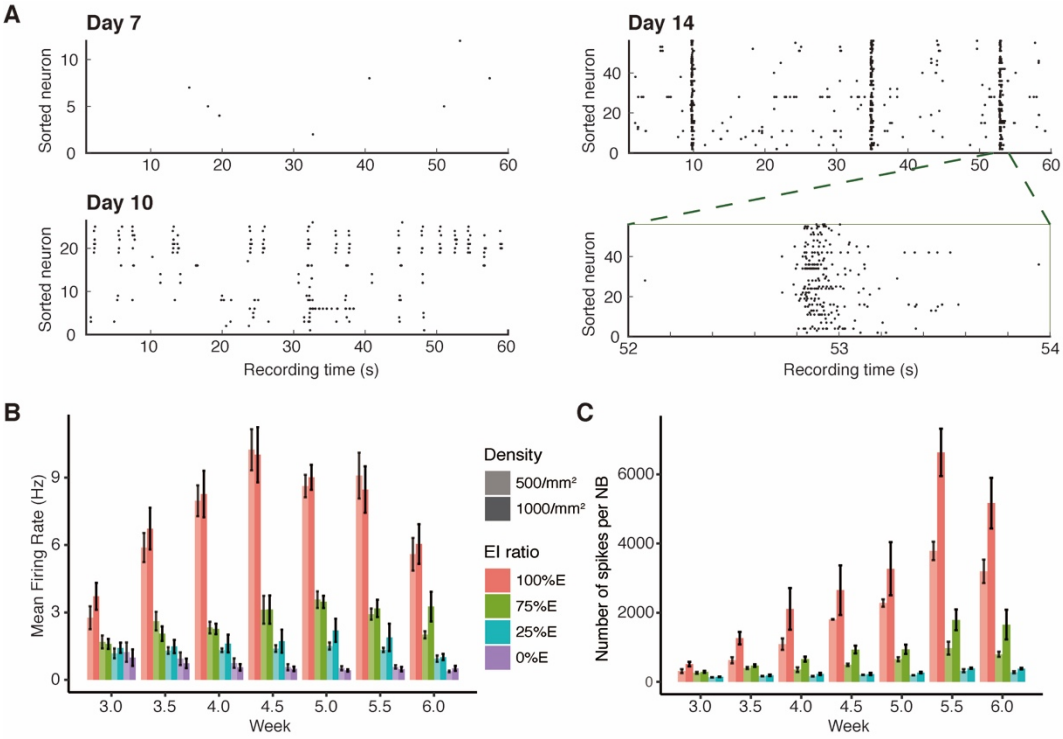

Figure 3-1-2 Functional characterization of forward programmed human neuronal cultures. (A) Example raster plot of human neuronal network activities during the first two weeks of development, the enlarged panel shows a synchronized network burst. The change of mean firing rate (B) and the number of spikes per NB (C) in different cultures during the first 6 weeks after seeding are shown. For each condition, data were collected from 6 cultures in 2 independent experiments.

At week 5, the composition of these cultures were assessed by immunofluorescence and modulation of synaptic transmissions. NeuN positive and GABA positive cells were counted in immunofluorescence pictures of the sister cultures of each condition, which gave an estimation of the survival rate and E-I ratios (Table 3-1). Although the survival rate of seeded neurons varied up to this point, E-I ratios remained close to the intended levels .

Table 3-1 Estimated neuronal density and E-I ratios of human forward programmed neuronal cultures at 5 weeks by immunofluorescence assessment of NeuN and GABA.

		Seeding E-I ratio (%E)			
		100%	75%	25%	0%
Seeding density (mm^{-2})	1000	160(98%)	319(67%)	540(34%)	710(3%)
	500	69(99%)	195(79%)	238(32%)	347(8%)

Application of 10 μM 6-cyano-7-nitroquinoxaline-2,3-dione (CNQX), an AMPA and kainate receptor antagonist, eliminated synchronized NBs, reducing the overall spike frequency in cultures containing iGlutNs while producing no significant difference in 100% iGABAN cultures (Figure 3-1-3, A&B). This confirmed the existence of functional glutamatergic synapses and their major roles in the formation of synchronized NBs. Application of 10 μM bicuculline, a GABA-A receptor antagonist, increased activity in all but the 100% iGlutN cultures. The number of spikes per NB also increased significantly after bicuculline application, with the 25% iGlutN networks showing significantly higher elevation than the 75% iGlutN networks (Figure 3-1-3, C&D). These findings are in line with the aforementioned observations of spontaneous activities, i.e., higher portion of iGABANs in the culture was associated with weaker NBs. Overall, these results suggest the existence of functional GABAergic synapses in the present cultures and that GABA has a modulatory effect on neural network activities.

In short, section 3.1.1 preliminarily depicts the functional characterization of developing forward-programmed human neuronal networks.

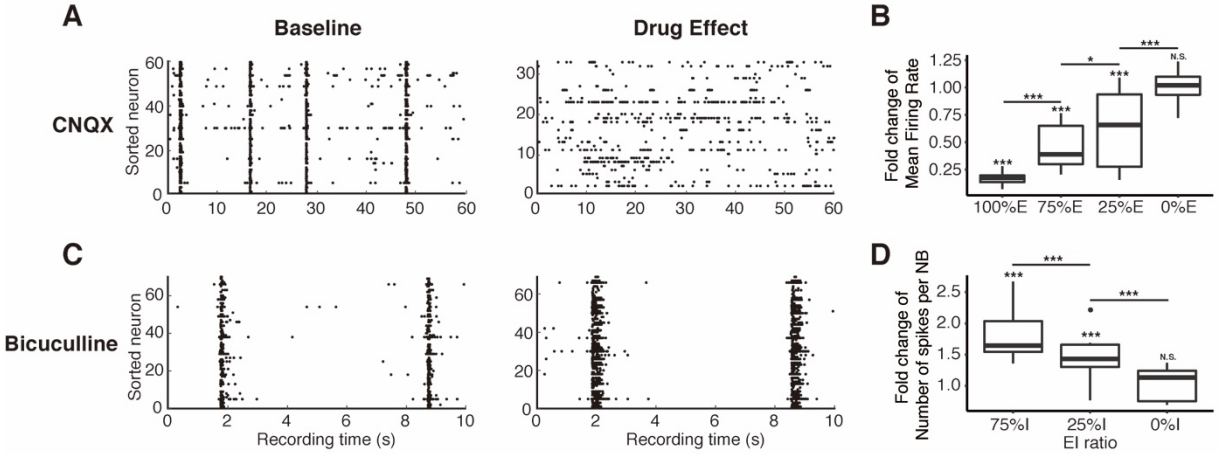

Figure 3-1-2 Synaptic modulation of forward programmed human neuronal networks. (A) Example raster plots showing the elimination of NBs by CNQX in one culture containing 75% iGlutN. (B) The fold change of overall firing rate comparing to the baseline after CNQX application. (C) Example raster plots showing the change of NB strength after the application of bicuculline in one culture containing 25% iGlutNs. (D) The fold change of the number of spikes per NB compared to the baseline after bicuculline application. Data were collected from 6 cultures of each condition from 2 independent experiments. N.S. not significant, * p<0.05, ** p<0.01, *** p<0.001.

3.1.2 Theoretical framework and computational simulation of *in vitro* human forward programmed neuronal networks

Forward programmed neurons *in vitro* can develop a substantial amount of synapses within two weeks in culture, leading to synchronized spikes and even NB activity which are hall markers of *in vitro* cortical neuronal cultures (Ito et al., 2010b; Odawara et al., 2016). It is believed NBs are initiated by the coincidental firing of several individual spontaneously active neurons. Within an excitatory neuronal network of sufficient synaptic connections, this coincidence is able to activate a larger group of neurons than the starting population, leading to an exponential increase of activated neurons and the overall firing rate. Within tens of milliseconds, virtually all neurons in the network would be activated, resulting in the peak of the burst. Afterwards, the neurons continue to recurrently activate each other, which quickly depletes presynaptic neural transmitter vesicles (i.e., the RRP) and thus attenuates excitatory post-synaptic potential (EPSP). Decreased EPSP means gradually fewer neurons can be activated and, as a result, the overall firing rate drops.

The final termination point comes when the average RRP level reaches a baseline where no additional neurons can be activated via synapses (Loebel and Tsodyks, 2002). The RRP takes some time to recover, which can be characterized by, in its simplest form, an exponential process (eq. 2-4, Wesseling and Lo, 2002). Due to the stochastic nature of NB initiation, the frequency of spontaneous NBs does not reflect the full bursting capacity of a network. Therefore, the frequency or interval of NBs is not a reliable indicator of neuronal network activities. The following discussions are mainly focused on the properties of single NBs.

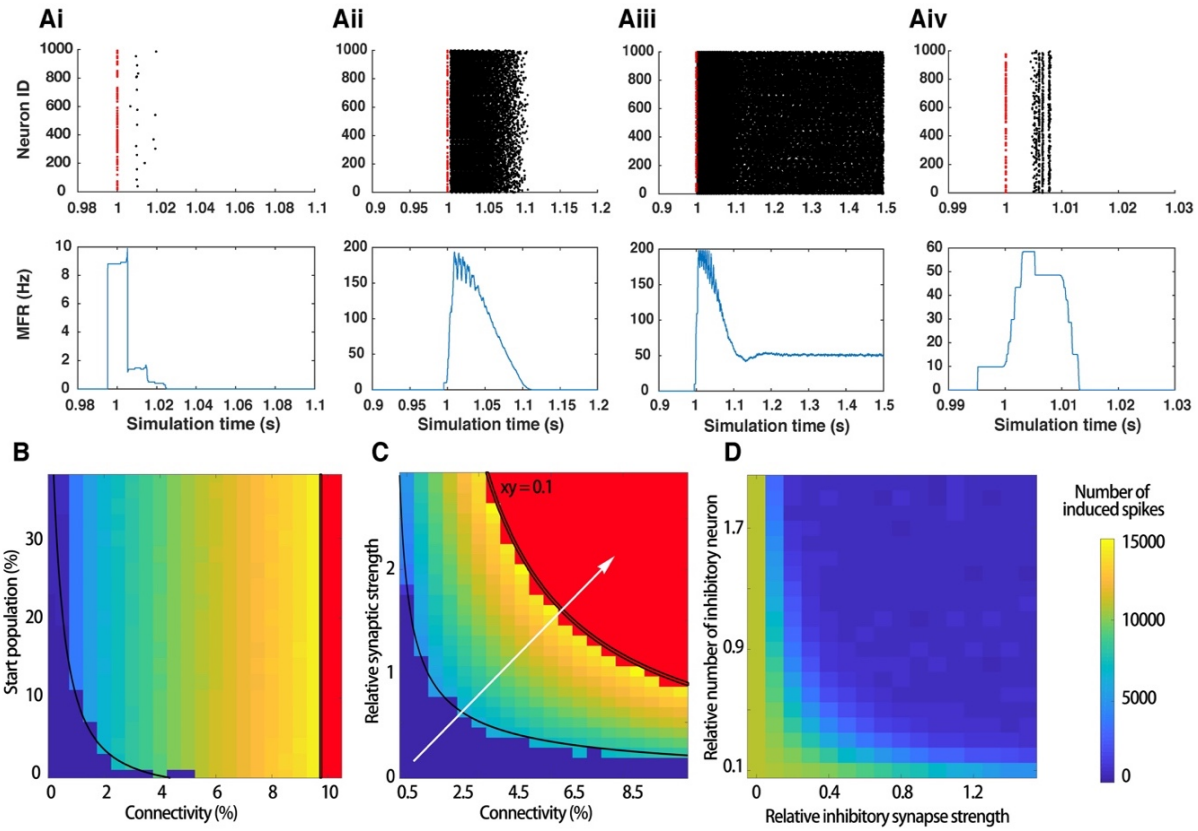

Figure 3-1-4 *In silico* simulation of NB generation in human neuronal cultures. (A) Example raster plot of induced network activities by external stimulation (red dots). i. failed network burst; ii. Successful network burst; iii. Sustained network burst; iv. Network burst in a mixed network, E/I cell number ratio = 1:1.5, E/I synapse strength ratio 1:1.5. (B) Network burst criteria and strength in relation to connectivity and start population in pure excitatory networks. The black curve marks the estimated boundary between failed and successful network bursts (Ai and Aii), and the red-colored area shows when a sustained burst occurs (Aiii). (C) Network burst criteria and strength in relation to connectivity and synaptic strength in pure excitatory networks with start population at 10%. The white arrowed line indicates the presumed network development route *in vitro*. (D) Network burst strength in relation to the number and synaptic strength of inhibitory neurons.

To illustrate the criteria for a network burst, a computational model was established. In a simulated pure excitatory neuronal network, with relatively low connectivity, artificial activation of a certain group of neurons can only activate a smaller population of downstream neurons, meaning exponential amplification or network bursts cannot be induced (Figure 3-1-4, Ai). When the network connectivity is increased, the activation of the same group can elicit a network burst (Figure 3-1-4, Aii). Additionally, the minimum starting population for NB depends on the connectivity. With the specified setting in Figure 3-1-4, for example, connectivity below 0.5% would effectively prevent any NBs, while increasing connectivity to over 5% requires only 1% of neurons to be activated for an NB (Figure 3-1-4, B). Note that once a NB can be initiated, the total number of spikes that can be induced, or the strength of NB, is only dependent on the connectivity and is independent of the starting population. If the connectivity continues to increase (above 10% here), there will be sustained network activation, i.e. an unstoppable network burst (Figure 3-1-4, Aiii). This is presumably due to the equilibrium between synaptic release and replenishment of the RRP. The biological significance of this scenario is to be discussed in the next section. Using the same starting population, relatively lower connectivity will be needed for a NB when the synaptic strength is increased (Figure 3-1-4, C). Both factors can affect the burst strength. Note, the threshold curve for sustained NB follows an inverse proportional function. Compared with experimental data, it is assumed that during network development the increasing number of synapses both strengthens the existing connections and creates new connections between neurons, which are respectively represented by synaptic strength and connectivity in this model.

One intriguing observation in the experiment was that the presence of an apparently overwhelming number of inhibitory neurons was unable to prevent NBs from occurring, although the strength of NBs was reduced significantly. This finding can also be partially seen in the computational simulation (Figure 3-1-4, Aiv and D). here, while increasing the number and synaptic strength of inhibitory neurons can reduce the elicited network activities, a relatively small but well-characterized NB can still be induced in very inhibitory networks.

In order to make the *in silico* model more realistic and recreate the spontaneous activity observed in their *in vitro* counterparts, a background Poisson input was implemented. By

introducing this, these models were able to spontaneously produce NBs and respond to simulated synaptic modulators in a similar way as *in vitro* (Figure 3-1-5).

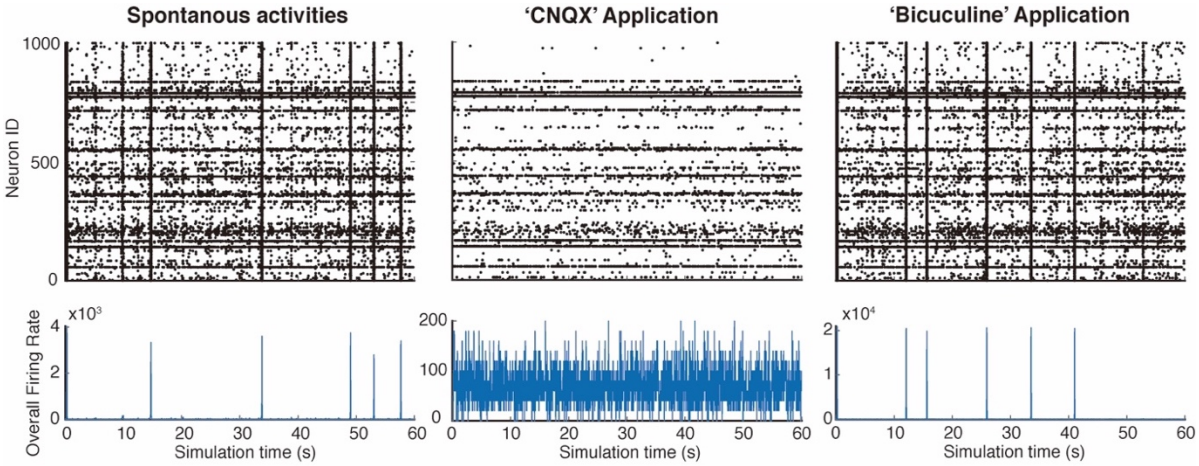

Figure 3-1-5 *In silico* simulation of spontaneously active human neuronal networks. Example activities of a simulated neural network containing 1000 neurons, of which 80% are glutamatergic.

To sum section 3.1.2 up, a preliminary *in silico* model of forward programmed human neuronal culture was established, which could recapitulate key *in vitro* observations shown in section 3.1.1. Furthermore, this simulation work supports the following assumptions regarding the formation of NBs: (1) the occurrence of a NB is due to the activation of a small group of spontaneously firing neurons, although the minimum starting population is dependent on the connectivity strength; (2) network connectivity, synaptic strength, and the presence of inhibitory elements determine the strength of NBs; (3) termination of NBs is dependent on the imbalance of fast depletion and slow replenishment of the RRP.

3.2 Sporadic response of the cultured human neuronal network to repetitive stimulation due to local circuit depletion

As NBs represent a hallmark of cultured neuronal networks (le Feber, 2019), further exploration of the networks focused on the properties of NBs in particular. Because neural networks are nonlinear systems with chaotic properties and short/long-term plasticity, the characteristics of NBs can vary. Additionally, due to being a continuous system, the current network state is dependent on previous activity. This principally violates the statistical rule of independent sampling. Therefore, in order to test whether the networks could be reset and subsequently produce relatively more homogenous output, local electric pulse stimulations were delivered via 1 of the 16 electrodes to the cultures. With sufficient interval (>5 s, i.e., <2 Hz), pulse stimulations were able to elicit robust homogeneous NBs in all cultures (Figure 3-2-1, A).

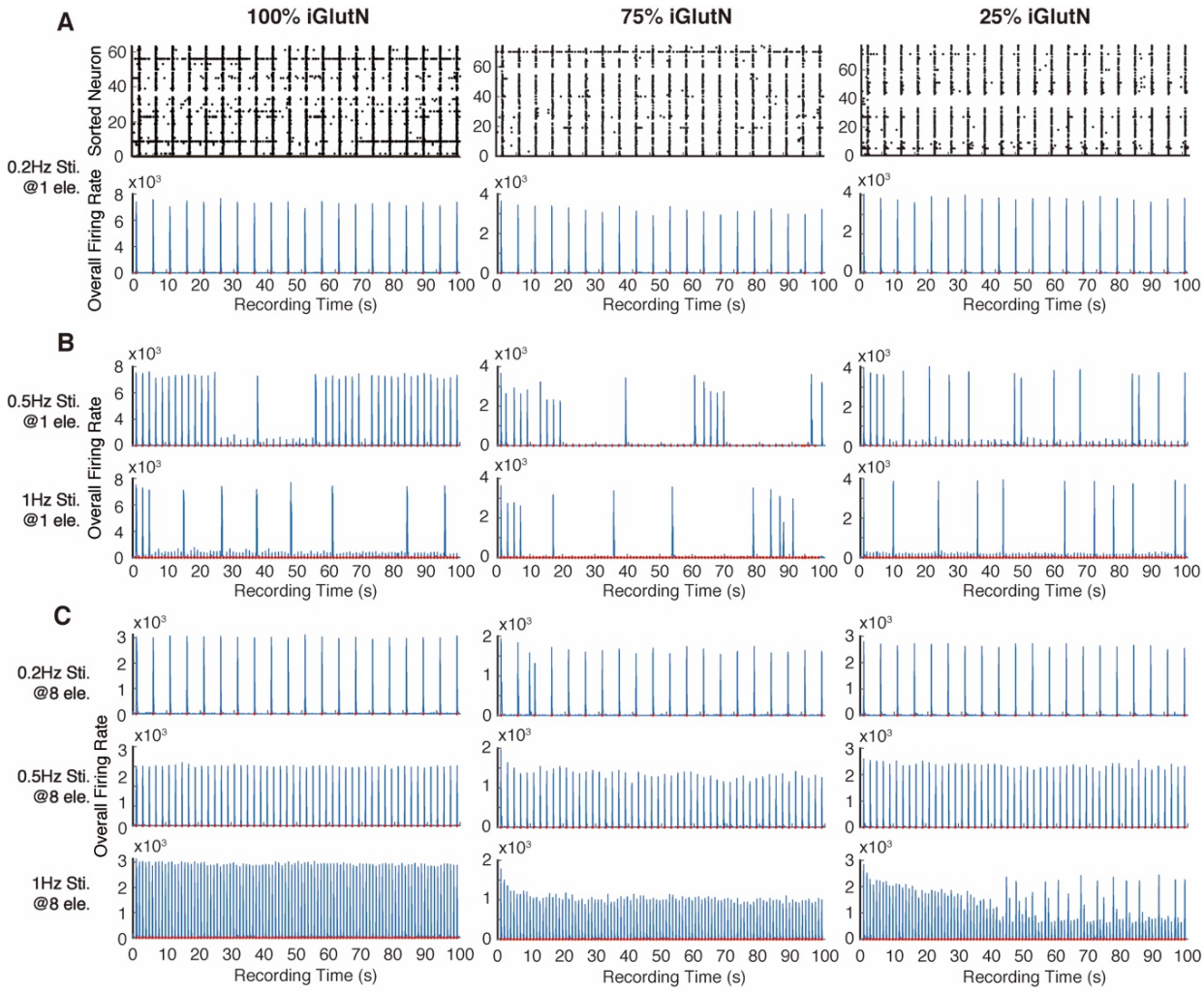

Figure 3-2-1 Network response of neuronal cultures to electrical stimulation *in vitro*. (A) Example of NBs elicited by low-frequency local pulse stimulations in cultures containing iGlutNs. Red dots indicate the onset of pulse stimulations. (B) Corresponding to A, local stimulations at higher frequency lead to sporadic NBs in the same cultures. (C) Network response to multi-site electrical stimulation. Multi-site stimulation at higher frequency elicited more robust network responses, although note that cultures containing 25% iGlutNs show inhomogeneous patterns.

Next, it was to observe how a fatigue network would respond to an external drive. It was reasoned that stimulations with shorter intervals would limit the level of RRP recovery, causing the network response to be weakened. Therefore, stimulations of higher frequency (>1 Hz) were applied to the cultures. Unexpectedly, most cultures displayed non-homogeneous responses to each stimulation. The networks burst only sporadically following stimulations (Figure 3-2-1, B). Furthermore, e.g., 2Hz stimulations elicited less NBs than 0.2 Hz stimulation within the same period of time. Interestingly, when 50% (8 out of 16) of available electrodes were stimulated, the network again responded robustly to the stimulations (Figure 3-2-1, C).

A possible explanation of this phenomenon is that local stimulation to a fatigue network could activate targeted neurons and induce the release of neural transmitters. Because the level of the RRP in a fatigue neuron was too low, however, few downstream neurons could subsequently be activated via the stimulation targets. Therefore, the rest of the network was not affected by the simulation. The following stimuli lead to a similar effect, i.e., keeping the targeted neuron fatigue, yet the majority of the network untouched. It is considered that local circuits which were directly stimulated were functionally paralyzed and isolated from the rest of the network and thus could not be used to control the whole network. The rest of the network could then replenish the RRP without interruption. At a certain point, a relatively small disturbance by the external stimulation would again elicit an NB. To test this hypothesis, *in silico* neuronal networks were administrated similar patterns of stimulation during which the RRP level of each neuron was recorded. Simulated low-frequency local stimulations could also elicit NBs, and high-frequency stimulations also elicited sporadic responses in computational models (Figure 3-2-2, A). It was shown that high-frequency local stimulations continuously depleted targeted local circuits, yet the majority of the remaining network could only be affected during NBs

(Figure 3-2-2, B). When a higher proportion (10%) of the network is stimulated, the networks show robust NBs (Figure 3-2-2, A) and the majority of neurons were depleted following each stimulation (Figure 3-2-2, B).

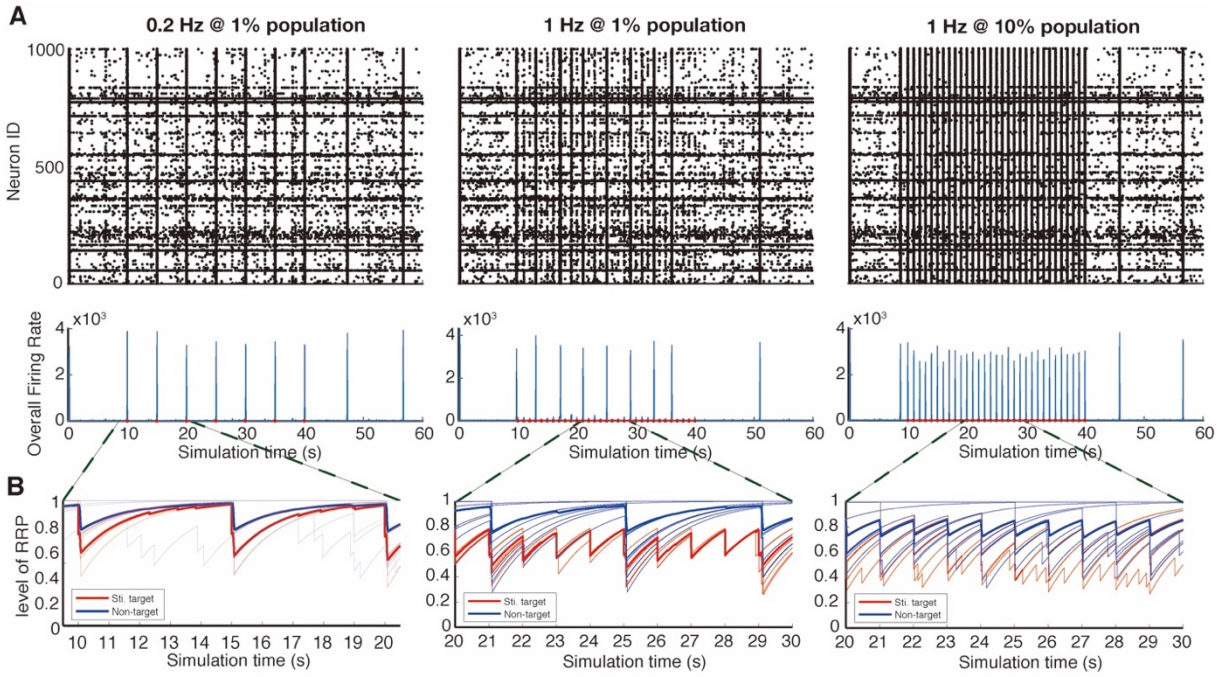

Figure 3-2-2 Simulated network response to electrical stimulation *in silico*. (A) Computational simulation of human neuronal networks. Example activities of a simulated neural network containing 1000 neurons, of which 80% are glutamatergic. (B) Corresponding to A, the RRP dynamics of simulated networks during electrical stimulation within the specified time windows. Bold lines depict the average RRP level of the specified population, and the RRP level of ten randomly chosen individual neurons from each population are shown in light-colored lines.

3.3 Presynaptic vesicle sustainability at the core of seizure-like activities in forward programmed excitatory human neuronal networks

In 100% iGlutN cultures, a spontaneous nested network phenomenon termed network super-burst (NSB) could be regularly observed after prolonged cultivation *in vitro*. Preliminary characterization indicated that NSBs share several key similarities with epileptic seizures. Based on the computational framework established in section 3.1, a modified *in silico* model with activity-dependent short-term facilitation and a hierarchy of presynaptic vesicle pools was established which could produce the seizure-like NSBs in unstructured pure excitatory neuronal networks. Some key predictions were then derived from the modified model and validated experimentally *in vitro*, indicating the reliability of the proposed framework. One seizure inducer, bicuculline, and two commonly used antiepileptic drugs, carbamazepine (CBZ) and levetiracetam (LEV), were then applied to investigate their impact on the seizure-like NSBs. While CBZ could effectively abolish NSB formation, bicuculline and LEV had no significant effect on seizure-like activities. *In silico*, preliminary exploration within the parameter space unveiled some basic properties of the proposed framework. In addition, probes into the possible mechanism of origin of rhythmic activities in a pure excitatory network indicated that tonic-to-clonic transition could be governed by a probability dependent on the state of the network. In brief, the framework of NSB activity in pure excitatory neuronal networks based on both *in vitro* and *in silico* observations could provide an alternative perspective of epileptic seizures.

3.3.1 Preliminary characterization of a nested-network activity and its implications in epileptic seizure

NSBs could be seen in iGlutN cultures derived from all 4 available hPSC lines in the present laboratory (hESCs: WA01 and WA09, hiPSCs: C14m-s11 and C35m-r1), with emerging time points vary from 4 weeks to 6 weeks. An NSB typically starts with a strong (measured by the number of spikes enclosed) and less defined sub-burst, followed by a train of weaker but comparatively more homogeneous sub-bursts (Figure 3-3-1, A&B). NSBs are composed of tens of sub-bursts lasting 5s to 20s but could sustain for longer than 1 minute in some observations. Interestingly, inter-sub-burst intervals (IBIs) within NSBs increase steadily from ~200ms to ~700ms, following a linear rule (Figure 3-3-1, C).

This type of NSB could dominate the network activity for hours of recording. Apart from asynchronous single spikes, few single NBs could be observed (Figure 3-3-1, A).

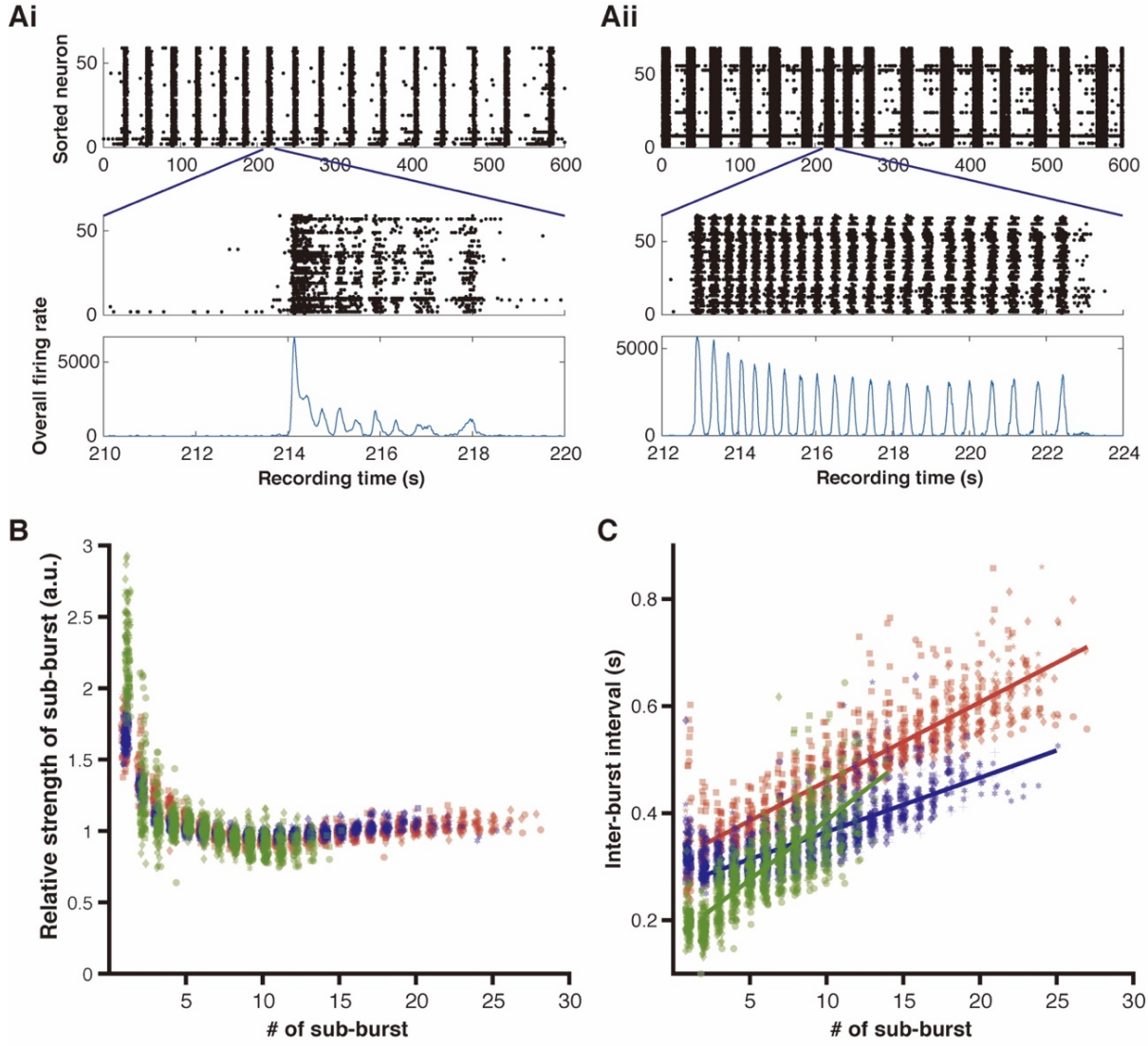

Figure 3-3-1 Preliminary characterization of NSBs. (Ai) Example recording from a 4-week-old 100% iGlutN culture with emerging NSBs. (Aii) Example recording from the save culture as in (Ai) at 7 weeks. (B) Profile of sub-bursts in NSBs at 7 weeks, sub-burst strengths are normalized to median number of spikes in sub-bursts during an NSB. Data are collected from 3 cell lines (marked by different colors), and more than 3 cultures from each cell lines (marked by different shapes). (C) Inter-sub-burst intervals (IBIs) within NSBs from the same recording as in (B). Linear fits of IBI changes are shown.

Nested super-burst activity has been reported in rodent neuronal cultures previously (Wagenaar et al., 2006b, 2006a; Stephens et al., 2012; Gladkov et al., 2018), yet not with such regularity as observed in human iGlutN cultures. In addition, the NSB described here

shares striking similarities with that of epileptic seizures. For example, absence seizures are characterized by a brief (usually not longer than 20 s) loss of consciousness, and regular 3-Hz spike-and-waves in electroencephalogram (Figure 3-3-2, A) (Gibbs et al., 1935). In children with absence seizures, the frequency of spike-and-wave reduces from ~4 Hz to ~ 3 Hz, and intervals increase from ~250 ms to 330 ms (Bai et al., 2010). Another type of seizure is the generalized tonic-clonic seizure. It is characterized by two successive phases, the tonic phase, during which the patients show stiffening and contraction of the muscles and irregular fast spike activity in cortical electrophysiological recording and the clonic phase, during which the patients show rhythmic twitching or jerking of muscles and slowing periodic bursting activity in cortical electrophysiological recording (Figure 3-3-2, B). The electrophysiological patterns of tonic-clonic seizures are universally observed in patients and in animal models established with different approaches and across spatial scales (Kramer et al., 2012; Boido et al., 2014; Jirsa et al., 2014; de Curtis and Avoli, 2015). Furthermore, it has been shown that during the clonic phase, spike numbers of each burst remained stable, but the inter-burst intervals also increased linearly from ~ 200 ms to ~1000 ms (Figure 3-3-2, B) (Boido et al., 2014; Bauer et al., 2017). These similarities strongly suggest that NSBs observed in iGlutN cultures shares a common electrophysiological mechanism with that of epileptic seizures.

Epilepsy is a type of neurological illness that was recognized and documented before the modern era but has yet to be fully understood (Magiorkinis et al., 2010). Epileptic seizures are generally believed to result from excessive excitation and/or excitability in addition to insufficient inhibition in the neural system. This is the theoretical basis of most anti-epilepsy drugs and many animal models of epilepsy (Sarkisian, 2001; Meldrum and Rogawski, 2007; Thijs et al., 2019). However, epileptic seizures are multistage processes, and there is no unanimous agreement on the mechanisms of their initiation, prolongation-propagation, and cessation. Several biophysiological changes are believed to play roles in the dynamics of seizure, including the alteration of icon concentrations, accumulation of metabolites, and the reorganization of microcircuits (Lado and Moshé, 2008; Van Gompel et al., 2014; Antonio et al., 2016; Bazzigaluppi et al., 2017; Weltha et al., 2019). These observations have been fed into computational models to gain more insight into the dynamics of seizures (Krishnan and Bazhenov, 2011; Liou et al., 2020). Of note, it seems to be generally accepted that it is the regaining of inhibition that terminates the

seizures, as opposed to the initiation (Boido et al., 2014; de Curtis and Avoli, 2015). This is unlikely the case, however, in the highly pure excitatory cultures presented here where there were few inhibitory synapses. These observations indicated that a randomly connected, purely excitatory neuronal network is fully capable of producing and terminating seizure-like activities. The relative simplicity of this system could provide unique opportunities to gain insight into the mechanism of epileptic seizures.

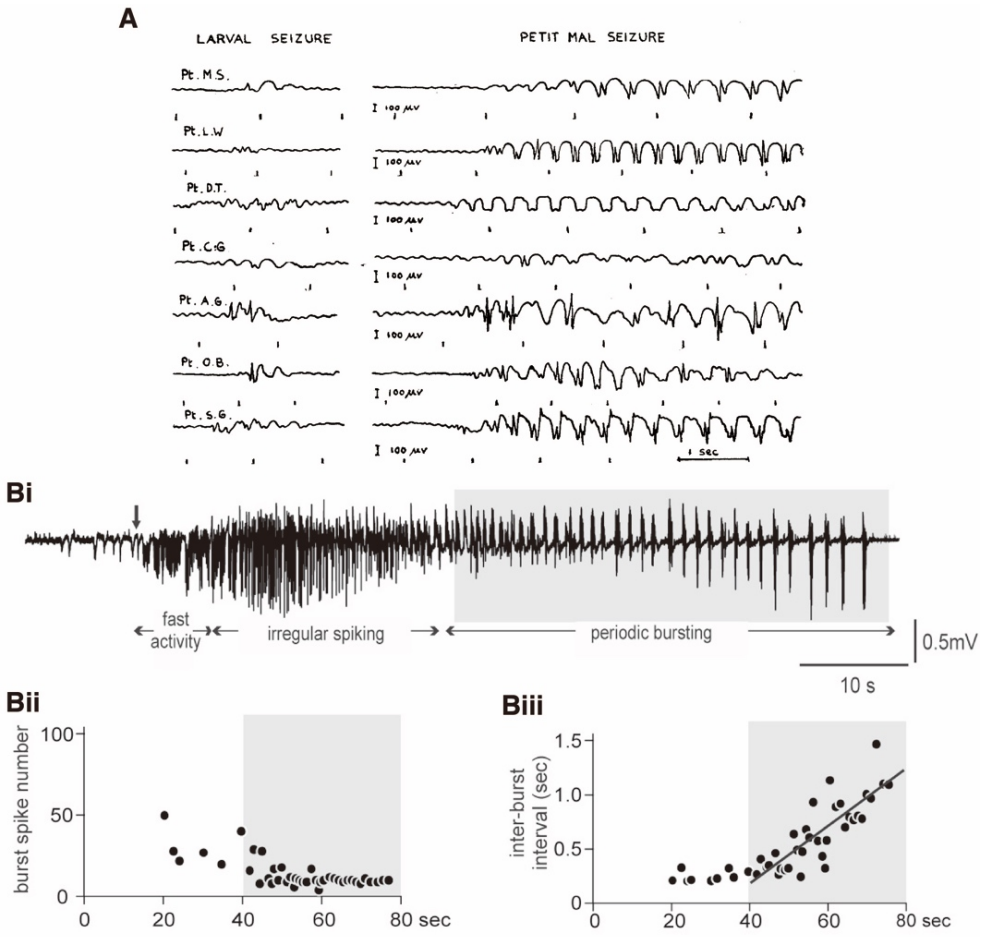

Figure 3-3-2 Typical electrophysiological features of seizures. (A) First published electroencephalogram of absence seizures from epilepsy patients. Adapted from Gibbs et al., 1935. (B) Typical electrophisiological profile of tonic-clonic seizure. Adapted from Boido et al. 2014. (Bi) Representative focal seizure recorded in the medial entorhinal cortex of the in vitro isolated guinea pig brain after 3-minute arterial perfusion of 50IM bicuculline methiodide. Note the progressive decrease in the burst rate approaching seizure end. (Bii) Changes in the number of spikes composing each burst during the periodic bursting phase are outlined in this and the following panels by the grey shading (as in Bi). (Biii) IBI distribution computed for the periodic bursting phase of the seizure.

3.3.2 Computational framework of seizure-like NSBs in iGlutN cultures

Some theoretical deductions could be drawn from these preliminary observations. First, NSBs occurs only after prolonged cultivation, indicating that further increase of connectivity and strengthening of synapses compared to earlier stages might play a role. In fact, as shown in the previous section, an increase of connectivity/synaptic strength along the development of networks could lead to a scenario where an unstoppable burst occurs (Figure 3-1-4, Aiii and C). Therefore, it's likely that excessive synaptic excitation is necessary for the sustainability of network bursting. Second, during the intervals of sub-bursts of NSBs, the overall network activity was not higher than the intervals between NSBs, yet the network was able to produce a succession of sub-bursts. This suggests that the first sub-burst might push the network into an easily excitable state, as do the following ones. In other words, there should be a facilitation effect after each sub-burst. Third, spontaneous activities, as have been shown, are the trigger of NBs and the first sub-burst of a NSB, but they could also contribute to the following sub-bursts.

To prove these concepts *in silico*, the computational model introduced previously was modified accordingly:

(1) Connectivity and synaptic strength were increased;

(2) An activity short-term facilitation mechanism was implemented. For this, another group of glutamate receptors G_{er} were added to the basal neuronal model (eq. 2-1), and the GABAergic parts were omitted:

$$T_m \frac{dv}{dt} = -(v - V_{rest}) + w_e(g_e + w_{er}G_{er})(E_e - v) + D_T e^{\left(\frac{v - V_{th}}{D_T}\right)} + \xi(t) \qquad \text{(eq. 3-1)}$$

Where w_{er} accounts for the strength of G_{er} relative to spike-triggered g_e. And G_{er} has the form:

$$\frac{dG_{er}}{dt} = -\sum_1^i \frac{g_{er}(i)}{\tau_{er}} \qquad \text{(eq. 3-2)}$$

Where τ_{er} = 800ms. And $g_{er}(i)$ denotes conductance contributed from the i^{th} synapse this neuron receives. $g_{er}(i)$ would be updated to 1 upon each presynaptic spike.

(3) Spontaneous spiking was realized with an external Poisson input.

After tuning these parameters, the modified network could produce a succession of sub-bursts, of which the first one was also relatively stronger and the rest smaller and homogeneous. This NSB did not have increasing intervals, however, nor could it stop (Figure 3-3-3, A). This supported the aforementioned assumptions, and, in addition, some more speculative mechanism could be deduced. For example, there is likely to be a threshold of the RRP to initiate a burst, which is lower than full capacity because the RRP has to recover from depletion to this threshold within only 200-300ms. After a sub-burst, activity-dependent facilitation keeps the network excitable for some time. When the RRP recovered to this threshold, a sub-burst happens again.

To further improve the model to fit experimental observations, it is reasoned that increasing intervals implies that the RRP needs more time to recover to the same level. In other words, the replenishment of the RRP slows down during an NSB. An intuitive mechanism would be that there is an upstream pool that supplies vesicles to the RRP, which leads to the notion of the presynaptic recycling pool (RCP) (Rizzoli and Betz, 2005). The RCP should be much bigger than the RRP, but repetitive depletion-replenishment cycles of the RRP could also lead to significant loss of the RCP. An incomplete RCP therefore could not supply the RRP as fast as before. This idea was realized with two sequential kinetics with parameters obtained from literature (Garcia-Perez et al., 2008). The RCP provides vesicles to the RRP at a rate depending on its own level, therefore eq. 2-4 now becomes:

$$\frac{dL_{RRP}}{dt} = \frac{(1-L_{RRP})L_{RCP}}{\tau_{RRP}} - L_{RRP}P_r\delta(t-t_{spk}) \qquad \text{(eq. 3-3)}$$

And respectively, the RCP has its own replenishment dynamics:

$$\frac{dL_{RCP}}{dt} = \frac{(1-L_{RCP})}{\tau_{RCP}} - \frac{(1-L_{RRP})L_{RCP}C_{RCP}}{\tau_{RRP}} \qquad \text{(eq. 3-4)}$$

Where τ_{RCP} is the replenishment time constant of the RCP, and C_{RCP} accounts for the size of the RCP relative to the RRP. Here, τ_{RCP} and C_{RCP} were set as 40s and 0.05 respectively.

With these modifications and the tuning of other parameters, the simulated network could now produce stoppable NSBs with increasing IBIs, just as observed in iGlutN cultures and reported in epilepsy studies (Figure 3-3-3, B-D).

This provides a preliminary computational framework of how the seizure-like NSB activity could emerge and terminate in the glutamatergic neuronal networks. First, a spontaneous or evoked NB (i.e., the first sub-burst) depletes the RRP, silencing the network for a while. In the meanwhile, short-term facilitation is induced, keeping the network highly excitable. After a short recovery, the RRP increases to a threshold level and another sub-burst can occur. During the cycles of RRP depletion-replenishment, the RCP slowly decreases, which results in the decreasing replenishment rate of the RRP. At a certain point, the RRP recovers too slowly to reach the threshold before the short-term facilitation faded away (Figure 3-3-3, C), a bifurcation point. After this, the network slowly returns to resting state again and requires some strong push to start a sub-burst and an NSB. Before that, the RCP would have fully recovered. Note that neither the RCP nor the RRP depleted completely during NSBs: the RRP depletes to the point where network sub-burst stops, whereas the RCP depletes to the point where it could not replenish the RRP 'fast' enough.

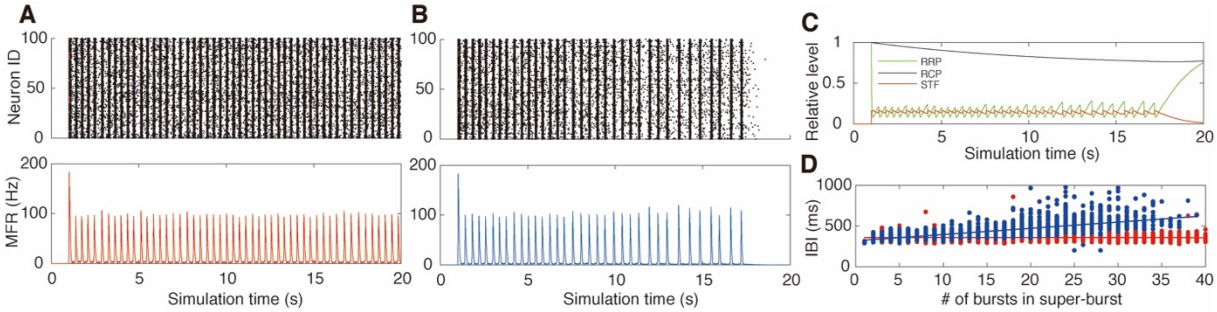

Figure 3-3-3 *In silico* simulation of NSB activities in pure glutamatergic networks. (A) An NSB produced in a simulated network employing a short-term facilitation mechanism does not terminate and show constant sub-burst intervals. (B) In contrast, an NSB generated in a model with a presynaptic recycling pool (RCP) mechanism shows increasing IBIs and a termination. (C) The dynamics of RRP, RCP and short-term facilitation level during the NSB. (D) Inter-burst interval within super burst from models without (red dots) and with (blue dots) RCP (e.g. A and B, respectively), each with 100 simulations.

3.3.3 Validating the 'dual-pool' model of NSBs in iGlutN cultures

According to the proposed model, the RCP level drops significantly during an NSB, which limits the recovery of the RRP and finally terminates the NSB. It is thus reasonable to assume that shortly after the termination of an NSB, before the RCP could fully recover, an external drive should be able to induce another significantly shorter NSB. Furthermore, if induced repetitively with fixed intervals, the network should in the end produce relatively homogeneous NSBs of which the strength (e.g., the total number of spikes enclosed) is

dependent on the repeating intervals. This idea was first tested in the computational model where stimulations with different intervals did yield NSBs of different strengths. And the recovery of NSBs could be fitted to an exponential curve with a time constant close to that preset in the model (Figure 3-3-4, A-D).

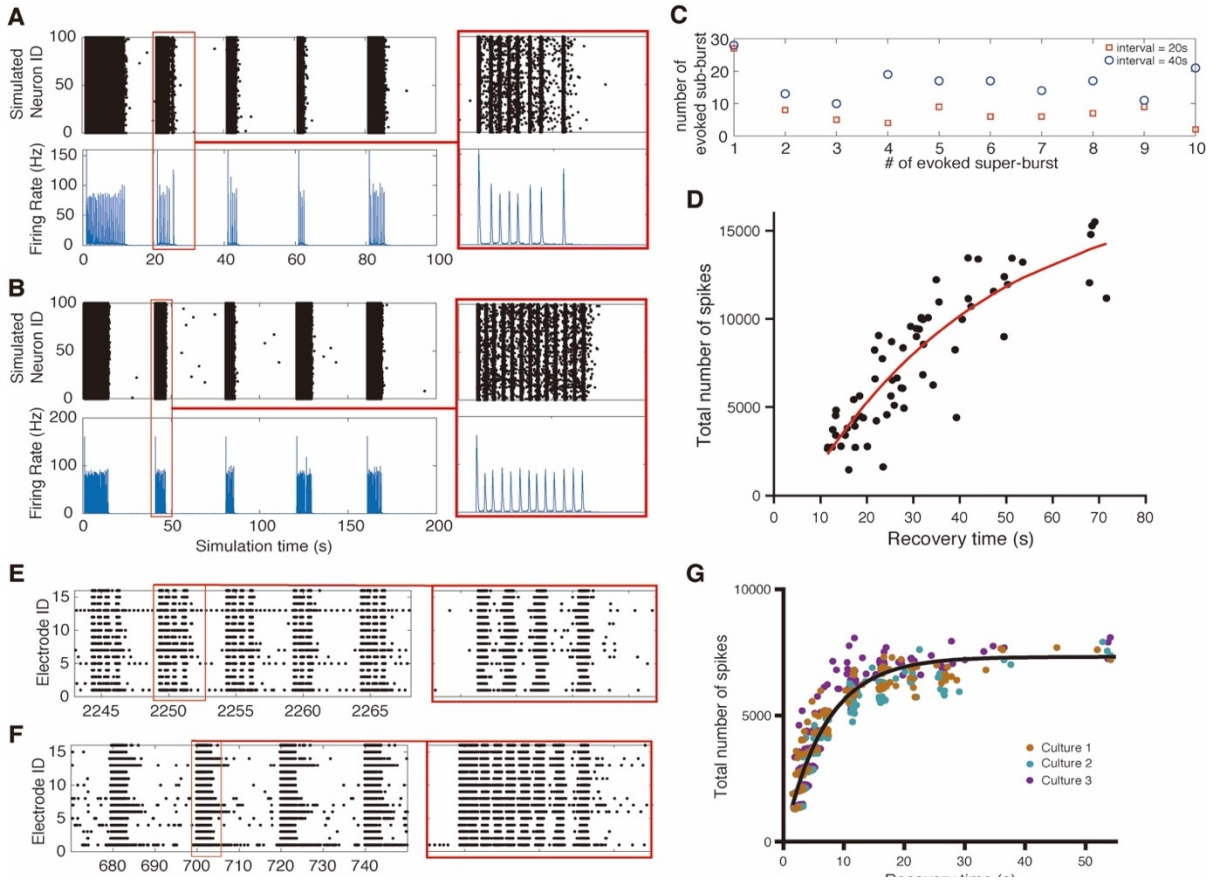

Figure 3-3-4 *In silico* prediction of interval-dependency of evoked NSB strength and in vitro validation. (A-D) *In silico* simulation. Example simulation of network response to stimulations with (A) 20s and (B) 40s intervals. (C) Comparison of super-burst strength evoked by 20s or 40s interval stimulations. (D) Exponential increase of super-burst strength in relation to stimulation interval. The fitted curve has a time constant of 39.2 seconds. (E-G) Evoked NSB in 7-week-old human iGlutN networks. Example recording of network responses to (E) 5s and (F) 20s interval stimulation. (G) Exponential increase of super-burst strength in relation to stimulated interval from 3 independent cultures. Note the fitted curve has a time constant of 6.4 seconds

Experiments were then performed with 7-week-old iGlutN cultures. When stimulated at different intervals, these cultures produced network responses that are similar to those produced in the model (Figure 3-3-4, E, F). This indicates at least the key assumptions about two-level vesicle replenishment in the model fit well with biological processes. However, fitting the result with a single exponential function yielded a recovery time

constant of 6.4 s (Figure 3-3-4, G). This is much shorter than the value set in the model as the RCP replenishment time constant. It is closer to the slower time constant in the bi-exponential fitting of RRP replenishment (Stevens and Wesseling, 1999). Therefore, it is more likely the 'RCP' mentioned earlier might instead be the rate-limiting step in RRP replenishment itself, or the so-called 'intermediate pool' as proposed by (Guo et al., 2015). For clarity, hereafter the two pools will be referred to as slow-recovery pool (SRP) and fast-recovery pool (FRP). And therefore eq. 3-3 and eq. 3-4 should now be written as:

$$\frac{dL_{FRP}}{dt} = \frac{(1-L_{FRP})L_{SRP}}{\tau_{FRP}} - L_{FRP}P_r\delta(t-t_{spk}) \quad \text{(eq. 3-3n)}$$

(n for 'new') and

$$\frac{dL_{SRP}}{dt} = \frac{(1-L_{SRP})}{\tau_{SRP}} - \frac{(1-L_{FRP})L_{SRP}C_{SRP}}{\tau_{FRP}} \quad \text{(eq. 3-4n)}$$

respectively.

3.3.4 *In silico* and *in vitro* modulation of the proposed framework

If the 'dual-pool' model should instead be slow- and fast- components of RRP recovery, specifically modulating these two processes respectively should yield different outcomes in the recovery curve of NSB. Specifically, since the FRP undergoes depletion-recovery cycle upon each sub-burst and its slowing recovery terminates NSBs, artificially slowing of its recovery should be able to terminate the NSB earlier or prevent a NSB from happening at all. In comparison, slowing down the recovery of SRP would not change the strength of NSB but the slope of the recovery. In presynaptic terminals, the dynamic of synaptic vesicles is composed of multiple delicately controlled and coordinated processes (Rizzoli, 2014). Among these processes, several key components could potentially be modulated that would affect the recovery of the SRP and the FRP. For example, it has been reported that the recovery of the RRP depends on Ca^{2+}/calmodulin/ mammalian uncoordinated-13 (Munc13) (Sakaba and Neher, 2001; Basu et al., 2007; Shin et al., 2010) and actin-myosin transportation system (Sakaba and Neher, 2003; Lee et al., 2012; Miki et al., 2016). Recently, Babu et al. reported that microtubule and actin mediated the recovery of the SRP and the FRP, respectively (Babu et al., 2020). Modulators of these components were thus applied to iGlutN cultures and the results were compared to that from *in silico* simulation.

As simulated by *in silico* models, moderate reduction of the FRP recovery would significantly attenuate the strength of evoked NSBs, whereas further slowing down would prevent NSB from emerging (Figure 3-3-5, A). The time constant for the NSB recovery curve should remain unchanged, however, which suggests the curve would be down-shifted (Figure 3-3-5, B). To test this prediction, iGlutN cultures were treated with different concentrations of Cytochalasin D (CytoD), a potent actin inhibitor (Casella et al., 1981). It was observed that while a high dosage of CytoD diminished NSB in the cultures, lower concentration indeed caused a down-shift of the curve as expected (Figure 3-3-5, C&D). The effect could also be reversed by washing off the drugs.

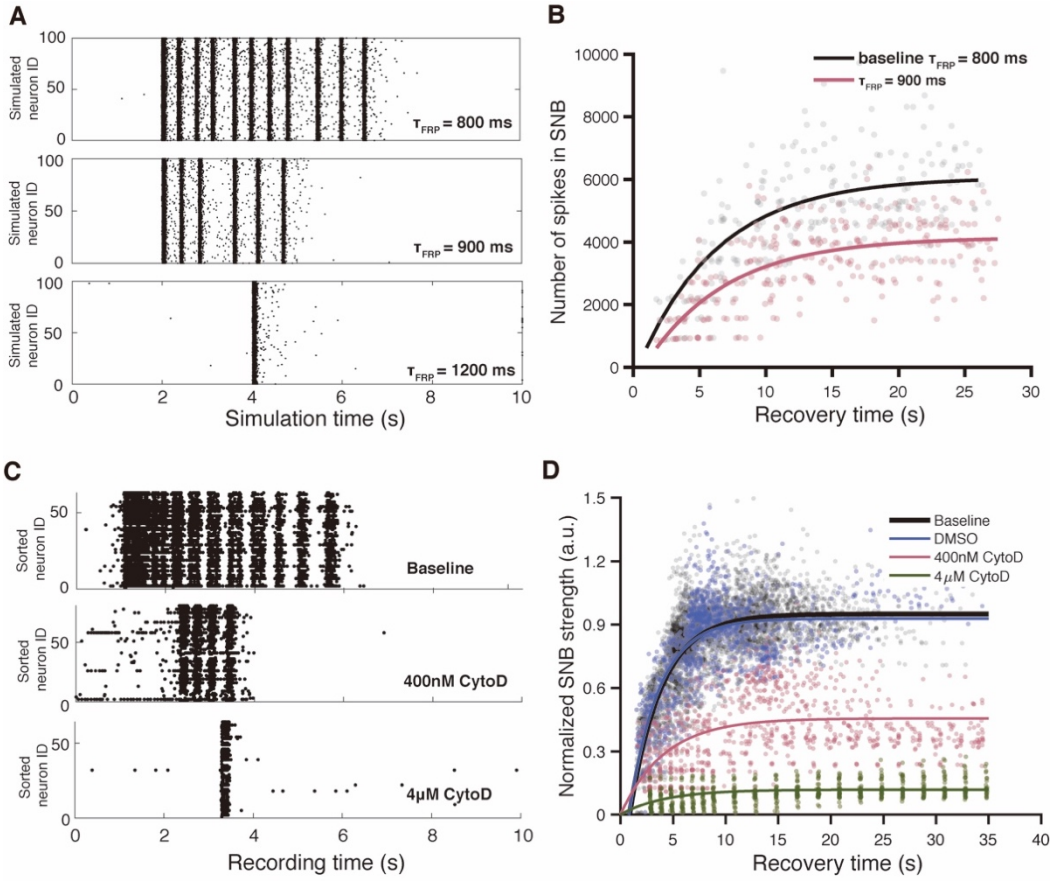

Figure 3-3-5 Deceleration of FRP recovery attenuates seizure-like NSB *in silico* and *in vitro*. (A) Example raster plot of evoked NSB at resting state in networks of all the same parameters but τ_{FRP}. (B) Increase of τ_{FRP} from 800 ms to 900 ms reduces maximum NSB strength from to 6065 ± 472 to 4154 ± 296, and keeps the time constant at comparable level (6.052 ± 2.008 s vs. 6.216 ± 2.226 s. (C) Example raster plot of spontaneous NSBs and a NB in 7-week-old iGlutN cultures in control condition or treated with CytoD. (D) 400nM CytoD reduced maximum evoked NSB by about 50 % (from 0.928 ± 0.015 to 0.4563 ± 0.016) but did not significantly change the recovery time constant (from 4.138 ± 1.23 s to 2.802 ± 0.28 s).

The next step was to test if inhibition of microtubule-dependent transportation could slow down the recovery of SRP, and thus result in a ‘right-shift’ of the NSB recovery curve. For this ispinesib, a kinesin inhibitor, was applied to the cultures. It was found that 100 nM ispinesib treatment for up to 5 hours did not resulted in significant changes of NSB profiles (data not shown). A microtubule destabilizer, vincristine, was also tested. 1 μM Vincristine treatment for 2 hours did not elicit significant changes in the NSB profile. However, after being washed and incubated overnight, the vincristine-treated cultures were severely damaged as few spikes could be observed. This indicated the slow, but potent and irreversible effect of vincristine on the microtubule. These results does not support the hypothesis that microtubule-dependent transportation is directly associated to SRP replenishment.

Phorbol 12, 13-Dibutyrate (PDBu) is a potent activator of PKC (Bazzi and Nelsestuen, 1989). Application of PDBu in neuronal tissues could dramatically elevate post-synaptic current, leading to a stronger activation of post-synaptic terminals. It is now known that, in the context of the presynaptic terminal, PDBu could activate MUNC13, which acts in one of the priming steps of presynaptic vesicles. Activation of MUNC13 increases the releasing probability (p_r) of vesicles triggered by calcium influx (Lou et al., 2008). It is not directly visible how the change of p_r could affect the NSB profile from the explicit equations. Computational simulations were therefore performed with different p_r. A moderate increase of p_r could prolong the NSB, i.e., resulting in more sub-bursts, but make each sub-burst weaker (Figure 3-3-6, A). However, further increase of p_r reduces both the number and strength of sub-bursts, thus decreasing the super burst strength overall. In the end, a very high p_r would effectively prevent the formation of NSB (Figure 3-3-6, Aiii and B-D). The nonlinear response of NSB to p_r could be explained as follows. A moderate increase of p_r makes the network more excitable, producing more sub-bursts, but also depletes vesicles too quickly, yielding fewer spikes within each sub-burst. Further increase of p_r, however, would produce too few spikes, therefore the activity-dependent facilitation would be too weak, which would in turn reduce the sustainability of the NSB. Different concentrations of PDBu were applied into the cultures to see if it could elicit the expected effect. While 5 nM PDBu did not cause observable alteration of NSB profiles (data not shown), 10 nM reduced both the number of sub-bursts and the number of spikes in sub-bursts, whereas 100 nM further reduce the number of spikes in each sub-burst

(Figure 3-3-6, E-G). As a result, a higher concentration of PDBu led to increased reduction of overall strength of NSBs (Figure 3-3-6, H). These observations fit with the downtrend predicted by the simulation. It is possible that the tested iGlutN cultures were already at the 'right side' of the peak in Figure 3-3-6, D, therefore no 'up-trend' could be observed. Overall, this intriguing finding suggests that changes of parameters on the single-cell level might lead to nonlinear consequences in neuronal networks. Importantly, the proposed model is robust enough to account for experimental observations.

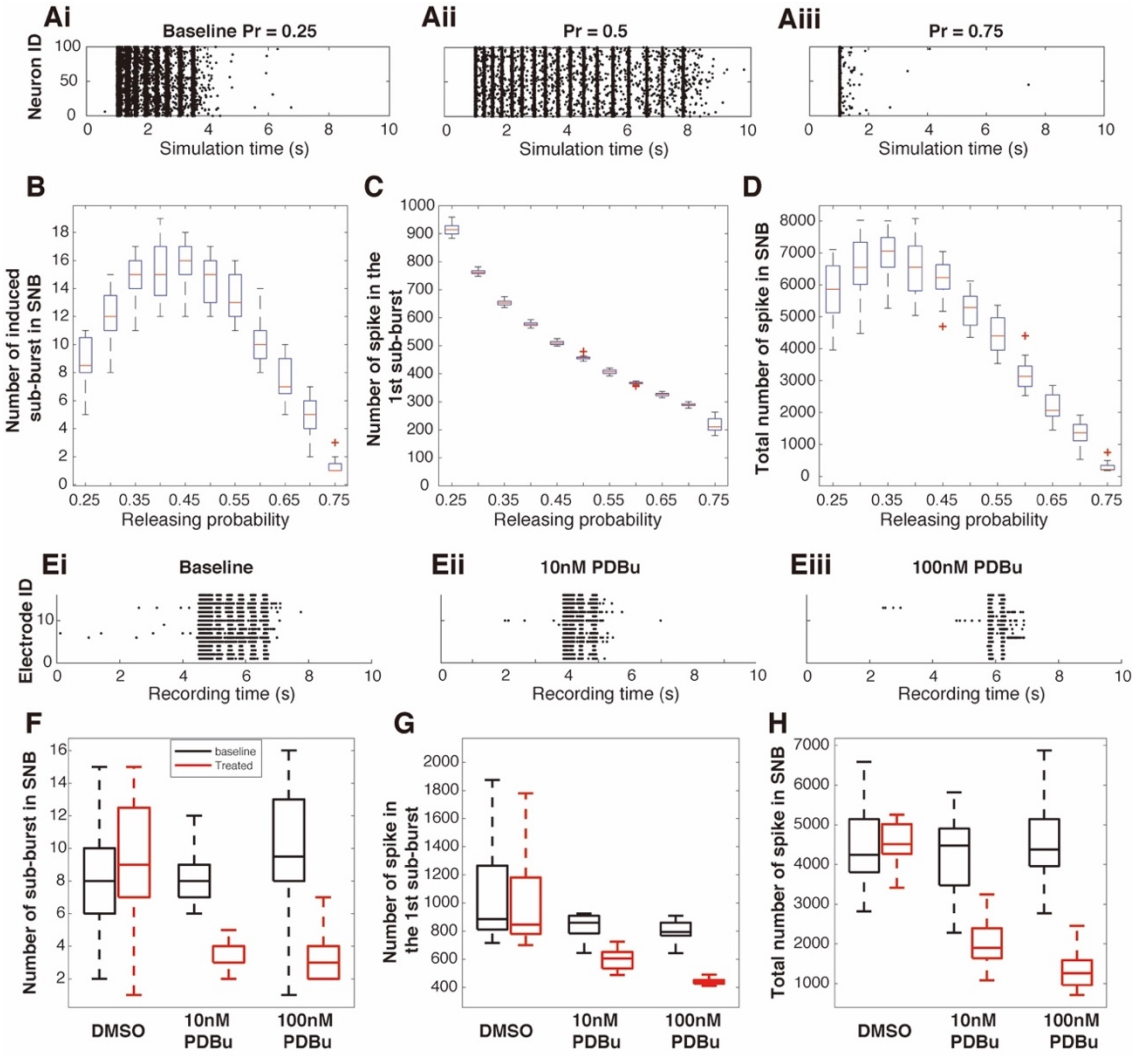

Figure 3-3-6 The effect of synaptic releasing probability on seizure-like NSB *in silico* and *in vitro*. (A) Example raster plot of evoked NSB at resting state in simulated networks of all the same parameters but p_r. (B-D) Quantification of number of sub-bursts (B), number of spikes in the 1st sub-burst (C) and total number of spikes in NSBs (D) at resting states in simulated networks of all the same parameters but p_r. n = 10 in each condition. (E) Example raster plot of spontaneous NSBs in 7-week-old iGlutN cultures in control condition or treated with PDBu. (F-H) Quantification of the same parameters as in (B-D), n = 6 cultures in each condition.

3.3.5 Effect of epileptic modulators on NSBs in iGlutN cultures

To investigate whether the observed NSBs could be blocked by anti-epileptic drugs (AEDs) or strengthened by epilepsy inducers, i.e., whether these iGlutN cultures could serve as a seizure model, two first-line AEDs, CBZ and LEV, as well as bicuculline were applied to the cultures, respectively. CBZ executes its anti-epileptic effect by binding to voltage-gated sodium channels and keeping them at inactivated state, thus reducing excessive open/close cycles during high-frequency activities (Ambrósio et al., 2002). LEV is relatively novel and was only approved for clinical use in 1999 in the US and in 2000 in Europe. LEV is structurally distinct from previous AEDs and also proved to act on a different target, synaptic vesicle protein 2A (SV2A) (Crepeau and Treiman, 2010). SV2A is believed to be important for the mobilization of synaptic vesicles, which suggests LEV could modulate vesicle recovery as proposed in the present framework. The precise mechanism for which this occurs remains unclear; it is not even known whether LEV promotes or inhibits SV2A (Alrabiah, 2019). Bicuculline is commonly used to induce epileptiform activity *in vivo* and *in vitro*.

0.1 mM CBZ abolished NSB and resulted in only a brief burst when evoked by electrical stimulations in iGlutN cultures, indicating its anti-epilepsy potency also inhibits seizure-like activities in iGlutN cultures (Figure 3-3-7). On the contrary, prolonged treatment (> 5 hours) of high dosage of LEV failed to exhibit significant alteration of NSB in iGlutN cultures. This result is not unexpected, however, it has been shown that in the central nervous system both SV2A and SV2B are expressed in glutamatergic neurons, but only SV2A is expressed in GABAergic inhibitory neurons (Bartholome et al., 2017). Animals with SV2A deletion or missense mutation show disruption in action potential induced-GABA but not -glutamate release, indicating the important role of SV2A-GABAergic system in epileptogenesis (Löscher et al., 2016). Therefore, these results are in line with the hypothesis that LEV probably maintains the sustainability of vesicle in GABAergic presynaptic terminals by enhancing SV2A mediated vesicle mobilization, inhibiting seizures. This is further supported by the fact that bicuculline did not cause any change of NSB activities in iGlutN cultures either. However, to verify this hypothesis, further experiments should be performed on cocultures of iGlutNs and iGABANs. Together, these results suggest the NSBs observed in iGlutN cultures could respond to at least some of

the AEDs, and it might also be able to help to dissect the action mechanism of AEDs of which the pharmacology is unclear.

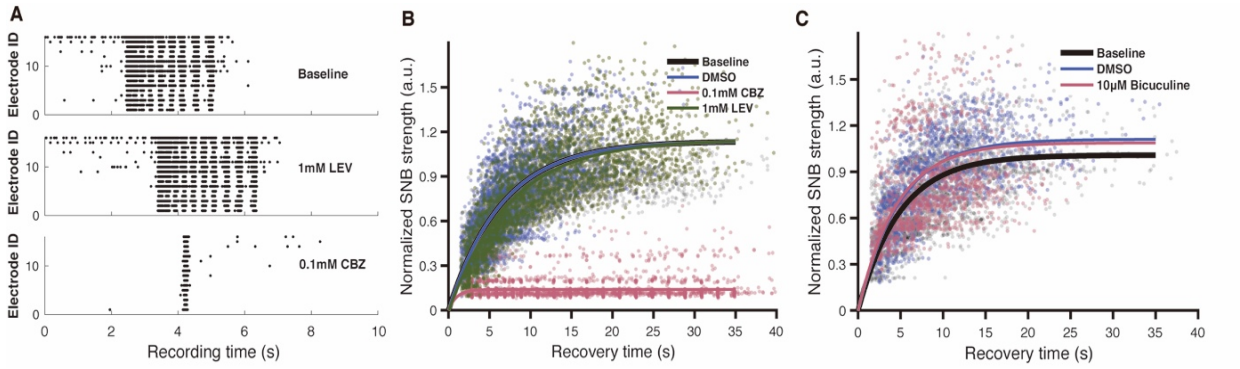

Figure 3-3-7 The effect of seizure modulators on NSB profiles. (A) example raster plot of spontaneous NSBs observed 7-week-old iGlutN cultures in control condition or treated with LEV or CBZ. (B) NSB recovery profile of cultures in control condition or treated with LEV or CBZ. Data were collected from 6 cultures of each condition. (C) NSB recovery profile of cultures in control condition or treated with bicuculline. Data were collected from 5 cultures of each condition.

3.3.6 Further exploration of the parameter space of the *in silico* epileptiform NSB model

This section described some preliminary exploration into the parameter space of NSB activity. The aim was to qualitatively describe different scenarios with recursive parameter tuning within defined limits, not to obtain a quantitively mathematic explanation of these phenomena.

There appears to be a convergence point at which all iGlutN networks developed NSB activity at a certain time in culture. However, during *in silico* simulation, the parameter conditions that could produce NSBs seems to be very narrow. For example, with a given strength of short-term facilitation, the Poisson input has to reach a threshold level of input frequency and strength to produce more than one burst, but the number of sub-bursts quickly exceed experimental observations (Figure 3-3-8, A&B). In addition, this threshold is not simply the product of input frequency and amplitude, demonstrating the non-linear properties of neural networks (Figure 3-3-8, B). Furthermore, given a fixed external input frequency, higher input amplitude makes the network more excitable, which in turn makes it easier to initiate a sub-burst and more difficult to prevent one from happening. As a consequence, the NSB elongates on both sides with increasing background input. On the left side, a tonic-to-clonic transition emerged (Figure 3-3-8, C-v), and on the right side, an unstoppable ‘status epilepticus’ appeared in the end (Figure 3-3-8, C-vi). Tonic-to-clonic

transition will be explored in the next section. Status epilepticus, on the other hand, can be addressed here briefly. Replenishment of both the SRP and the FRP depends on the level of the SRP, in opposite ways, i.e., a decrease of the SRP level would limit the rate of its FRP recovery but accelerate its own recovery in quantity. As a consequence, under the circumstance of high network excitability, the SRP could reach an equilibrium state before the FRP recovery reaches its threshold to stop the NSB, enabling epilepticus (Figure 3-3-8 C-vi). Apart from background input, a similar conclusion might be applicable for other factors affecting the overall network excitability, e.g., the strength of short-term facilitation and the network connectivity (Figure 3-3-8 D&E).

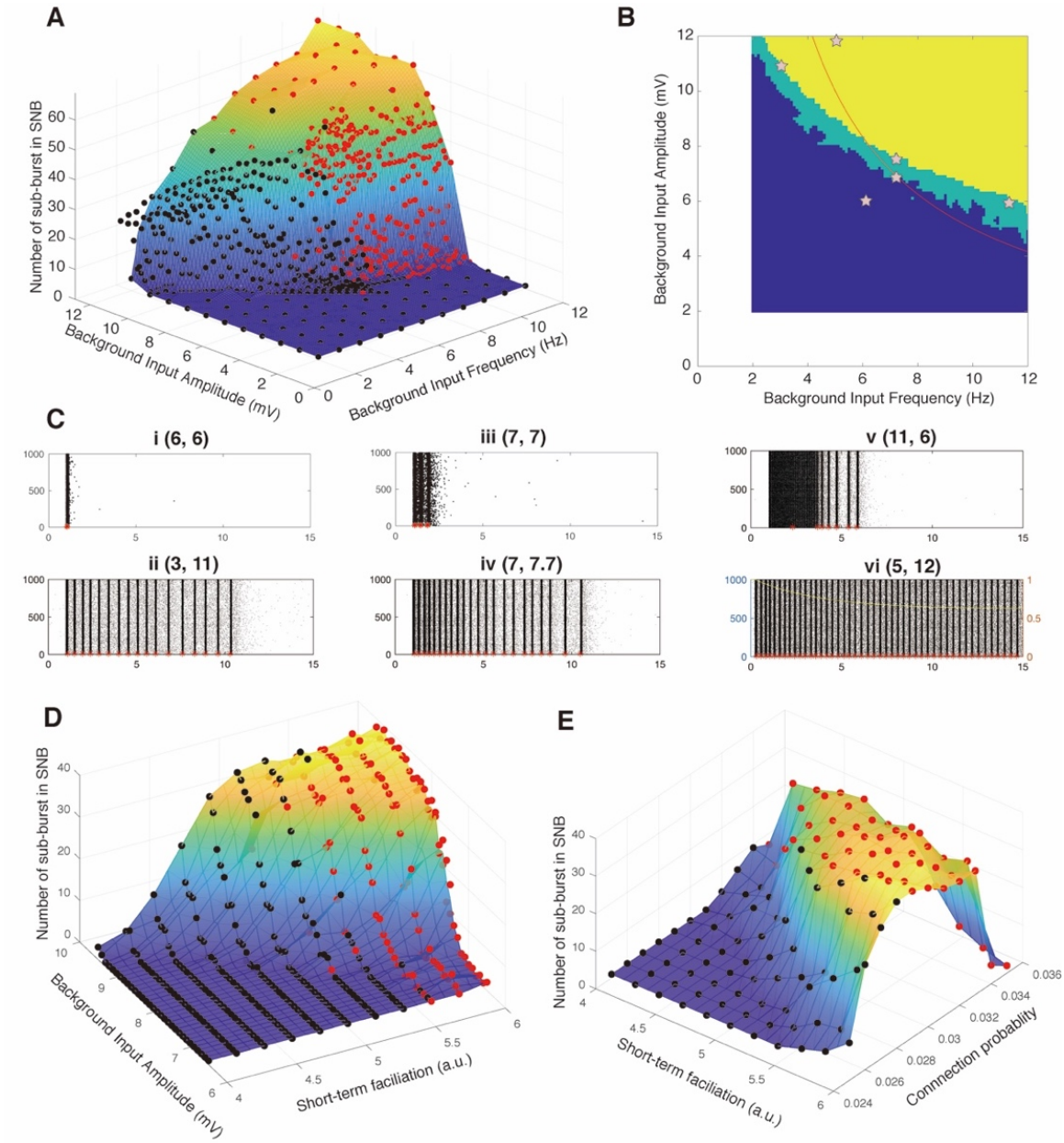

Figure 3-3-8 Network excitability and the generation of NSBs. (A) The strength of NSB produced in networks with different background input. Black dots show NSB without tonic activities, red dots show elicited NSB contains tonic activity, only clonic sub-bursts are counted. (B) Plan view of (A), dark blue = single NB, light blue = limited NSB, yellow = NSB longer than simulation time. Stars indicates example simulations shown in (C). (C) Raster blot of different simulation results as shown in (B). (D) The strength of NSB produce in networks of different background input and short-term facilitation. (E) The strength of NSBs produce in networks of different short-term facilitation and connectivity. Note in the sunk top-right corner, the drop of the number of sub-bursts was due to predominant presence of tonic activity during the simulated period of time.

In epilepsy models and aforementioned *in silico* simulations, tonic activities precede clonic activities and indicate that faster FRP recovery is necessary for tonic activity. Slowing down of FRP recovery would appear to lead to a tonic-to-clonic transition. In the aforementioned simulations (Figure 3-3-8), two interesting features could be seen in tonic-to-clonic transitions. First, there seemed to be no 'hard boundary' when a tonic-clonic transition could be observed. With the same parameters, the network might start with tonic activity and then transform into clonic activity but could also directly start from clonic activities. Second, the transition happens very quickly with no obvious intermediate state.

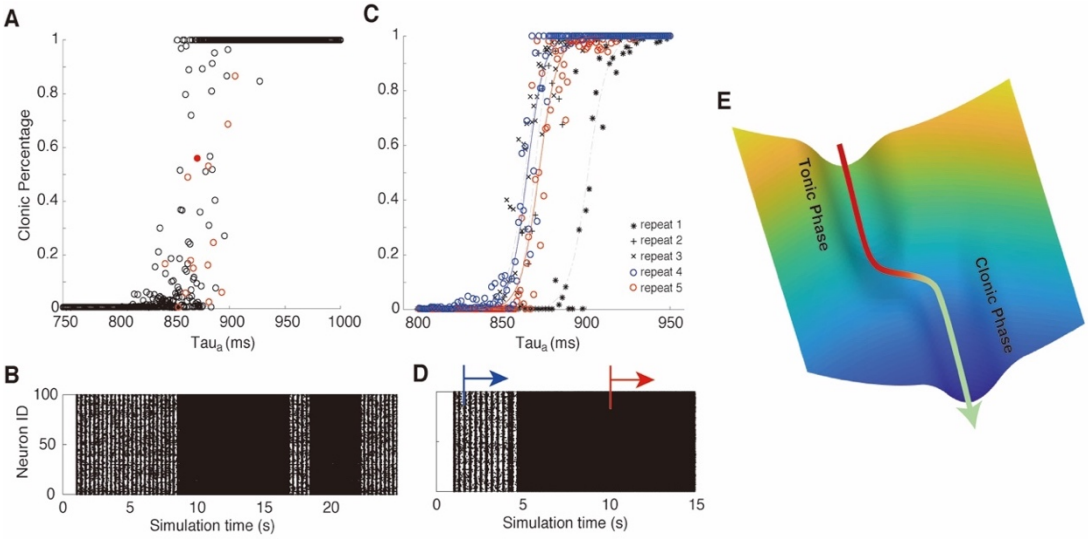

Figure 3-3-9 *In silico* exploration of tonic-clonic transition. (A) Percentage of clonic state in 25s simulation along the increase of FRP recovery time constant. Filled red circle depict a sample run shown in B). (C) Percentage of clonic state in 50s simulation started from a tonic state (repeat 1-3, and 5) and a clonic state (repeat 4). Repeats 1-3 are from different networks of the same parameters, repeat 4-5 are from the same network of different starting point as illustrated in (D). Dashed gray lines and colored lines indicate sigmoid fitting of the observations. (E) Visualization of bi-stability during tonic-to-clonic transition.

To further explore this phenomenon within the proposed theoretical framework, simulations were performed with the FRP recovery time constant (τ_{FRP}) fixed at different values.

With faster FRP recovery, the networks stayed in tonic state. Then along with the increase of τ_{FRP}, the network starts to show tonic-clonic transition (Figure 3-3-9, A). Interestingly, tonic and clonic states appeared to be interchangeable, as networks can switch between the two states multiple times (e.g., Figure 3-3-9, B). Networks with higher τ_{FRP} appeared to transform into clonic states earlier and stay in clonic states for longer, until τ_{FRP} is long enough that only clonic activity can be seen. It is worth noting that a pulse stimulation always elicits a NB, thus clonic activity would be more likely to follow. To address this problem, a simulated network was run until it enters the tonic state, then its τ_{FRP} was changed to a different value and run for another 50 seconds. Similar tonic-to-clonic shifting patterns could be observed again, although networks with the same parameters showed a slightly different transition curve (Figure 3-3-9, C&D). The starting state also appeared to affect the probability of tonic and clonic states within the recording time. Taken together, these results suggest these networks have a tonic-clonic bi-stability and slowing down FRP recovery should increase the probability of clonic states (Figure 3-3-9, E). In more realistic *in silico* models, as well as possibly in experimental observations, the FRP recovery slows down continuously, and, therefore, only tonic-to-clonic transition could be recorded.

When stimulated with shorter intervals, cultures derived from one cell line showed sporadic responses of NSBs (Figure 3-3-10, A). Some preliminary explorations were also performed, and a speculative mechanism of this phenomenon was proposed by introducing a Ca^{2+}-mediated saturable short-term facilitation mechanism. For this, eq. 3-2 was modified as follows:

$$\frac{dG_{er}}{dt} = -\sum_1^i \left(\frac{g_{er}(i)}{\tau_{er}} + C_{ger}(g_{max} - g_{er}(i))\delta(t - t_{spk})\right) \qquad \text{(eq. 3-5)}$$

C_{ger} defines relative accumulation speed and g_{max} defines maximum facilitation level. If facilitation saturates relatively quickly, every sub-burst should lead to a similar level of facilitation. The occurrence of the following sub-burst depends only on the recovery of the FRP, allowing homogenous NSBs to be elicited. However, if the first sub-burst could not

saturate facilitation, both recovery of the FRP and facilitation became the limiting factor of NSBs. At the beginning of stimulation, the SRP was at a high level. Therefore, faster FRP recovery would need less prominent facilitation to produce a second sub-burst. The following sub-burst could saturate facilitation and produce an NSB as before. When the second stimulation was delivered before the SRP could recover, the FRP could not recover quickly enough, the first elicited NB thus failed to elicit a second sub-burst which could produce an NSB. A successful NSB could only be elicited when the SRP recovered to a high level (Figure 3-3-10).

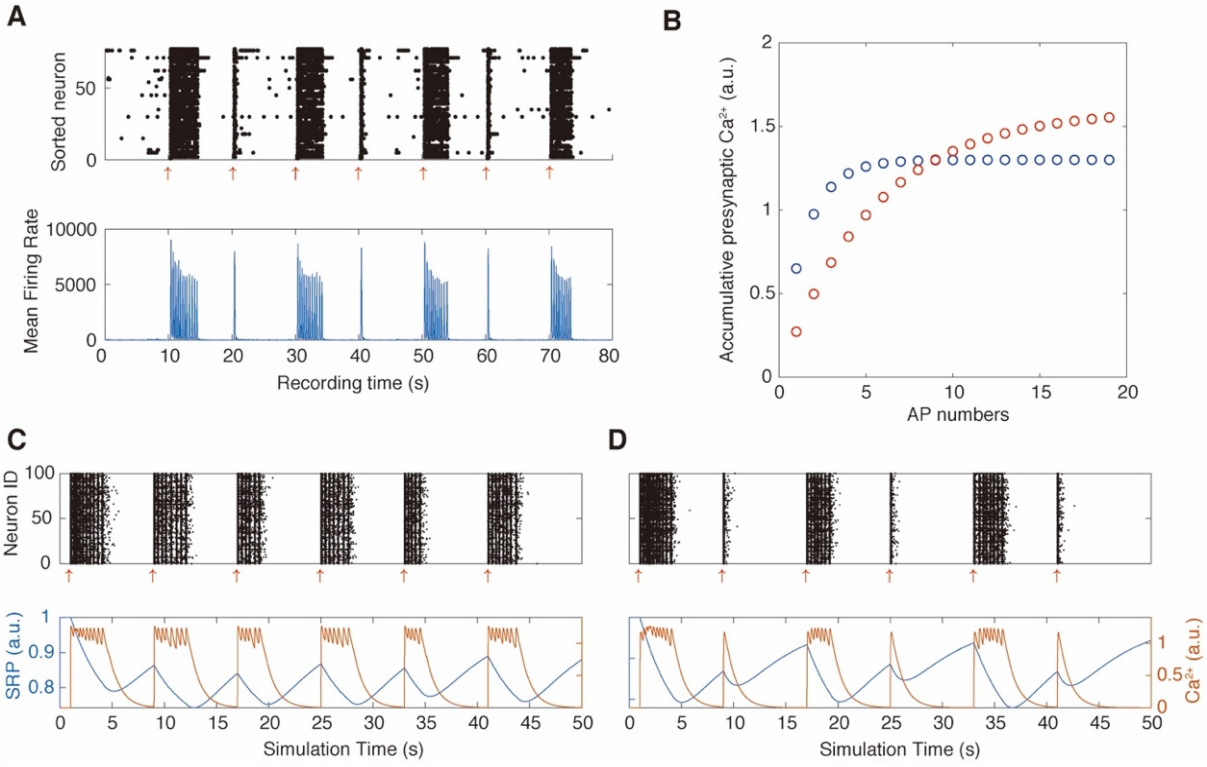

Figure 3-3-10 Mechanism of sporadic NSB induced by repetitive stimulations. (A) Example of sporadic NSB observed in one culture. (B) Two different calcium accumulation dynamic resulted different NSB response in simulation. Blue dots correspond to (C) and red dots correspond to (D). (C) Homogenous NSBs could be elicited if calcium saturates quickly thus the same level of facilitation could be elicited after each sub-burst. (D) Sporadic NSBs occur when calcium saturates relatively slower and there are minor differences of short-term facilitation after each sub-burst. (C_{ger}, $g_{\max}$) were set as (0.17, 1.6) in (C) and (0.5, 1.3) in (D), respectively.

3.4 Morphological and functional consequences of RB1CC1 loss of function in forward programmed human glutamatergic neurons

After establishment and systematic characterization of the human-specific platform based on forward programmed neurons, Section 3.4 aims at exploring this platform as a way to study the functions of RB1CC1, a gene that has been associated with psychiatric disorders. For this experiment, isogenic hPSC lines with RB1CC1 loss of function mutations were established using the CRISPR-Cas9 system. From these cell lines, iGlutNs were produced using the forward-programming technique, and the morphological as well as electrophysiological consequences of RB1CC1 loss of function were explored. In addition, to investigate which mechanism could mediate these alterations, autophagy- and FAK-dependent pathways were further assessed with pharmacological modulations. These results have the potential to help uncover possible etiological and pathogenic mechanisms of psychiatric disorders such as schizophrenia.

3.4.1 Establishment of isogenic RB1CC1^{KO} hPSC lines and iGlutNs

Two hPSC lines (C14ms11, human induced pluripotent stem cell line; WA01, human embryonic stem cell line) carrying a doxycycline inducible NGN2 expression cassette in both alleles of the AAVS1 “genomic safe harbor” locus kindly provided by Dr. Matthias Hebisch were used in this study. Single-cell-derived clones with CRISPR/Cas9-mediated loss of function mutations of RB1CC1 were obtained (Figure 3-4-1, A). From each background, two homozygous knockout lines (referring to RB1CC1 CCDS34892.1: C14KO1, 124_125insT/125_131del; C14KO2, 125_126del/125_126del; WA01KO1, 124_125insC/125_126del; WA01KO2, 124_125insT/125del) were picked, and one unedited wild type subclone as a control, respectively. Parental lines were also used as control. Amplicon sequencing was performed to confirm Sanger sequencing data and to exclude mosaic clones (Supplementary Figure S1). SNP-based virtual karyotyping was performed to verify genome integrity (Supplementary Figure S2). Full-length RB1CC1 was not detectable in RB1CC1 mutated clones as revealed by western blot (Figure 3-4-1, C). Expression of pluripotency markers in the obtained cell lines were assessed, TRA-1-60 with flow cytometry and both SOX2 and OCT4 with immunofluorescence (Figure 3-4-1, B). These pluripotency markers are robustly expressed in all PSC cell lines, indicating that neither the insertion of a doxycycline inducible NGN2 expression cassette in AAVS1 nor

the loss of function of RB1CC1 affected pluripotency in either genetic background. RB1CC1^{KO} and control hPSC lines were then subjected to the forward-programming protocol for the generations of iGlutNs. No difference was observed during this process (Figure 3-4-1, D).

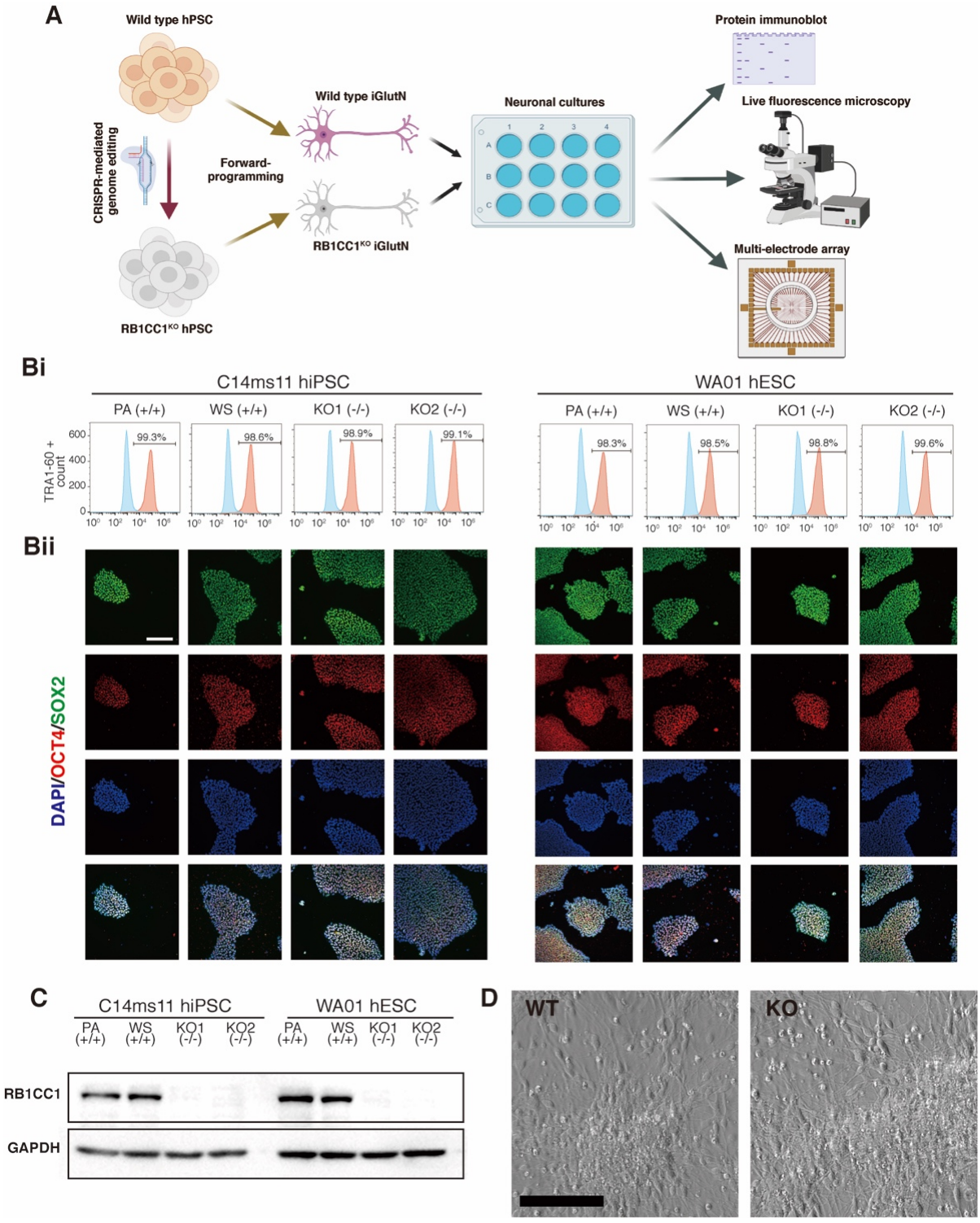

Figure 3-4-1 Schematic of the experimental procedure and the establishment of isogenic RB1CC1^{KO} hPSC lines. (A) Schematic of the experimental procedure. (Bi) Flow cytometry for the pluripotency marker TRA-1-60, and (Bii) immunofluorescence assessment for the pluripotent markers OCT4 and SOX2 in obtained hPSC lines. (C) Western blot analysis of RB1CC1 in obtained hPSC lines. (D) Example microscopy pictures of iGlutNs induced from wild type and RB1CC1^{KO} hPSCs. Scale bar = 100 μm.

3.4.2 RB1CC1^{KO} human glutamatergic neurons show axonal pathology and deficient autophagy

After replated for maturation for 3 weeks, multiple swelling-like structures could be observed in RB1CC1^{KO} iGlutNs cultures (Figure 3-4-2, A). To further investigate the quantity and distribution of these swelling structures on the neuronal level, iGlutN cultures were transfected with a plasmid expressing hrGFP under the control of a DCX promoter. The transfection efficiency was adjusted to around 5% in order to dissect the profile of single neurons in dense cultures. It was found that swelling structures were predominantly present along axons, especially close to the distal axonal terminal, whereas they were rarely present on soma and dendrites. In fact, it was observed that new swellings formed just behind the axonal growth cone (Figure 3-4-2, B). Compared to wild-type controls, the number of swellings per axonal terminal was significantly higher in RB1CC1^{KO} iGlutNs (median count 4 vs. 0, $F(1,187) = 170.4$, $p<0.0001$, Figure 3-4-2, C). Nevertheless, loss of function of RB1CC1 did not appear to affect dendrite or axon outgrowth, as no significant difference could be observed in the speed of axon outgrowth between cultures of different genotypes (median speed 2.7 vs. 2.1 μm/h, $F(1,48) = 3.06$, $p=0.087$, Figure 3-4-2, D) or the dendrite complexity as assessed with the Sholl analysis (Figure 3-4-2, E&F).

To assess the effect of RB1CC1 loss of function on autophagy, the cultures were transfected with a plasmid expressing mRFP-GFP tandem fluorescent-tagged LC3 (Kimura et al., 2007). With this setup, mRFP and GFP are equally distributed before and during the early stages of autophagy. However, after the fusion of autophagosome and lysosome, GFP is quenched in acidic and degradative conditions, whereas mRFP-LC3 is not, marking autolysosomes with red fluorescence (Figure 3-4-3, A).

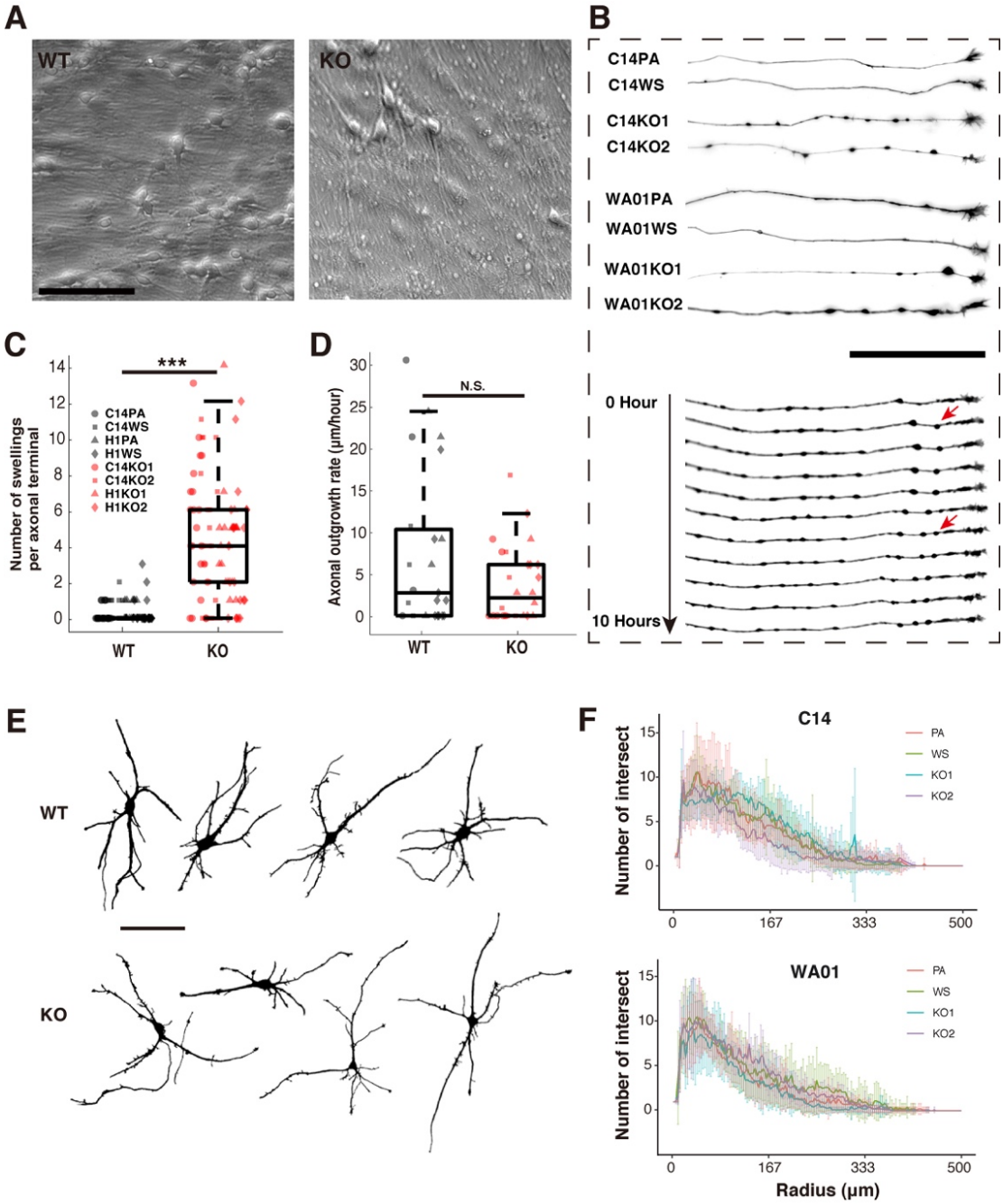

Figure 3-4-2 Morphological alteration observed in RB1CC1^{KO} iGlutN. (A) Example pictures from live phase contrast microscopy of wild type and RB1CC1^{KO} iGlutN cultures, 3-week-old. (B) Upper, examples from inverted live fluorescence pictures of axonal terminal in wild type and RB1CC1^{KO} iGlutN cultures. Lower, example of live time-lapse microscopy of an axonal terminal in RB1CC1^{KO} cultures obtained every hour. Red arrows indicates newly formed swellings. Quantification of (C) axonal swellings and (D) axonal outgrowth rate in wild type and RB1CC1^{KO} iGlutN cultures. For each cell line, >20 axons from 3 independent experiments were analyzed. (E) Example pictures of iGlutN in wild type and RB1CC1^{KO} cultures. (F) Sholl analysis results showing the number of dendritic intersections at fixed distances from the soma in concentric circles. For each cell line, >10 pictures from 2 independent experiments were analyzed. All scale bars = 100 µm.

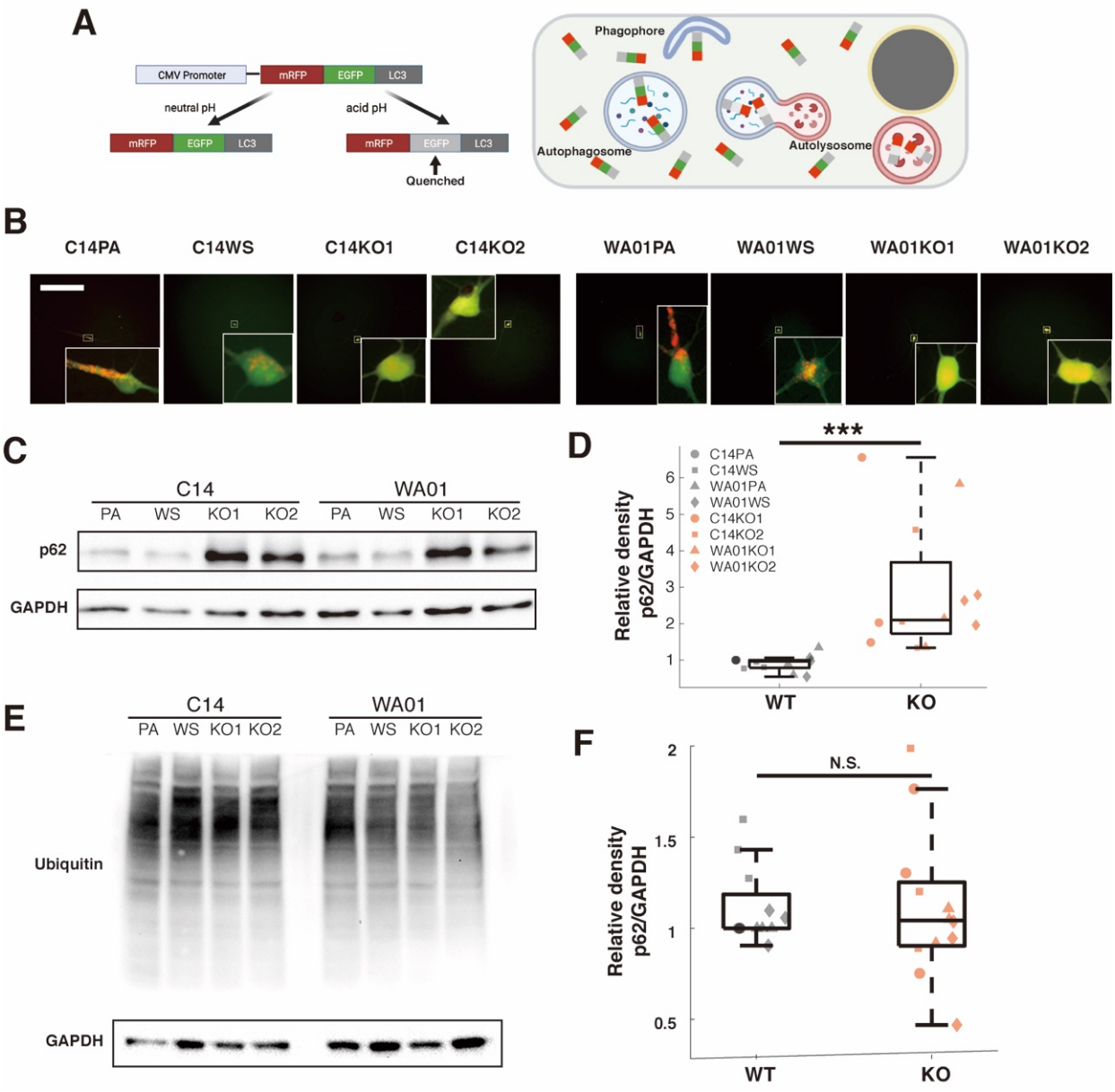

Figure 3-4-3 RB1CC1 loss of function led to autophagy deficiency in iGlutN. (A) Schematic illustration of the autophagy reporter used in the present study. (B) Example live fluorescence microscopy pictures of iGlutN cultures 7 days after transfected with an autophagy reporter plasmid (ptfLC3). Scale bar = 100 μm. Western blot analysis of p62 in wild type and RB1CC1^{KO} iGlutN (C) and quantification (D), N = 3. Western blot analysis of ubiquitin in wild type and RB1CC1^{KO} iGlutN (E) and quantification (F), N = 3.

Red-colored vacuoles could be found near or within the soma of wild type iGlutNs but not RB1CC1^{KO} iGlutNs (Figure 3-4-3, B). Autophagy deficiency also left p62 labeled cellular waste accumulated in the cytoplasm. This was confirmed in RB1CC1^{KO} iGlutNs, in which

the amount p62 was significantly higher than wild-type controls after 3 weeks in culture as revealed by western blot analysis (median fold change = 1.09, $F(1,23) = 22.4$, $p=0.00014$, Figure 3-4-3, C&D). By contrast, ubiquitin did not seem to accumulate in RB1CC1^{KO} iGlutNs, indicating the function of the proteasome was not impaired (median fold change = 0.04, $F(1,23) = 0$, $p = 0.96$, Figure 3-4-3, E&F). Together, these results confirmed that loss of function of RB1CC1 could lead to the failure of autophagy induction.

3.4.3 RB1CC1-deficient human cortical glutamatergic neuronal networks are hyperactive

To assess possible electrophysiological alterations result from deletion of RB1CC1, iGlutNs were cocultured with mouse astrocytes on MEA plates. After 3 weeks, RB1CC1^{KO} iGlutN cultures exhibited more spike activity than wild-type controls (median of mean firing rate: 1.77 Hz vs. 0.83 Hz, $F(1,143) = 16.23$, $p<0.0001$, Figure 3-4-4, A and C). The hyperactivity was unlikely a result of a higher level of spontaneous spiking activity, as after the application of CNQX, an AMPA and kainate receptor antagonist, no significant difference of spiking activity between genotypes could be observed (median of mean firing rate: 0.11 Hz vs. 0.14 Hz, $F(1,119) = 0.02$, $p=0.891$,, Figure 3-4-4, B and D). The hyperactivity did not appear to be due to less GABAergic inhibition either, as bicuculline, a GABA-A receptor antagonist, did not alter the difference between genotypes (median fold change of mean firing rate: 0.1 vs. 0.06, $F(1,23) = 1.43$, $p=0.241$, Figure 3-4-4, E). Stronger spiking activity in RB1CC1^{KO} iGlutNs could be observed 30 mins after washing off of CNQX (median of mean firing rate: 1.62 Hz, vs. 1.15 Hz, $F(1,71) = 4.45$, $p=0.0387$, Figure 3-4-4, F). Therefore, the observed hyperactivity was believed to be due to strengthened glutamatergic synaptic activation. The next step was to investigate what mechanism mediated the strengthened glutamatergic activation. Quantification of pre- and post-synaptic markers, synapsin1 and PSD95, failed to reveal significant differences (median fold change: 0.15, $F(1,23) = 0.09$, $p=0.764$ for synapsin1, and median fold change: 0.05, $F(1,23) = 0.64$, $p=0.432$ for PSD95, respectively, Figure 3-4-4, G, H, and I). Therefore, the strengthened glutamatergic excitation in RB1CC1^{KO} iGlutN was likely not due to differing amounts of synapses.

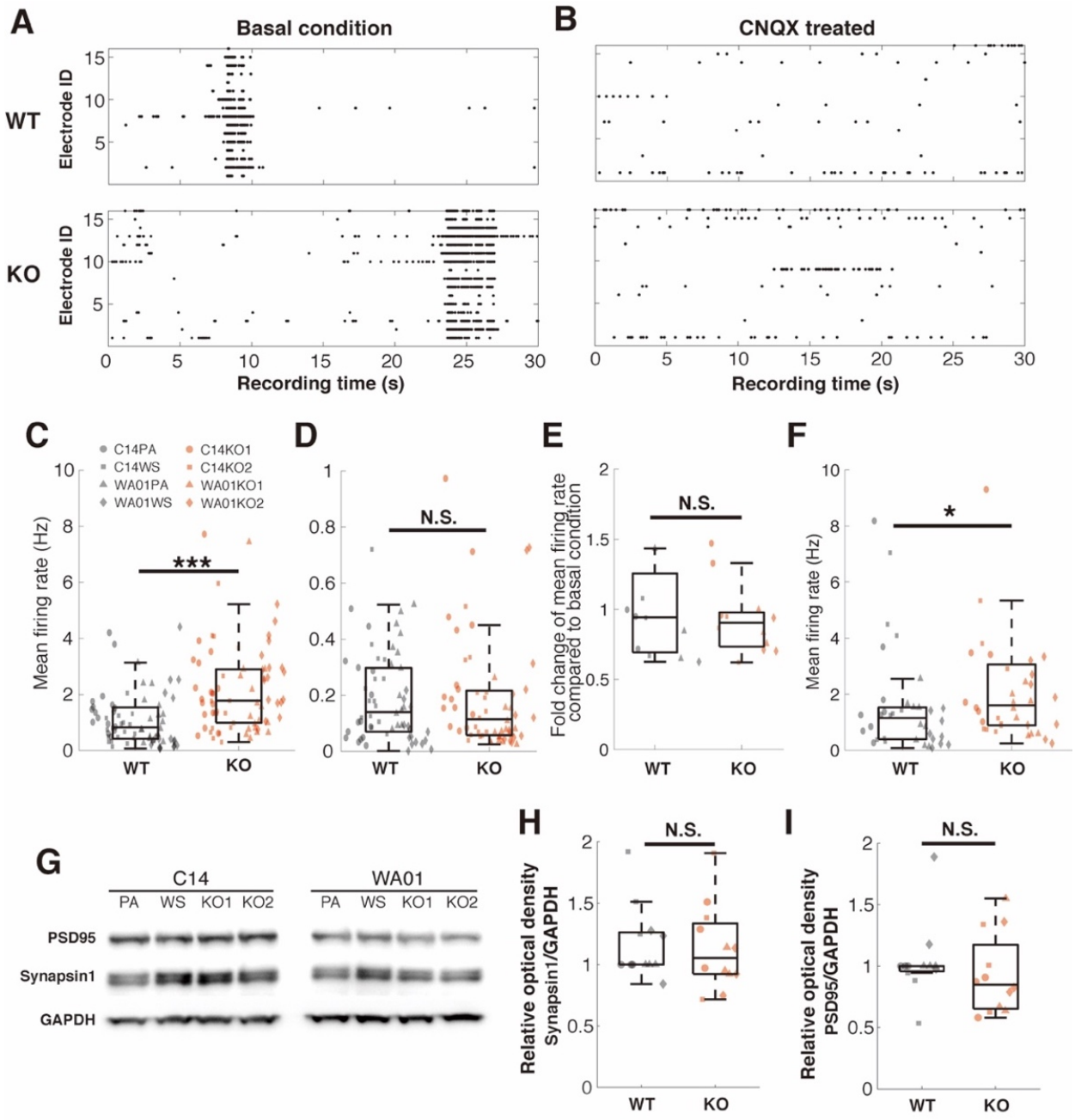

Figure 3-4-4 Electrophysiological characterization of RB1CC1^{KO} iGlutN cultures with MEAs. Example raster plot of spike activities recorded of wild-type and RB1CC1^{KO} iGlutN cultures in basal condition (A) and treated with 10μM CNQX (B). Quantification of spike activities recorded of wild-type and RB1CC1^{KO} iGlutN cultures in basal condition (C), and treated with 10 μM CNQX (D), 10 μM bicuculline (E), and after washing off (F). For each cell line, 9 cultures from 3 independent experiments were analyzed. (G), (H) and (I) Quantification of synaptic markers synapsin1 and PSD95 assessed with western blot, N=3.

3.4.4 RB1CC1^{KO} neurons show altered metabolic processes and dysregulation of cell-adhesion-related processes

Because proteins that directly support the electrophysiological machinery of neurons mostly reside on the membrane. To further investigate which components mediated the observed hyperactivity in RB1CC1^{KO} iGlutN cultures, we did membrane proteomic analysis with 3-week-old human iGlutN and mouse astrocyte cocultures. Among the 2007 proteins identified in all samples, 1249 could be mapped to the human proteome. And two proteins showed significantly lower expression in RB1CC1^{KO} samples than in controls: family with sequence similarity 171 member B (FAM171B) and receptor-type tyrosine-protein phosphatase T (PTPRT) (Figure 3-4-5, A-C). FAM171B is a single-pass type I membrane protein containing a polyglutamine (polyQ) stretch (Tran et al., 2021). It is widely expressed in the brain and can be recruited into polyQ aggregates and thus contribute to the development of polyQ diseases (Kirlin and Goellner, 2019). While it is unclear how FAM171B can be related to RB1CC1, PTPRT could be linked to RB1CC1 via FAK pathways. PTPRT is exclusively expressed in the brain and regulates synapse formation through interaction with cell adhesion molecules (Lim et al., 2009). Its reduction in neurons where FAK is presumably disinhibited by RB1CC1^{KO} indicated a dysregulation of protein tyrosine kinase - phosphatases activity in processes related to cell adhesion. Gene ontology (GO) term enrichment analysis further strengthened this hypothesis. It is shown that the most significantly down-regulated GO term in RB1CC1^{KO} neurons is cell-cell adhesion, and other significantly down-regulated terms are also related to cell-adhesion, e.g., axon development, neuron projection, morphogenesis, and migration. Interestingly, GO terms that are positively enriched point to the other function of RB1CC1: the autophagy. RB1CC1^{KO} neurons show upregulated generation of precursor metabolites and many metabolic processes, as well as expression of proteins involved in redox homeostasis and proteolysis (Figure 3-4-5**,** D). In short, the loss of FAK- and autophagy-related functions of RB1CC1 in human glutamatergic neurons resulted in distinct consequences respectively.

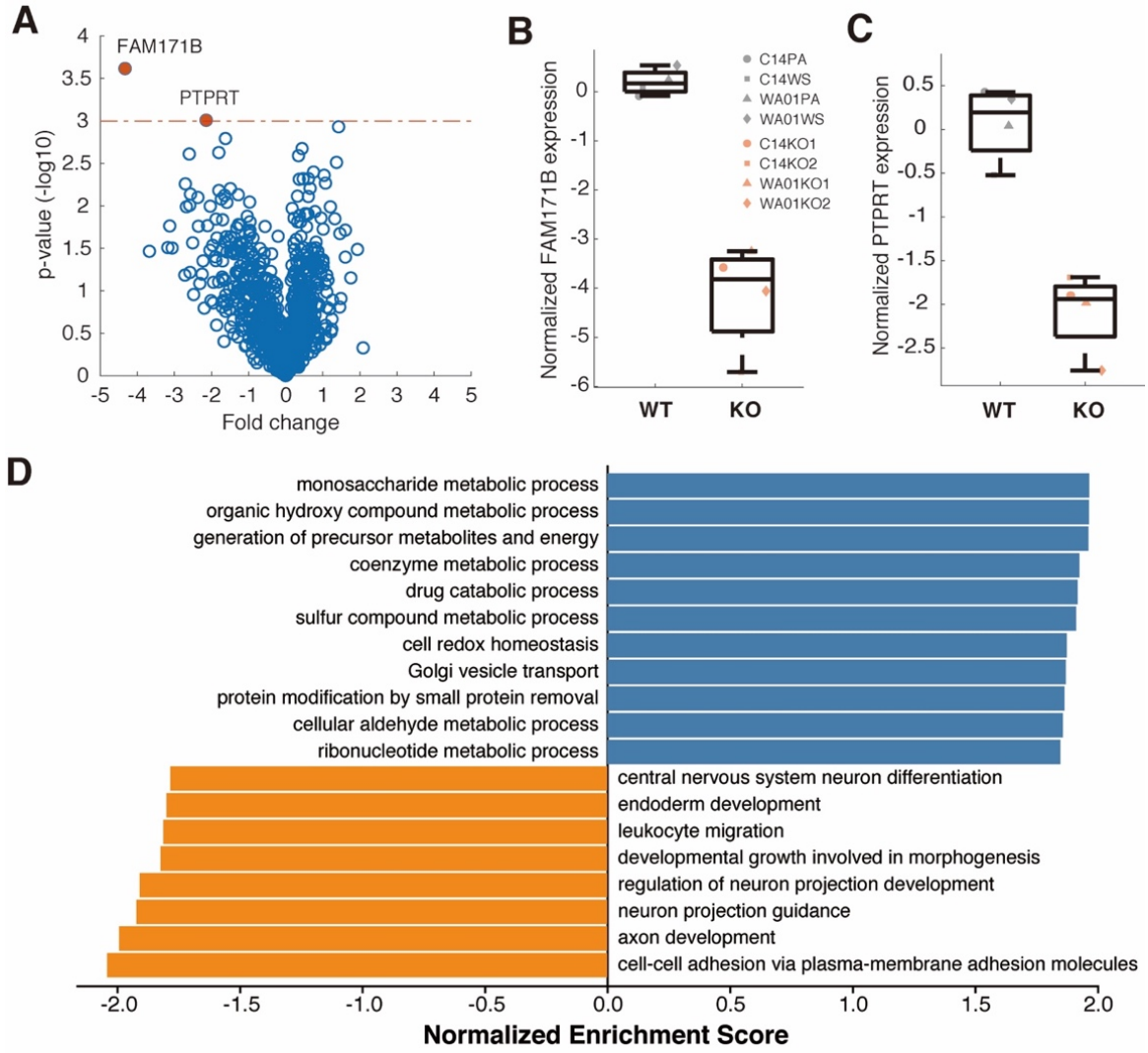

Figure 3-4-5 Membrane proteomic analysis of RB1CC1^{KO} iGlutN cultures. (A) Volcano plot of all 1249 proteins identified. Cut off by FDR $p < 0.05$. FAM171B (B) and PTPRT (C) showed significant down-regulation in RB1CC1^{KO} iGlutN cultures than in controls. (D) Gene set enrichment analysis revealed biological processes that were significantly up- or down-regulated in RB1CC1^{KO} iGlutN cultures compared to controls. One 3-week-old sample from each of the eight cell lines were used for membrane proteomic analysis.

3.4.5 Autophagy-dependent and -independent mechanisms underlying RB1CC1 loss of function mediated hyperactivity in glutamatergic neurons

This study then proceeded to interfere with autophagy- and FAK-dependent pathways in iGlutNs to verify the hypothesis. As RB1CC1 functions as a member of ULK1 complex in autophagy, we reasoned that inhibition of ULK1 complex in wild type cultures should lead

to similar autophagy deficiency as RB1CC1 loss of function. We used MRT68921 (hereafter referred as MRT), which is a potent inhibitor of ULK1 and ULK2, and can block autophagy at early stage and cause accumulation of stalled early autophagosomal structures (Petherick et al., 2015). And for FAK signaling, we treated the iGlutN cultures with PF573228 (hereafter referred as PF228), a potent FAK inhibitor (Slack-Davis et al., 2007), see if the hyperactivity could be rescued in RB1CC1^{KO} iGlutN cultures.

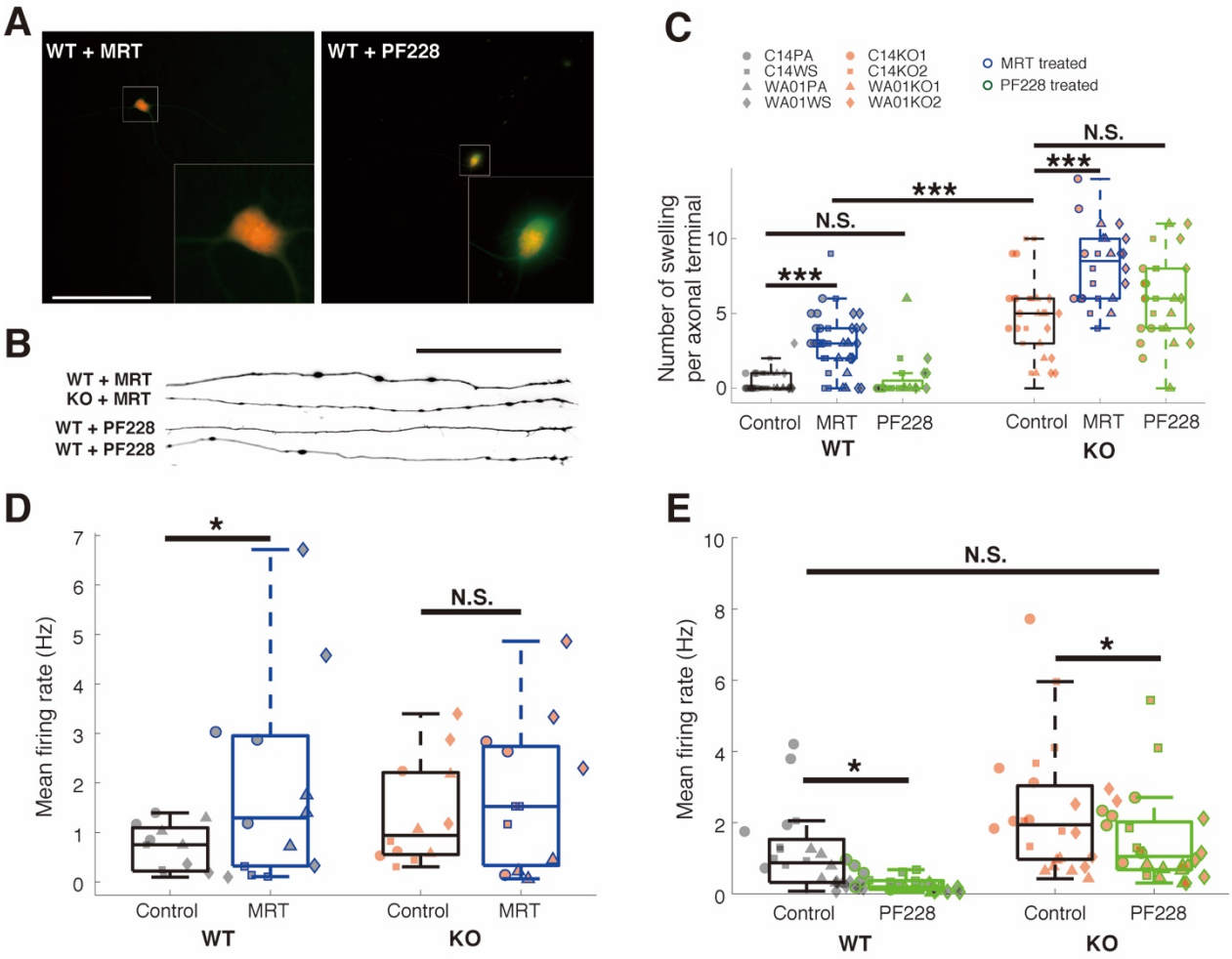

Figure 3-4-6 Morphological and electrophysiological alterations induced by modulators of autophagy-dependent and -independent pathways in wild type and RB1CC1^{KO} iGlutN cultures of 3-week-old. (A) Example live fluorescence microscopy pictures of wild type iGlutN cultures 7 days after transfection with an autophagy reporter plasmid. (B) Examples from inverted live fluorescence pictures of an axonal terminal in wild type iGlutN cultures treated with 3.5 μM MRT or 1 μM PF228 for 3 weeks. (C) Quantification of axonal swellings in iGlutN cultures with and without modulators treatment. For each condition, >20 axons from 2 independent experiments were analyzed. (D) and (E) Quantification of spike activities recorded from iGlutN cultures in basal medium or treated with modulators.

The two chemicals were applied all along after reseeding for 3-4 weeks. MRT arrested autophagy at the initial stage in wild type iGlutN cultures, whereas PF228 did not, both of which were expected (Figure 3-4-6, A). MRT also led to axonal swellings in control iGlutN cultures, of which the number was significantly higher than in control conditions (2.99 ± 0.2818 vs. 0.0685 ± 0.3043, $p < 0.0001$), but not as prominent as those observed in RB1CC1^{KO} cultures in control conditions (2.99 ± 0.3116 vs. 5.04 ± 0.3116, $p < 0.0001$). MRT also further increased the number of axonal swellings in RB1CC1^{KO} cultures (5.04 ± 0.3116 vs. 7.9605 ± 0.3266, $p < 0.0001$,), indicating an additive effect. By contrast, PF228 treatment did not lead to a significant difference in axonal swelling in wild type ($p = 0.568$), or RB1CC1^{KO} ($p = 0.568$) iGlutN cultures (Figure 3-4-6, B and C). As for electrophysiological properties, MRT treatment led to marginally but significantly higher activity in wild-type iGlutN cultures (1.352 ± 0.088 Hz vs. 1.755 ± 0.012 Hz, $p = 0.0264$, trailed t-test), whereas in RB1CC1^{KO} cultures no significant effect could be observed ($p = 0.2259$, Figure 3-4-6, D). In comparison, PF228 treatment led to a decrease of spike activity in both wild type (1.418 ± 0.278 Hz vs. 0.393 ± 0.278 Hz, $p = 0.0103$) and RB1CC1^{KO} cultures (2.395 ± 0.278 Hz vs. 1.37 ± 0.278 Hz, $p = 0.0159$). Interestingly, PF228 treatment brought the activity in RB1CC1^{KO} iGlutN cultures to a comparable level of that of wild-type cultures in the control conditions ($p = 0.9996$), suggesting a successful rescue (Figure 3-4-6**,** E). Together, these results indicate that autophagy deficiency leads to axonal swellings in RB1CC1^{KO} iGlutNs, whereas both autophagy deficiency and FAK disinhibition could lead to hyperactivity.

4. Discussion

4.1 Basic characterization of forward-programmed human neuronal networks

Transcription factor-based forward programming enables the generation of homogenous excitatory and inhibitory neurons from hPSCs as well as the composition of defined neuronal networks. Forward-programmed human neurons inside these networks showed expected responses to glutamate receptor and GABA receptor antagonists, confirming the presence of functional excitatory and inhibitory synapses. Overall, network activity increased within the first two weeks before reaching a plateau phase after 3-6 weeks post-plating. While synchronized NBs could be observed in all conditions containing glutamatergic neurons, cultures with a higher E/I ratio, a higher density, and more maturity showed significantly stronger NBs. Therefore, the strength of NBs could be a distinctive feature to characterize the functional state of *in vitro* neuronal networks forward programmed from hPSCs. This is in accordance with a recent study employing similar techniques (Mossink et al., 2021a), where they found the duration of NB is a distinctive feature of human *in vitro* network activity.

In neurons, action potentials are initiated at the initial segment of the axon upon the opening of voltage-gated sodium channels after membrane potential reaches their activation thresholds (Shu et al., 2007). A typical cortical neuron has a much lower resting potential (ca. -70 mV) than the threshold of sodium channels (ca. -55 mV), meaning it will not fire by itself without external stimulation. However, it is common both *in vivo* and *in vitro* that some neurons have spontaneous spiking activity (Turrigiano et al., 1995; Tsodyks, 1999). While some spontaneous activity is responsible for essential physiological functions, e.g. ‘pacemakers’ (Ramirez et al., 2004), other forms may reflect an immature or pathological state. For example, immature neurons usually do not have enough transporters to pump ions across the membrane in order to lower the threshold, genetic deficiencies related to lipid organization may lead to a too ‘leaky’ membrane that cannot be polarized enough, or mutant voltage-gated sodium channels may simply have a lower threshold (Blankenship and Feller, 2010). Regardless of the reasons, previous work has revealed that a significant proportion of the induced neurons can fire spontaneously (Rhee et al., 2019a) and are the trigger of all network-level phenomena.

NBs are almost always observable in dissociated neuronal cultures, yet are rare events in a healthy brain (le Feber, 2019). Lack of external input and random connections are thought to be the reason for the difference (Eytan and Marom, 2006). One of the original objectives of this work was to see how different E/I ratios could affect NB activity. Although a greater proportion of inhibitory neurons in a network led to less prominent NBs, they were unable to eliminate NB when in a proportion of up to 75%. These findings underline the importance of structural organization for maintaining the functional E/I balance in the nervous system. While these *in vitro* cultures need further improvement to resemble their *in vivo* counterparts more closely, it represents a valuable contribution towards personalized *in vitro* studies of the human neural system.

Previous computational modeling work suggested that glutamatergic synapses play a critical role in the initiation of NBs, and STD leads to the cease and interval of NBs (Tsodyks et al., 2000). This was confirmed with the *in silico* model proposed in section 3.1.2. Here, a primary framework of how functional activity could emerge and develop in forward programmed neuronal cultures was established. There are several key components in the framework: (1) A sub-group of neurons could generate spontaneous action potentials. (2) Neurons were linked by increasing the number and strength of synapses during development, which gave rise to network-level phenomena. (3) Synaptic neural transmitter vesicle depletion-mediated short-term depression was found to be important for NBs. (4) GABAergic inhibition in a randomly connected network had a modulatory effect on NBs.

4.2 Nonlinear response of neuronal cultures to repetitive stimulation due to local synaptic fatigue and its implications in brain modulation

The sporadic NB response of neuronal networks to high-frequency local stimulations reflects the intrinsic nonlinearity of the nervous system. One early study reported the response of rat cortical neuronal culture to different frequencies of stimulation, which was similar to the results shown here (Tal et al., 2001). The authors attributed this phenomenon to the mechanism of excitability on a molecular level. Later, Wagenaar et al. explored how to control bursts in rat cortical neuronal culture with different patterns of stimulation, including single-site and multi-site stimulations at different frequencies (Wagenaar, 2005). Their results were also largely in line with the present work, yet they

did not investigate the mechanism of these phenomena. The present work shows this phenomenon can emerge without any change in excitability of single neurons, and an STD-mediated local circuit depletion mechanism led to the sporadic response of neuronal cultures to high-frequency local stimulation.

Direct or indirect interference with the nervous system is necessary for both fundamental and clinical neuroscience studies. Oftentimes, however, the exact mechanisms by which external stimulation can modulate neural networks are unclear. Interestingly, one of the brain modulation technique, the transcranial magnetic stimulation (TMS), shares some similarities with the present work. Typical TMS applications deliver pulse stimulations at a frequency between 1Hz and 5Hz (Fitzgerald et al., 2006; Klomjai et al., 2015). A recent study showed that magnetic pulse elicits a similar effect on the single-cell level as found in the present study (Romero et al., 2019). While most TMS studies focus on the transient effect of single pulse stimulation or the long-term effect of a train of repetitive simulations, there are two early studies that reported the response profile of single stimulations within a train of repetitive TMS (Valzania et al., 1994; Jennum et al., 1995). Both studies reported that low-frequency stimulation on the motor cortex can elicit robust motor evoked potentials (MEP) recorded at the abductor pollicis brevis muscle, yet high-frequency stimulation only resulted in sporadic MEPs. Although MEPs originate from descending tracts of the motor pathway, which is intrinsically different from NBs in cortical neuronal cultures, the net patterns are strikingly similar to the results presented here. This suggests common mechanisms are at play in both cases, most likely the synaptic short-term depression. In addition, they reported higher critical frequency at 5-10 Hz, which could be explained by the structural differences of the nervous system in the study. In neuronal cultures, recurrent activation within a single NB could drive the RRP to a very low level. In comparison, repetitive TMS elicits motor evoked potentials via unidirectional descending tracts of motor pathway, thus higher stimulation frequency is needed to deplete the RRP to a threshold level.

Accompanied with computational modeling, a possible mechanism for the response of a human nervous system to stimulations was established. Although the work is based on *in vitro* neuronal cultures and electrical pulse stimulation and recording, two important corollaries are applicable in all neural stimulation techniques and are especially applicable

for techniques employing pulse trains of stimulation such as TMS (Romero et al., 2019), deep brain stimulation (Kringelbach et al., 2007), and optogenetic implements (Mattis et al., 2012). First, in a repetitive stimulation paradigm, only a limited number of stimulations can elicit a successful or effective whole-scale response. The second corollary, based on the first, is that if a relatively large network is to be modulated with repetitive stimulations, distributed multi-site stimulation should yield a more reliable outcome.

4.3 A novel theoretical framework of epileptiform activity observed in forward programmed human glutamatergic neuronal networks

A nested network super-burst phenomenon, i.e., NSB, which emerged from highly excitatory neuronal networks was systematically investigated. It is scientifically and clinically significant due to their striking similarity with 3-Hz epileptic seizures. The existence of this phenomenon could challenge the common belief that GABAergic synapses are directly involved in the generation of 3 Hz spike-and-wave oscillations (Destexhe and Sejnowski, 1995) and the cessation of epileptic seizures when inhibitory neurons ‘regain’ control (Boido et al., 2014; de Curtis and Avoli, 2015). This claim is supported by the finding that the inhibitory population was controlled to a minimum level (<5%) (Rhee et al., 2019b) and that the application of bicuculline had no observable effect.

Based on the initial *in silico* work, a modified computational model which demonstrates two-order RRP recovery dynamics (Guo et al., 2015) and activity-dependent short-term facilitation was established. The randomly connected homogenous excitatory neuronal network with corresponding mechanisms can largely recapitulate the observed NSBs. These findings confirmed that GABAergic inhibition and dedicated defined network connections are not necessary for generating 3-Hz seizure-like activity (Destexhe, 1998). In fact, the homogeneity and structurelessness of the proposed framework makes it a good model for comprehensive assessment of neuronal function, as well as making it easier to directly link neuronal properties such as ion channels, transporters, and synaptic functions to circuit and network activities.

Further exploration of the biological basis of the proposed model suggests that: (1) the recovery time constant of NSBs fits that of slow components of RRP recovery (SRP) (Rizzoli and Betz, 2005; Neher, 2015); (2) actin mediates the replenishment of fast components of RRP (FRP), of which inhibition appears to attenuate NSB strength but not

its recovery; (3) PDBu increases synaptic vesicle releasing probability, which resulted in a non-linear alteration of the overall network activity and ultimately abolished NSBs. Glutamate depletion/replenishment and asynchronous release have been proposed to modulate synchronized bursting activity in slice preparations (Staley et al., 1998; Jones et al., 2007). In the earlier work, the authors documented two distinguished time constants of glutamate recovery and bursting strength, with the latter only manifesting after GABA blockage. They did not, however, point out the sequential or hierarchy relationship of the two processes. It is likely that with inhibition NBs could only proceed within the 'first FRP cycle' because GABA release counteracted the asynchronous release-mediated facilitation and no further burst could be induced. Without GABAergic inhibition, a burst or super-burst could proceed until the bifurcation point where facilitation decay outpaced FRP replenishment. It has been revealed that there are distinct steps before presynaptic vesicles could be primed and readied for release (Rizzoli, 2014; Neher and Brose, 2018). These works were mainly performed on the single cell level with artificial manipulations of presynaptic releasing. How these steps may manifest on the macro-network level and modulate neural activities under physiological conditions has yet to be elucidated. As aforementioned, the present work directly links synaptic properties to network level activity.

Results from experiments with two anti-epileptic drugs (AEDs), CBZ and LEV, indicated their different mechanism of action. The hypothesis that LEV promotes vesicle sustainability in GABAergic synapses (Ohno and Tokudome, 2017) could be investigated in the future with iGlutN-iGABAN co-cultures. It has also been suggested that to produce an NSB, the network needs to be within a relatively narrow parameter space. The fact that all cell lines developed NSBs indicated that this could be a result of intrinsic developmental coordination. Of note, it was also shown that tonic-clonic transition in a seizure-like processes happens as a probability depending on the availability of synaptic vesicles and could be bi-directional. Therefore, the present platform could facilitate the study of epileptic seizures in many ways.

In summary, these results have potential significance in several aspects: (1) a novel model based on human forward programmed neuronal cultures was established which could serve as a research platform for novel AED screening; (2) these results elucidate a simple yet mathematically accurate mechanism of seizure termination based solely on

glutamatergic synapses; (3) these results support the theory of sequential steps in RRP replenishment under physiological conditions and at the macro-network level.

4.4 Loss of function of RB1CC1 in human pluripotent stem cell-derived neurons leads to axonal pathology and hyperactivity

It has been proposed that transient activation of autophagy is required for somatic cell reprogramming to pluripotency (He et al., 2012; Wang et al., 2013b), and that autophagy is highly active in pluripotent stem cells (Sotthibundhu et al., 2016). Yet to the best of the author's knowledge, no hPSC line with canonical autophagy-related gene (ATG) knockout has been reported in the literature so far. Therefore, it is unknown whether autophagy is needed for pluripotency maintenance. Here, hPSC lines with loss of function of RB1CC1, one of the core ATGs, were established. Although it is beyond the scope of this study, the present data suggests that, at least in the short-term, RB1CC1 loss of function does not lead to an impaired self-renewal or observable pluripotency marker alteration, nor does it appear to impair the forward programming from hPSC to forebrain glutamatergic neurons.

Axonal swelling (or 'beading') is a hallmark of axonopathy that has been documented since as early as Ramon y Cajal (Ramon y Cajal, 1928), which is usually followed by axonal retraction and synaptic pathology (Yang et al., 2013). The causes of this phenomenon varies from toxins and genetic defects to inflammation and metabolic disturbances, which eventually impairs axonal transportation, and leads to jamming and accumulation of disorganized neurofilaments, microtubules, organelles, and multi-lamellar vesicles (Lin et al., 2003; Coleman, 2005). Interestingly, both insufficient and excessive autophagy could contributes to axonal degeneration (Wang et al., 2018). In neurons, autophagy follows pathways not differently from that have been established in yeast, yet with distinct spatial patterns (Maday and Holzbaur, 2014; Stavoe and Holzbaur, 2019). In axons, autophagosomes form at distal growth cones, and have to be transported retrogradely towards soma to fuse with lysosome there, which is necessary for the following acidification and the degradation of engulfed cargos (Maday et al., 2012; Fu et al., 2014). Whereas in soma and dendrite, autophagosomes are formed and also confined locally along their lifetime (Maday and Holzbaur, 2016). This is in line with the observation with the autophagy reporter assay, where acidized autophagy vacuoles could be robustly observed near or within the soma of wild type iGlutNs, but not in RB1CC1^{KO} or MRT

treated neurons. It was also showed that blockage of autophagy initiation, either by RB1CC1 loss of function mutation or ULK1 inhibition, could lead to pathological axonal swellings. These observation is in agreement with a previous report that axonal swelling could be observed in cerebellar neurons lacking RB1CC1 (Liang et al., 2010). However, a recent study did not reveal significant axonal swelling induction in RB1CC1 knock-down neurons, but only in ATG5 and ATG16L1 knock-out neurons (Negrete-Hurtado et al., 2020). This could possibly be due to the insufficiency of shRNA-mediated knock-down of RB1CC1. RB1CC1^{KO} induced autophagy deficiency also likely leads to a shift of metabolic and redox homeostasis as well as proteolysis in human glutamatergic neurons. Despite the blockage of autophagy initiation, accumulation of p62, and initial axonopathy, no major difference in axonal or dendrite growth has been observed in RB1CC1^{KO} iGlutNs. However, these findings could be limited by the relatively early time point these observation were made, and/or due to nutrient-rich in vitro system, which could make autophagy functionally disposable. Future studies with long-term characterizations and/or autophagy-inducing conditions are therefore needed for a comprehensive understanding of the function of RB1CC1 in neurons.

RB1CC1^{KO} did not compromise the electrophysiological function of iGlutNs in the present work either, rather, it led to hyperactivity that can be attributed to stronger glutamatergic synaptic transmission. And data from MRT-treated cultures suggested that autophagy deficiency could also have played a role. Previous studies have reported that autophagy blockage could lead to stronger overall synaptic transmission by regulating presynaptic vesicles (Hernandez et al., 2012), or reducing spine pruning (Tang et al., 2014). Recently, Lieberman et al. reported that loss of autophagy resulted in hyperexcitability of a specific type of spiny projection neurons in striatum, which might be due to reduced function of the inwardly rectifying potassium channel, Kir2 (Lieberman et al., 2020). And Kuijpers et al. found that autophagy deficiency led to gain of synaptic neurotransmission at glutamatergic synapses in CA1 and CA3 of the hippocampus, which was due to elevated calcium release from accumulated endoplasmic reticulum (Kuijpers et al., 2021). No significant difference in synaptic protein quantification between RB1CC1^{KO} and wild type neurons was observed in the present work. But the other pathways were not ruled out in the present study, therefore it needs to be further explored which mechanisms mediated autophagy deficiency-induced hyperactivity in the present system. In addition,

data indicates that another function of RB1CC1, i.e., FAK inhibition, could also modulate neuronal activity. FAK regulates dendrite arborization under the control of protocadherins (Garrett et al., 2012; Keeler et al., 2015; Molumby et al., 2016). And disruption of this pathway has recently been shown in iPSC-derived cortical interneurons from schizophrenia patients (Shao et al., 2019). RB1CC1^{KO} induced FAK disinhibition also likely leads to the down-regulation of PTPRT and dysregulation of cell-adhesion-related processes. Cell-adhesion is crucial for the morphological development, neurite outgrowth, migration, and other functions of neurons (Honig and Shapiro, 2020; Tan and Eroglu, 2021). Although no significant difference in neurite outgrowth between RB1CC1^{KO} and wild type neurons was observed, the successful rescue of hyperactivity by FAK re-inhibition in RB1CC1^{KO} neurons suggested that other mechanisms could have played a role. Future studies focusing on cell-adhesion related processes, especially FAK and PTPRT signaling pathways, should be helpful to find an answer.

Human brain imaging studies have consistently observed hippocampal hyperactivity in schizophrenia patients (Talati et al., 2014, 2015; Tregellas et al., 2014). It is also proposed that hippocampal hyperactivity could mediate both positive symptoms and cognitive impairments in schizophrenia patients (Zierhut et al., 2010; Tregellas et al., 2014; Wolff et al., 2018) and could present a possible target for intervention (Perez and Lodge, 2013; Perez et al., 2013; Smucny et al., 2015; Kätzel et al., 2020). Several mechanisms have been proposed regarding the origin of hippocampal hyperactivity, e.g., glutamate (Schobel et al., 2013), GABA (Heckers and Konradi, 2015), or dopamine dysregulation (Lodge and Grace, 2007). These observations implicated that RB1CC1 loss of function could mediate hyperactivity in glutamatergic neurons via autophagy-dependent and/or -independent pathways, and thus could increase the risk of developing schizophrenia.

4.5 Outlook

One of the unexpected findings in this study was the observation of seizure-like activity in human glutamatergic neuronal networks, from which a ‘pure presynaptic’ framework of epileptiform activity developed thereafter. This framework could be further developed at both lower and higher levels. Electrophysiological patch clamping on single cells or synapses would provide more detailed information on the dynamics of the observed seizure-like activity and could further verify the proposed mechanisms. The hypothesis

that levetiracetam could inhibit seizure generation by preferably promoting neurotransmitter vesicle mobilization in GABAergic inhibitory synapses should also be investigated with basic electrophysiological implementations. The antiepileptic effect of actin inhibitors, e.g., cytochalasin D, should be tested with established *ex vivo* or *in vivo* animal models of epilepsy.

The specific roles of RB1CC1 in human PSC-derived glutamatergic neurons also need to be further investigated with basic electrophysiological characterizations. Specifically, it is yet to be found out which mechanisms mediated the strengthened glutamatergic activation in $RB1CC1^{KO}$ neurons and how these to-be-defined mechanisms could be linked to autophagy and FAK pathways. It is unclear whether a gain of function or a reduction/loss of function of RB1CC1 could promote the development of schizophrenia and other neuropsychiatric conditions, either of which could be pathogenic. Therefore, future work with patient-specific mutations of RB1CC1 is needed in order to obtain a clearer picture.

5. Abstract

This study established an *in vitro* platform based on forward programmed neuronal cultures derived from human pluripotent stem cells. Firstly, the electrophysiological properties of the obtained neuronal networks were systematically characterized with multi-electrode arrays. The obtained data were then fed into *in silico* computational models of neuronal networks, that were able to reproduce key experimental observations, including network bursts and expected response to simulated synaptic modulations. The combined *in vitro* and *in silico* approach helped to elucidate a possible mechanism by which local synaptic depletion leads to sporadic responses of the neural networks to repetitive external stimulations. The potential implications of these findings on common brain modulation techniques were discussed. Secondly, a seizure-like nested network activity observed in highly pure glutamatergic neuronal cultures was described. In-depth *in vitro* exploration of this phenomenon combined with *in silico* simulation resulted in a novel theoretical framework of epileptiform activities observed in human neuronal cultures, which was characterized by pure excitatory composition, unstructured network organization, and a hierarchy of presynaptic vesicle pools. The proposed framework elucidates a possible mechanism which may relate to how seizures initiate, evolve, and terminate. It was also shown that forward programmed human neuronal cultures could be used to dissect the pharmacological basis of known anti-epileptic drugs in addition to potentially providing a method to screen for novel ones. Thirdly, to explore the utilization of human forward programmed neurons in brain disease modelling, this study generated isogenic neural cultures derived from human pluripotent stem cells carrying a loss of function of mutation of RB1CC1, a gene that is associated with schizophrenia. Neurons lacking RB1CC1 showed autophagy deficiency and pathological axonal swellings, a phenomenon that could be partially phenocopied with an ULK1/2-specific autophagy inhibitor in control cells. Moreover, monitoring electrophysiological activities of neuronal cultures on multi-electrode arrays revealed that RB1CC1-deficiency resulted in a hyperactive network. Pharmacological inhibition of FAK signaling could normalize the hyperactivity of RB1CC1-deficient neurons, whereas inhibition of autophagy in control neurons led to hyperactivity. These results suggest that both impaired autophagy and disinhibition of FAK contribute to the hyperactivity phenotype of RB1CC1-deficient neuronal networks. The observed consequences of RB1CC1-deficiency in human

glutamatergic neurons might help to understand cellular pathomechanisms contributing to neuropsychiatric conditions. In summary, this thesis characterized human forward programmed neuronal cultures derived from pluripotent stem cells and demonstrated its versatility in studies of neural modulation, epilepsy, and psychiatric diseases.

6. List of figures

7. References

Abbi S, Ueda H, Zheng C, Cooper LA, Zhao J, Christopher R, Guan J-L. Regulation of focal adhesion kinase by a novel protein inhibitor FIP200. Mol Biol Cell 2002; 13:3178–3191

Alrabiah H. Levetiracetam. In: . Profiles of Drug Substances, Excipients and Related Methodology. Academic Press Inc., 2019: 167–204

Ambrósio AF, Soares-da-Silva P, Carvalho CM, Carvalho AP. Mechanisms of action of carbamazepine and its derivatives, oxcarbazepine, BIA 2-093, and BIA 2-024. Neurochem Res 2002; 27:121–130

Amin H, Marinaro F, De Pietri Tonelli D, Berdondini L. Developmental excitatory-to-inhibitory GABA-polarity switch is disrupted in 22q11.2 deletion syndrome: a potential target for clinical therapeutics. Sci Rep 2017; 7:15752

Antonio LL, Anderson ML, Angamo EA, Gabriel S, Klaft ZJ, Liotta A, Salar S, Sandow N, Heinemann U. In vitro seizure like events and changes in ionic concentration. J Neurosci Methods 2016; 260:33–44

Arcangeli A, Becchetti A, Mannini A, Mugnai G, De Filippi P, Tarone G, Del Bene MR, Barletta E, Wanke E, Olivotto M. Integrin-mediated neurite outgrowth in neuroblastoma cells depends on the activation of potassium channels. J Cell Biol 1993; 122:1131–1143

Arnsten AFT. Stress signalling pathways that impair prefrontal cortex structure and function. Nat Rev Neurosci 2009; 10:410–422

Babu LPA, Wang HY, Eguchi K, Guillaud L, Takahashi T. Microtubule and actin differentially regulate synaptic vesicle cycling to maintain high-frequency neurotransmission. J Neurosci 2020; 40:131–142

Badel L, Lefort S, Berger TK, Petersen CCH, Gerstner W, Richardson MJE. Extracting non-linear integrate-and-fire models from experimental data using dynamic I-V curves. Biol Cybern 2008; 99:361–370

Bai X, Vestal M, Berman R, Negishi M, Spann M, Vega C, Desalvo M, Novotny EJ, Constable RT, Blumenfeld H. Dynamic Time Course of Typical Childhood Absence Seizures: EEG, Behavior, and Functional Magnetic Resonance Imaging. J Neurosci 2010;

30:5884 LP – 5893

Bakkum DJ, Frey U, Radivojevic M, Russell TL, Müller J, Fiscella M, Takahashi H, Hierlemann A. Tracking axonal action potential propagation on a high-density microelectrode array across hundreds of sites. Nat Commun 2013; 4:1–12

Bakkum DJ, Radivojevic M, Frey U, Franke F, Hierlemann A, Takahashi H. Parameters for burst detection. Front Comput Neurosci 2014; 7:193

Ballini M, Müller J, Livi P, Chen Y, Frey U, Stettler A, Shadmani A, Viswam V, Jones IL, Jäckel D. A 1024-channel CMOS microelectrode array with 26,400 electrodes for recording and stimulation of electrogenic cells in vitro. IEEE J Solid-State Circuits 2014; 49:2705–2719

Bamba N, Chano T, Taga T, Ohta S, Takeuchi Y, Okabe H. Expression and regulation of RB1CC1 in developing murine and human tissues. Int J Mol Med 2004; 14:583–590

Barbey AK. Network Neuroscience Theory of Human Intelligence. Trends Cogn Sci 2018; 22:8–20

Bartholome O, Van Den Ackerveken P, Gil JS, Bonardeaux O de la B, Leprince P, Franzen R, Rogister B. Puzzling out synaptic vesicle 2 family members functions. Front Mol Neurosci 2017; 10:148

Basu J, Betz A, Brose N, Rosenmund C. Munc13-1 C1 Domain Activation Lowers the Energy Barrier for Synaptic Vesicle Fusion. J Neurosci 2007; 27:1200–1210

Bauer PR, Thijs RD, Lamberts RJ, Velis DN, Visser GH, Tolner EA, Sander JW, Lopes da Silva FH, Kalitzin SN. Dynamics of convulsive seizure termination and postictal generalized EEG suppression. Brain 2017; 140:655–668

Bazzi MD, Nelsestuen GL. Properties of the Protein Kinase C-Phorbol Ester Interaction. Biochemistry 1989; 28:3577–3585

Bazzigaluppi P, Ebrahim Amini A, Weisspapir I, Stefanovic B, Carlen P. Hungry Neurons: Metabolic Insights on Seizure Dynamics. Int J Mol Sci 2017; 18:2269

Benítez-King G, Riquelme A, Ortíz-López L, Berlanga C, Rodríguez-Verdugo MS, Romo F, Calixto E, Solís-Chagoyán H, Jímenez M, Montaño LM, Ramírez-Rodríguez G, Morales-Mulia S, Domínguez-Alonso A. A non-invasive method to isolate the neuronal

linage from the nasal epithelium from schizophrenic and bipolar diseases. J Neurosci Methods 2011; 201:35–45

Biedler JL, Schachner M. Multiple Neurotransmitter Synthesis by Human Neuroblastoma Cell Lines and Clones. Cancer Res 1978; 38:3751–3757

Bitanihirwe BKY, Woo T-UW. Oxidative stress in schizophrenia: An integrated approach. Neurosci Biobehav Rev 2011; 35:878–893

Blankenship AG, Feller MB. Mechanisms underlying spontaneous patterned activity in developing neural circuits. Nat Rev Neurosci 2010; 11:18–29

Boido D, Gnatkovsky V, Uva L, Francione S, De Curtis M. Simultaneous enhancement of excitation and postburst inhibition at the end of focal seizures. Ann Neurol 2014; 76:826–836

Borgmann-Winter K, Willard SL, Sinclair D, Mirza N, Turetsky B, Berretta S, Hahn C-G. Translational potential of olfactory mucosa for the study of neuropsychiatric illness. Transl Psychiatry 2015; 5:e527–e527

Bower JM, Beeman D. The book of GENESIS: exploring realistic neural models with the GEneral NEural SImulation System. Springer Science & Business Media.

Brennand KJ, Gage FH. Concise Review: The Promise of Human Induced Pluripotent Stem Cell-Based Studies of Schizophrenia. Stem Cells 2011; 29:1915–1922

Brennand KJ, Simone A, Jou J, Gelboin-Burkhart C, Tran N, Sangar S, Li Y, Mu Y, Chen G, Yu D, McCarthy S, Sebat J, Gage FH. Modelling schizophrenia using human induced pluripotent stem cells. Nature 2011; 473:221–225

Brown AS. Prenatal Infection as a Risk Factor for Schizophrenia. Schizophr Bull 2006; 32:200–202

Brown AS, Susser ES. Prenatal Nutritional Deficiency and Risk of Adult Schizophrenia. Schizophr Bull 2008; 34:1054–1063

Burkitt AN. A Review of the Integrate-and-fire Neuron Model: I. Homogeneous Synaptic Input. Biol Cybern 2006; 95:1–19

Cannon M, Jones PB, Murray RM. Obstetric Complications and Schizophrenia: Historical and Meta-Analytic Review. Am J Psychiatry 2002; 159:1080–1092

Cantor-Graae E, Selten J-P. Schizophrenia and Migration: A Meta-Analysis and Review. Am J Psychiatry 2005; 162:12–24

Capitanio JP, Emborg ME. Contributions of non-human primates to neuroscience research. Lancet 2008; 371:1126–1135

Carnevale NT, Hines ML. The NEURON book. Cambridge University Press.

Casella JF, Flanagan MD, Lin S. Cytochalasin D inhibits actin polymerization and induces depolymerization of actin filaments formed during platelet shape change. Nature 1981; 293:302–305

Caviness VS, Takahashi T, Nowakowski RS. Numbers, time and neocortical neuronogenesis: a general developmental and evolutionary model. Trends Neurosci 1995; 18:379–383

Chambers SM, Fasano CA, Papapetrou EP, Tomishima M, Sadelain M, Studer L. Highly efficient neural conversion of human ES and iPS cells by dual inhibition of SMAD signaling. Nat Biotechnol 2009; 27:275–280

Chano T, Ikebuchi K, Ochi Y, Tameno H, Tomita Y, Jin Y, Inaji H, Ishitobi M, Teramoto K, Nishimura I, Minami K, Inoue H, Isono T, Saitoh M, Shimada T, Hisa Y, Okabe H. Bauer JA, ed RB1CC1 Activates RB1 Pathway and Inhibits Proliferation and Cologenic Survival in Human Cancer. PLoS One 2010; 5:e11404

Chano T, Ikegawa S, Kontani K, Okabe H, Baldini N, Saeki Y. Identification of RB1CC1, a novel human gene that can induce RB1 in various human cells. Oncogene 2002a; 21:1295

Chano T, Kontani K, Teramoto K, Okabe H, Ikegawa S. Truncating mutations of RB1CC1 in human breast cancer. Nat Genet 2002b; 31:285

Chano T, Okabe H, Hulette CM. RB1CC1 insufficiency causes neuronal atrophy through mTOR signaling alteration and involved in the pathology of Alzheimer's diseases. Brain Res 2007; 1168:97–105

Chano T, Saji M, Inoue H, Minami K, Kobayashi T, Hino O, Okabe H. Neuromuscular abundance of RB1CC1 contributes to the non-proliferating enlarged cell phenotype through both RB1 maintenance and TSC1 degradation. Int J Mol Med 2006; 18:425–432

Chen S, Wang C, Yeo S, Liang CC, Okamoto T, Sun S, Wen J, Guan JL. Distinct roles of autophagy-dependent and -independent functions of FIP200 revealed by generation and analysis of a mutant knock-in mouse model. Genes Dev 2016; 30:856–869

Chen Y-C, Ma N-X, Pei Z-F, Wu Z, Do-Monte FH, Keefe S, Yellin E, Chen MS, Yin J-C, Lee G, Minier-Toribio A, Hu Y, Bai Y-T, Lee K, Quirk GJ, Chen G. A NeuroD1 AAV-Based Gene Therapy for Functional Brain Repair after Ischemic Injury through In Vivo Astrocyte-to-Neuron Conversion. Mol Ther 2020; 28:217–234

Cheung AYL, Horvath LM, Grafodatskaya D, Pasceri P, Weksberg R, Hotta A, Carrel L, Ellis J. Isolation of MECP2-null Rett Syndrome patient hiPS cells and isogenic controls through X-chromosome inactivation. Hum Mol Genet 2011; 20:2103–2115

Chiang C-H, Su Y, Wen Z, Yoritomo N, Ross CA, Margolis RL, Song H, Ming G. Integration-free induced pluripotent stem cells derived from schizophrenia patients with a DISC1 mutation. Mol Psychiatry 2011; 16:358–360

Chiappalone M, Bove M, Vato A, Tedesco M, Martinoia S. Dissociated cortical networks show spontaneously correlated activity patterns during in vitro development. Brain Res 2006; 1093:41–53

Cohen D, Segal M. Network bursts in hippocampal microcultures are terminated by exhaustion of vesicle pools. J Neurophysiol 2011; 106:2314–2321

Coleman M. Axon degeneration mechanisms: commonality amid diversity. Nat Rev Neurosci 2005; 6:889–898

Cong L, Ran FA, Cox D, Lin S, Barretto R, Habib N, Hsu PD, Wu X, Jiang W, Marraffini LA, Zhang F. Multiplex Genome Engineering Using CRISPR/Cas Systems. Science (80-) 2013; 339:819–823

Cooper GM et al. A copy number variation morbidity map of developmental delay. Nat Genet 2011; 43:838–846

Crepeau AZ, Treiman DM. Levetiracetam: A comprehensive review. Expert Rev Neurother 2010; 10:159–171

Crow TJ. ‘The missing genes: what happened to the heritability of psychiatric disorders?’ Mol Psychiatry 2011; 16:362–364

de Curtis M, Avoli M. Initiation, propagation, and termination of partial (Focal) seizures. Cold Spring Harb Perspect Med 2015; 5:1–15

Degenhardt F et al. Duplications in RB1CC1 are associated with schizophrenia; identification in large European sample sets. Transl Psychiatry 2013; 3:e326–e326

Destexhe A. Spike-and-Wave Oscillations Based on the Properties of GABAB Receptors. J Neurosci 1998; 18:9099 LP – 9111

Destexhe A, Sejnowski TJ. G protein activation kinetics and spillover of gamma-aminobutyric acid may account for differences between inhibitory responses in the hippocampus and thalamus. Proc Natl Acad Sci 1995; 92:9515 LP – 9519

Di Lullo E, Kriegstein AR. The use of brain organoids to investigate neural development and disease. Nat Rev Neurosci 2017; 18:573–584

Dimos JT, Rodolfa KT, Niakan KK, Weisenthal LM, Mitsumoto H, Chung W, Croft GF, Saphier G, Leibel R, Goland R, Wichterle H, Henderson CE, Eggan K. Induced Pluripotent Stem Cells Generated from Patients with ALS Can Be Differentiated into Motor Neurons. Science (80-) 2008; 321:1218 LP – 1221

Du Y, Wang J, Jia J, Song N, Xiang C, Xu J, Hou Z, Su X, Liu B, Jiang T, Zhao D, Sun Y, Shu J, Guo Q, Yin M, Sun D, Lu S, Shi Y, Deng H. Human Hepatocytes with Drug Metabolic Function Induced from Fibroblasts by Lineage Reprogramming. Cell Stem Cell 2014; 14:394–403

Ebert AD, Yu J, Rose FF, Mattis VB, Lorson CL, Thomson JA, Svendsen CN. Induced pluripotent stem cells from a spinal muscular atrophy patient. Nature 2009; 457:277–280

Eiraku M, Watanabe K, Matsuo-Takasaki M, Kawada M, Yonemura S, Matsumura M, Wataya T, Nishiyama A, Muguruma K, Sasai Y. Self-Organized Formation of Polarized Cortical Tissues from ESCs and Its Active Manipulation by Extrinsic Signals. Cell Stem Cell 2008; 3:519–532

Errichiello E, Giorda R, Gambale A, Iolascon A, Zuffardi O, Giglio S. RB1CC1 duplication and aberrant overexpression in a patient with schizophrenia: further phenotype delineation and proposal of a pathogenetic mechanism. Mol Genet Genomic Med 2020:1–7

Eytan D, Marom S. Dynamics and Effective Topology Underlying Synchronization in Networks of Cortical Neurons. J Neurosci 2006; 26:8465–8476

Falk A, Heine VM, Harwood AJ, Sullivan PF, Peitz M, Brüstle O, Shen S, Sun Y-M, Glover JC, Posthuma D, Djurovic S. Modeling psychiatric disorders: from genomic findings to cellular phenotypes. Mol Psychiatry 2016; 21:1167–1179

Ferreira TA, Blackman A V., Oyrer J, Jayabal S, Chung AJ, Watt AJ, Sjöström PJ, van Meyel DJ. Neuronal morphometry directly from bitmap images. Nat Methods 2014; 11:982–984

Filomeni G, De Zio D, Cecconi F. Oxidative stress and autophagy: the clash between damage and metabolic needs. Cell Death Differ 2015; 22:377–388

Fitzgerald P, FOUNTAIN S, DASKALAKIS Z. A comprehensive review of the effects of rTMS on motor cortical excitability and inhibition. Clin Neurophysiol 2006; 117:2584–2596

Flitsch LJ, Laupman KE, Brüstle O. Transcription factor-based fate specification and forward programming for neural regeneration. Front Cell Neurosci 2020; 14:121

Flores G, Morales-Medina JC, Diaz A. Neuronal and brain morphological changes in animal models of schizophrenia. Behav Brain Res 2016; 301:190–203

Frega M, Linda K, Keller JM, Gümüş-Akay G, Mossink B, van Rhijn J-R, Negwer M, Klein Gunnewiek T, Foreman K, Kompier N, Schoenmaker C, van den Akker W, van der Werf I, Oudakker A, Zhou H, Kleefstra T, Schubert D, van Bokhoven H, Nadif Kasri N. Neuronal network dysfunction in a model for Kleefstra syndrome mediated by enhanced NMDAR signaling. Nat Commun 2019; 10:4928

Frey U, Sedivy J, Heer F, Pedron R, Ballini M, Mueller J, Bakkum D, Hafizovic S, Faraci FD, Greve F. Switch-matrix-based high-density microelectrode array in CMOS technology. IEEE J Solid-State Circuits 2010; 45:467–482

Fromer M et al. Gene expression elucidates functional impact of polygenic risk for schizophrenia. Nat Neurosci 2016; 19:1442–1453

Fu M, Nirschl JJ, Holzbaur ELF. LC3 Binding to the Scaffolding Protein JIP1 Regulates Processive Dynein-Driven Transport of Autophagosomes. Dev Cell 2014; 29:577–590

Gammoh N, Florey O, Overholtzer M, Jiang X. Interaction between FIP200 and ATG16L1

distinguishes ULK1 complex-dependent and -independent autophagy. Nat Struct Mol Biol 2013; 20:144–149

Gan B, Melkoumian ZK, Wu X, Guan KL, Guan JL. Identification of FIP200 interaction with the TSC1-TSC2 complex and its role in regulation of cell size control. J Cell Biol 2005; 170:379–389

Gan B, Peng X, Nagy T, Alcaraz A, Gu H, Guan J-L. Role of FIP200 in cardiac and liver development and its regulation of TNFα and TSC–mTOR signaling pathways. J Cell Biol 2006; 175:121–133

Ganley IG, Lam du H, Wang J, Ding X, Chen S, Jiang X. ULK1.ATG13.FIP200 complex mediates mTOR signaling and is essential for autophagy. J Biol Chem 2009; 284:12297–12305

Gao R, Penzes P. Common mechanisms of excitatory and inhibitory imbalance in schizophrenia and autism spectrum disorders. Curr Mol Med 2015; 15:146–167

Garcia-Perez E, Lo DC, Wesseling JF. Kinetic isolation of a slowly recovering component of short-term depression during exhaustive use at excitatory hippocampal synapses. J Neurophysiol 2008; 100:781–795

Garrett AM, Schreiner D, Lobas MA, Weiner JA. γ-Protocadherins Control Cortical Dendrite Arborization by Regulating the Activity of a FAK/PKC/MARCKS Signaling Pathway. Neuron 2012; 74:269–276

Gerstner W, Kistler WM, Naud R, Paninski L. Neuronal Dynamics. Cambridge: : Cambridge University Press.

Gibbs FA, Davis H, Lennox WG. The electro-encephalogram in epilepsy and in conditions of impaired consciousness. Arch Neurol Psychiatry 1935; 34:1133–1148

Giovanoli S, Engler H, Engler A, Richetto J, Voget M, Willi R, Winter C, Riva MA, Mortensen PB, Feldon J, Schedlowski M, Meyer U. Stress in Puberty Unmasks Latent Neuropathological Consequences of Prenatal Immune Activation in Mice. Science (80-) 2013; 339:1095–1099

Gladkov A, Grinchuk O, Pigareva Y, Mukhina I, Kazantsev V, Pimashkin A. Cymbalyuk G, ed Theta rhythm-like bidirectional cycling dynamics of living neuronal networks in vitro.

PLoS One 2018; 13:e0192468

Gritsun T, Le Feber J, Stegenga J, Rutten WLC. Experimental analysis and computational modeling of interburst intervals in spontaneous activity of cortical neuronal culture. Biol Cybern 2011; 105:197–210

Gritsun TA, le Feber J, Rutten WLC. Wennekers T, ed Growth Dynamics Explain the Development of Spatiotemporal Burst Activity of Young Cultured Neuronal Networks in Detail. PLoS One 2012; 7:e43352

Gross GW, Rieske E, Kreutzberg GW, Meyer A. A new fixed-array multi-microelectrode system designed for long-term monitoring of extracellular single unit neuronal activity in vitro. Neurosci Lett 1977; 6:101–105

Guo J, Ge J, Hao M, Sun Z, Wu X, Zhu J, Wang W, Yao P, Lin W, Xue L. A Three-Pool Model Dissecting Readily Releasable Pool Replenishment at the Calyx of Held. Sci Rep 2015; 5:9517

Hara T, Mizushima N. Role of ULK-FIP200 complex in mammalian autophagy: FIP200, a counterpart of yeast Atg17? Autophagy 2009; 5:85–87

Hara T, Takamura A, Kishi C, Iemura S, Natsume T, Guan J-L, Mizushima N. FIP200, a ULK-interacting protein, is required for autophagosome formation in mammalian cells. J Cell Biol 2008; 181:497–510

Harrison PJ, Cader MZ, Geddes JR. Reprogramming psychiatry: stem cells and bipolar disorder. Lancet 2016; 387:823–825

Hartley BJ, Tran N, Ladran I, Reggio K, Brennand KJ. Dopaminergic differentiation of schizophrenia hiPSCs. Mol Psychiatry 2015; 20:549–550

He J, Kang L, Wu T, Zhang J, Wang H, Gao H, Zhang Y, Huang B, Liu W, Kou Z, Zhang H, Gao S. An Elaborate Regulation of Mammalian Target of Rapamycin Activity Is Required for Somatic Cell Reprogramming Induced by Defined Transcription Factors. Stem Cells Dev 2012; 21:2630–2641

Heckers S, Konradi C. GABAergic mechanisms of hippocampal hyperactivity in schizophrenia. Schizophr Res 2015; 167:4–11

Heikkilä TJ, Ylä-Outinen L, Tanskanen JMA, Lappalainen RS, Skottman H, Suuronen R,

Mikkonen JE, Hyttinen JAK, Narkilahti S, Heikkila TJ, Yla-Outinen L, Tanskanen JMA, Lappalainen RS, Skottman H, Suuronen R, Mikkonen JE, Hyttinen JAK, Narkilahti S. Human embryonic stem cell-derived neuronal cells form spontaneously active neuronal networks in vitro. Exp Neurol 2009; 218:109–116

Hernandez D, Torres CA, Setlik W, Cebrián C, Mosharov E V., Tang G, Cheng HC, Kholodilov N, Yarygina O, Burke RE, Gershon M, Sulzer D. Regulation of Presynaptic Neurotransmission by Macroautophagy. Neuron 2012; 74:277–284

Hockemeyer D, Jaenisch R. Induced Pluripotent Stem Cells Meet Genome Editing. Cell Stem Cell 2016; 18:573–586

Hodgkin AL, Huxley AF. A quantitative description of membrane current and its application to conduction and excitation in nerve. J Physiol 1952; 117:500–544

Hoffman GE, Schrode N, Flaherty E, Brennand KJ. New considerations for hiPSC-based models of neuropsychiatric disorders. Mol Psychiatry 2019; 24:49–66

Hong G, Lieber CM. Novel electrode technologies for neural recordings. Nat Rev Neurosci 2019; 20:330–345

Honig B, Shapiro L. Adhesion Protein Structure, Molecular Affinities, and Principles of Cell-Cell Recognition. Cell 2020; 181:520–535

Hou P, Li Y, Zhang X, Liu C, Guan J, Li H, Zhao T, Ye J, Yang W, Liu K, Ge J, Xu J, Zhang Q, Zhao Y, Deng H. Pluripotent Stem Cells Induced from Mouse Somatic Cells by Small-Molecule Compounds. Science (80-) 2013; 341:651 LP – 654

Howes OD, McCutcheon R, Owen MJ, Murray RM. The Role of Genes, Stress, and Dopamine in the Development of Schizophrenia. Biol Psychiatry 2017; 81:9–20

Huang YT, Chang YL, Chen CC, Lai PY, Chan CK. Positive feedback and synchronized bursts in neuronal cultures. PLoS One 2017; 12:1–19

Hulshoff Pol HE, Kahn RS. What Happens After the First Episode? A Review of Progressive Brain Changes in Chronically Ill Patients With Schizophrenia. Schizophr Bull 2007; 34:354–366

Hyvärinen T, Hyysalo A, Kapucu FE, Aarnos L, Vinogradov A, Eglen SJ, Ylä-Outinen L, Narkilahti S. Functional characterization of human pluripotent stem cell-derived cortical

networks differentiated on laminin-521 substrate: comparison to rat cortical cultures. Sci Rep 2019; 9:17125

Iismaa SE, Kaidonis X, Nicks AM, Bogush N, Kikuchi K, Naqvi N, Harvey RP, Husain A, Graham RM. Comparative regenerative mechanisms across different mammalian tissues. npj Regen Med 2018; 3:6

Isomura T, Kotani K, Jimbo Y. Cultured Cortical Neurons Can Perform Blind Source Separation According to the Free-Energy Principle. PLoS Comput Biol 2015; 11:1–29

Israel MA, Yuan SH, Bardy C, Reyna SM, Mu Y, Herrera C, Hefferan MP, Van Gorp S, Nazor KL, Boscolo FS, Carson CT, Laurent LC, Marsala M, Gage FH, Remes AM, Koo EH, Goldstein LSB. Probing sporadic and familial Alzheimer's disease using induced pluripotent stem cells. Nature 2012; 482:216–220

Ito D, Tamate H, Nagayama M, Uchida T, Kudoh SN, Gohara K. Minimum neuron density for synchronized bursts in a rat cortical culture on multi-electrode arrays. Neuroscience 2010a; 171:50–61

Ito D, Tamate H, Nagayama M, Uchida T, Kudoh SN, Gohara K. Minimum neuron density for synchronized bursts in a rat cortical culture on multi-electrode arrays. Neuroscience 2010b; 171:50–61

Jennum P, Winkel H, Fuglsang-Frederiksen A. Repetitive magnetic stimulation and motor evoked potentials. Electroencephalogr Clin Neurophysiol Mot Control 1995; 97:96–101

Jiang H, Ren Y, Yuen EY, Zhong P, Ghaedi M, Hu Z, Azabdaftari G, Nakaso K, Yan Z, Feng J. Parkin controls dopamine utilization in human midbrain dopaminergic neurons derived from induced pluripotent stem cells. Nat Commun 2012; 3:668

Jinek M, Chylinski K, Fonfara I, Hauer M, Doudna JA, Charpentier E. A programmable dual-RNA–guided DNA endonuclease in adaptive bacterial immunity. Science (80-) 2012; 337:816–821

Jirsa VK, Stacey WC, Quilichini PP, Ivanov AI, Bernard C. On the nature of seizure dynamics. Brain 2014; 137:2210–2230

Jones J, Stubblefield EA, Benke TA, Staley KJ. Desynchronization of glutamate release prolongs synchronous CA3 network activity. J Neurophysiol 2007; 97:3812–3818

Kamioka H, Maeda E, Jimbo Y, Robinson HPC, Kawana A. Spontaneous periodic synchronized bursting during formation of mature patterns of connections in cortical cultures. Neurosci Lett 1996; 206:109–112

Kätzel D, Wolff AR, Bygrave AM, Bannerman DM. Hippocampal Hyperactivity as a Druggable Circuit-Level Origin of Aberrant Salience in Schizophrenia. Front Pharmacol 2020; 11

Kawasaki F, Stiber M. A simple model of cortical culture growth: Burst property dependence on network composition and activity. Biol Cybern 2014; 108:423–443

Keeler AB, Schreiner D, Weiner JA. Protein Kinase C Phosphorylation of a γ-Protocadherin C-terminal Lipid Binding Domain Regulates Focal Adhesion Kinase Inhibition and Dendrite Arborization. J Biol Chem 2015; 290:20674–20686

Kendler KS. Twin Studies of Psychiatric Illness. Arch Gen Psychiatry 1993; 50:905

Kendler KS. Twin Studies of Psychiatric Illness. Arch Gen Psychiatry 2001; 58:1005

Kim JH, Lee HJ, Choi W, Lee KJ. Encoding information into autonomously bursting neural network with pairs of time-delayed pulses. Sci Rep 2019; 9:1394

Kim T-G, Yao R, Monnell T, Cho J-H, Vasudevan A, Koh A, Peeyush KT, Moon M, Datta D, Bolshakov VY, Kim K-S, Chung S. Efficient Specification of Interneurons from Human Pluripotent Stem Cells by Dorsoventral and Rostrocaudal Modulation. Stem Cells 2014; 32:1789–1804

Kimura S, Noda T, Yoshimori T. Dissection of the Autophagosome Maturation Process by a Novel Reporter Protein, Tandem Fluorescent-Tagged LC3. Autophagy 2007; 3:452–460

Kirlin J, Goellner G. The Novel Protein FAM171B is recruited into Intracellular PolyQ Aggregates. In: . Annual meeting of the Society for Neuroscience2019

Klink PC et al. Combining brain perturbation and neuroimaging in non-human primates. Neuroimage 2021; 235:118017

Klomjai W, Katz R, Lackmy-Vallée A. Basic principles of transcranial magnetic stimulation (TMS) and repetitive TMS (rTMS). Ann Phys Rehabil Med 2015; 58:208–213

Knight BW. Dynamics of encoding in a population of neurons. J Gen Physiol 1972;

59:734–766

Koob GF, Zimmer A. Animal models of psychiatric disorders. In: . Handbook of Clinical Neurology. Elsevier B.V., 2012: 137–166

Koplin JJ, Savulescu J. Moral Limits of Brain Organoid Research. J Law, Med Ethics 2019; 47:760–767

Kovalevich J, Langford D. Considerations for the use of SH-SY5Y neuroblastoma cells in neurobiology. Methods Mol Biol 2013; 1078:9–21

Krabbendam L. Schizophrenia and Urbanicity: A Major Environmental Influence--Conditional on Genetic Risk. Schizophr Bull 2005; 31:795–799

Kramer MA, Truccolo W, Eden UT, Lepage KQ, Hochberg LR, Eskandar EN, Madsen JR, Leek JW, Maheshwari A, Halgren E, Chu CJ, Cash SS. Human seizures self-terminate across spatial scales via a critical transition. Proc Natl Acad Sci U S A 2012; 109:21116–21121

Kringelbach ML, Jenkinson N, Owen SLF, Aziz TZ. Translational principles of deep brain stimulation. Nat Rev Neurosci 2007; 8:623–635

Krishnan GP, Bazhenov M. Ionic dynamics mediate spontaneous termination of seizures and postictal depression state. J Neurosci 2011; 31:8870–8882

Krogh A. What are artificial neural networks? Nat Biotechnol 2008; 26:195–197

Kuijpers M, Kochlamazashvili G, Stumpf A, Puchkov D, Swaminathan A, Lucht MT, Krause E, Maritzen T, Schmitz D, Haucke V. Neuronal Autophagy Regulates Presynaptic Neurotransmission by Controlling the Axonal Endoplasmic Reticulum. Neuron 2021; 109:299-313.e9

Kuma A, Komatsu M, Mizushima N. Autophagy-monitoring and autophagy-deficient mice. Autophagy 2017; 13:1619–1628

Ladewig J, Koch P, Brüstle O. Leveling Waddington: the emergence of direct programming and the loss of cell fate hierarchies. Nat Rev Mol Cell Biol 2013; 14:225–236

Ladewig J, Koch P, Endl E, Meiners B, Opitz T, Couillard-Despres S, Aigner L, Brüstle O. Lineage Selection of Functional and Cryopreservable Human Embryonic Stem Cell-

Derived Neurons. Stem Cells 2008

Ladewig J, Mertens J, Kesavan J, Doerr J, Poppe D, Glaue F, Herms S, Wernet P, Kögler G, Müller F-J, Koch P, Brüstle O. Small molecules enable highly efficient neuronal conversion of human fibroblasts. Nat Methods 2012; 9:575–578

Lado FA, Moshé SL. How do seizures stop? Epilepsia 2008; 49:1651–1664

le Feber J. In Vitro Models of Brain Disorders. In: . In Vitro Neuronal Networks. Springer, 2019: 19–49

Le Feber J, Witteveen T, Van Veenendaal TM, Dijkstra J. Repeated stimulation of cultured networks of rat cortical neurons induces parallel memory traces. Learn Mem 2015; 22:594–603

Lee JS, Ho WK, Lee SH. Actin-dependent rapid recruitment of reluctant synaptic vesicles into a fast-releasing vesicle pool. Proc Natl Acad Sci U S A 2012; 109:765–774

Lenk K, Priwitzer B, Yla-Outinen L, Tietz LH, Narkilahti S, Hyttinen JA. Simulation of developing human neuronal cell networks. Biomed Eng Online 2016; 15:105

Liang CC, Wang C, Peng X, Gan B, Guan JL. Neural-specific deletion of FIP200 leads to cerebellar degeneration caused by increased neuronal death and axon degeneration. J Biol Chem 2010; 285:3499–3509

Liao Y, Wang J, Jaehnig EJ, Shi Z, Zhang B. WebGestalt 2019: gene set analysis toolkit with revamped UIs and APIs. Nucleic Acids Res 2019; 47:W199–W205

Lieberman OJ, Frier MD, McGuirt AF, Griffey CJ, Rafikian E, Yang M, Yamamoto A, Borgkvist A, Santini E, Sulzer D. Cell-type-specific regulation of neuronal intrinsic excitability by macroautophagy. Elife 2020; 9:1–39

Lim S-H, Kwon S-K, Lee MK, Moon J, Jeong DG, Park E, Kim SJ, Park BC, Lee SC, Ryu S-E, Yu D-Y, Chung BH, Kim E, Myung P-K, Lee J-R. Synapse formation regulated by protein tyrosine phosphatase receptor T through interaction with cell adhesion molecules and Fyn. EMBO J 2009; 28:3564–3578

Lin W-L, Lewis J, Yen S-H, Hutton M, Dickson DW. Ultrastructural neuronal pathology in transgenic mice expressing mutant (P301L) human tau. J Neurocytol 2003; 32:1091–1105

Liou J, Smith EH, Bateman LM, Bruce SL, McKhann GM, Goodman RR, Emerson RG, Schevon CA, Abbott L. A model for focal seizure onset, propagation, evolution, and progression. Elife 2020; 9:1–27

Lodge DJ, Grace AA. Aberrant Hippocampal Activity Underlies the Dopamine Dysregulation in an Animal Model of Schizophrenia. J Neurosci 2007; 27:11424–11430

Loebel A, Tsodyks M. Computation by ensemble synchronization in recurrent networks with synaptic depression. J Comput Neurosci 2002; 13:111–124

Löscher W, Gillard M, Sands ZA, Kaminski RM, Klitgaard H. Synaptic Vesicle Glycoprotein 2A Ligands in the Treatment of Epilepsy and Beyond. CNS Drugs 2016; 30:1055–1077

Lou X, Korogod N, Brose N, Schneggenburger R. Phorbol esters modulate spontaneous and Ca2+-evoked transmitter release via acting on both Munc13 and protein kinase C. J Neurosci 2008; 28:8257–8267

Lu J, Zhong X, Liu H, Hao L, Huang CT-L, Sherafat MA, Jones J, Ayala M, Li L, Zhang S-C. Generation of serotonin neurons from human pluripotent stem cells. Nat Biotechnol 2016; 34:89–94

MacDonald ML, Alhassan J, Newman JT, Richard M, Gu H, Kelly RM, Sampson AR, Fish KN, Penzes P, Wills ZP, Lewis DA, Sweet RA. Selective Loss of Smaller Spines in Schizophrenia. Am J Psychiatry 2017; 174:586–594

Maday S, Holzbaur ELF. Autophagosome biogenesis in primary neurons follows an ordered and spatially regulated pathway. Dev Cell 2014; 30:71–85

Maday S, Holzbaur ELF. Compartment-specific regulation of autophagy in primary neurons. J Neurosci 2016; 36:5933–5945

Maday S, Wallace KE, Holzbaur ELF. Autophagosomes initiate distally and mature during transport toward the cell soma in primary neurons. J Cell Biol 2012; 196:407–417

Magiorkinis E, Sidiropoulou K, Diamantis A. Hallmarks in the history of epilepsy: Epilepsy in antiquity. Epilepsy Behav 2010; 17:103–108

Marchetto MCN, Carromeu C, Acab A, Yu D, Yeo GW, Mu Y, Chen G, Gage FH, Muotri AR. A Model for Neural Development and Treatment of Rett Syndrome Using Human

Induced Pluripotent Stem Cells. Cell 2010; 143:527–539

Marshall CR et al. Structural Variation of Chromosomes in Autism Spectrum Disorder. Am J Hum Genet 2008; 82:477–488

Martens MB, Frega M, Classen J, Epping L, Bijvank E, Benevento M, van Bokhoven H, Tiesinga P, Schubert D, Nadif Kasri N. Euchromatin histone methyltransferase 1 regulates cortical neuronal network development. Sci Rep 2016; 6:35756

Matigian N et al. Disease-specific, neurosphere-derived cells as models for brain disorders. Dis Model Mech 2010; 3:785–798

Mattis J, Tye KM, Ferenczi EA, Ramakrishnan C, O'Shea DJ, Prakash R, Gunaydin LA, Hyun M, Fenno LE, Gradinaru V, Yizhar O, Deisseroth K. Principles for applying optogenetic tools derived from direct comparative analysis of microbial opsins. Nat Methods 2012; 9:159–172

Meijer M, Rehbach K, Brunner JW, Classen JA, Lammertse HCAA, van Linge LA, Schut D, Krutenko T, Hebisch M, Cornelisse LN, Sullivan PF, Peitz M, Toonen RF, Brüstle O, Verhage M, Brustle O, Verhage M. A Single-Cell Model for Synaptic Transmission and Plasticity in Human iPSC-Derived Neurons. Cell Rep 2019; 27:2199-2211 e6

Meldrum BS, Rogawski MA. Molecular targets for antiepileptic drug development. Neurotherapeutics 2007; 4:18–61

Mertens J et al. Differential responses to lithium in hyperexcitable neurons from patients with bipolar disorder. Nature 2015a; 527:95–99

Mertens J, Paquola ACM, Ku M, Hatch E, Böhnke L, Ladjevardi S, McGrath S, Campbell B, Lee H, Herdy JR, Gonçalves JT, Toda T, Kim Y, Winkler J, Yao J, Hetzer MW, Gage FH. Directly Reprogrammed Human Neurons Retain Aging-Associated Transcriptomic Signatures and Reveal Age-Related Nucleocytoplasmic Defects. Cell Stem Cell 2015b; 17:705–718

Miki T, Malagon G, Pulido C, Llano I, Neher E, Marty A. Actin- and Myosin-Dependent Vesicle Loading of Presynaptic Docking Sites Prior to Exocytosis. Neuron 2016; 91:808–823

Molumby MJ, Keeler AB, Weiner JA. Homophilic Protocadherin Cell-Cell Interactions

Promote Dendrite Complexity. Cell Rep 2016; 15:1037–1050

Mossink B et al. Cadherin-13 is a critical regulator of GABAergic modulation in human stem-cell-derived neuronal networks. Mol Psychiatry 2021a

Mossink B, Verboven AHA, van Hugte EJH, Klein Gunnewiek TM, Parodi G, Linda K, Schoenmaker C, Kleefstra T, Kozicz T, van Bokhoven H, Schubert D, Nadif Kasri N, Frega M. Human neuronal networks on micro-electrode arrays are a highly robust tool to study disease-specific genotype-phenotype correlations in vitro. Stem Cell Reports 2021b

Moyer CE, Shelton MA, Sweet RA. Dendritic spine alterations in schizophrenia. Neurosci Lett 2015; 601:46–53

Muratore CR, Zhou C, Liao M, Fernandez MA, Taylor WM, Lagomarsino VN, Pearse R V, Rice HC, Negri JM, He A, Srikanth P, Callahan DG, Shin T, Zhou M, Bennett DA, Noggle S, Love JC, Selkoe DJ, Young-Pearse TL. Cell-type Dependent Alzheimer's Disease Phenotypes: Probing the Biology of Selective Neuronal Vulnerability. Stem Cell Reports 2017; 9:1868–1884

Murray MR, Stout AP. Distinctive Characteristics of the Sympathicoblastoma Cultivated in Vitro: A Method for Prompt Diagnosis. Am J Pathol 1947; 23:429–441

Murrell W, Féron F, Wetzig A, Cameron N, Splatt K, Bellette B, Bianco J, Perry C, Lee G, Mackay-Sim A. Multipotent stem cells from adult olfactory mucosa. Dev Dyn 2005; 233:496–515

Musk E. An integrated brain-machine interface platform with thousands of channels. J Med Internet Res 2019; 21:1–14

Napoli A, Obeid I. Comparative Analysis of Human and Rodent Brain Primary Neuronal Culture Spontaneous Activity Using Micro-Electrode Array Technology. J Cell Biochem 2016; 117:559–565

Negrete-Hurtado A, Overhoff M, Bera S, De Bruyckere E, Schätzmüller K, Kye MJ, Qin C, Lammers M, Kondylis V, Neundorf I, Kononenko NL. Autophagy lipidation machinery regulates axonal microtubule dynamics but is dispensable for survival of mammalian neurons. Nat Commun 2020; 11:1535

Neher E. Merits and Limitations of Vesicle Pool Models in View of Heterogeneous Populations of Synaptic Vesicles. Neuron 2015; 87:1131–1142

Neher E, Brose N. Dynamically Primed Synaptic Vesicle States: Key to Understand Synaptic Short-Term Plasticity. Neuron 2018; 100:1283–1291

Nelson SB, Valakh V. Excitatory/Inhibitory Balance and Circuit Homeostasis in Autism Spectrum Disorders. Neuron 2015; 87:684–698

Ni P, Noh H, Park G-H, Shao Z, Guan Y, Park JM, Yu S, Park JS, Coyle JT, Weinberger DR, Straub RE, Cohen BM, McPhie DL, Yin C, Huang W, Kim H-Y, Chung S. iPSC-derived homogeneous populations of developing schizophrenia cortical interneurons have compromised mitochondrial function. Mol Psychiatry 2020; 25:2873–2888

Novellino A, Scelfo B, Palosaari T, Price A, Sobanski T, Shafer TJ, Johnstone AFM, Gross GW, Gramowski A, Schroeder O, Jügelt K, Chiappalone M, Benfenati F, Martinoia S, Tedesco MT, Defranchi E, D'Angelo P, Whelan M. Development of Micro-Electrode Array Based Tests for Neurotoxicity: Assessment of Interlaboratory Reproducibility with Neuroactive Chemicals. Front Neuroeng 2011; 4

Obien MEJ, Deligkaris K, Bullmann T, Bakkum DJ, Frey U. Revealing neuronal function through microelectrode array recordings. Front Neurosci 2015; 8

Odawara A, Katoh H, Matsuda N, Suzuki I. Physiological maturation and drug responses of human induced pluripotent stem cell-derived cortical neuronal networks in long-term culture. Sci Rep 2016; 6:26181

Odawara A, Matsuda N, Ishibashi Y, Yokoi R, Suzuki I. Toxicological evaluation of convulsant and anticonvulsant drugs in human induced pluripotent stem cell-derived cortical neuronal networks using an MEA system. Sci Rep 2018; 8:10416

Oh Y, Jang J. Directed Differentiation of Pluripotent Stem Cells by Transcription Factors. Mol Cells 2019; 42:200–209

Ohno Y, Tokudome K. Therapeutic Role of Synaptic Vesicle Glycoprotein 2A (SV2A) in Modulating Epileptogenesis. CNS Neurol Disord - Drug Targets 2017; 16

Ohnstad AE, Delgado JM, North BJ, Nasa I, Kettenbach AN, Schultz SW, Shoemaker CJ. Receptor-mediated clustering of FIP200 bypasses the role of LC3 lipidation in autophagy.

EMBO J 2020; 39

Okujeni S, Egert U. Self-organization of modular network architecture by activity-dependent neuronal migration and outgrowth. Elife 2019; 8:1–29

Opitz T, De Lima AD, Voigt T. Spontaneous Development of Synchronous Oscillatory Activity During Maturation of Cortical Networks In Vitro. J Neurophysiol 2002; 88:2196–2206

Owen MJ, Sawa A, Mortensen PB. Schizophrenia. Lancet 2016; 388:86–97

Pak C, Danko T, Zhang Y, Aoto J, Anderson G, Maxeiner S, Yi F, Wernig M, Südhof TC. Human Neuropsychiatric Disease Modeling using Conditional Deletion Reveals Synaptic Transmission Defects Caused by Heterozygous Mutations in NRXN1. Cell Stem Cell 2015; 17:316–328

Pang ZP, Yang N, Vierbuchen T, Ostermeier A, Fuentes DR, Yang TQ, Citri A, Sebastiano V, Marro S, Südhof TC, Wernig M. Induction of human neuronal cells by defined transcription factors. Nature 2011; 476:220–223

Paolicelli RC, Bolasco G, Pagani F, Maggi L, Scianni M, Panzanelli P, Giustetto M, Ferreira TA, Guiducci E, Dumas L, Ragozzino D, Gross CT. Synaptic Pruning by Microglia Is Necessary for Normal Brain Development. Science (80-) 2011; 333:1456–1458

Pasquale V, Martinoia S, Chiappalone M. Stimulation triggers endogenous activity patterns in cultured cortical networks. Sci Rep 2017; 7:9080

Patel V, Chisholm D, Parikh R, Charlson FJ, Degenhardt L, Dua T, Ferrari AJ, Hyman S, Laxminarayan R, Levin C, Lund C, Medina-Mora ME, Petersen I, Scott JG, Shidhaye R, Vijayakumar L, Thornicroft G, Whiteford H. Global Priorities for Addressing the Burden of Mental, Neurological, and Substance Use Disorders. In: . Disease Control Priorities, Third Edition (Volume 4): Mental, Neurological, and Substance Use Disorders. The World Bank, 2016: 1–27

Peitz M, Krutenko T, Brüstle O. Protocol for the Standardized Generation of Forward Programmed Cryopreservable Excitatory and Inhibitory Forebrain Neurons. STAR Protoc 2020; 1:100038

Pelt J van, Wolters PS, Corner MA, Rutten WLC, Ramakers GJA. Long-term

characterization of firing dynamics of spontaneous bursts in cultured neural networks. IEEE Trans Biomed Eng 2004; 51:2051–2062

Perez SM, Lodge DJ. Hippocampal interneuron transplants reverse aberrant dopamine system function and behavior in a rodent model of schizophrenia. Mol Psychiatry 2013; 18:1193–1198

Perez SM, Shah A, Asher A, Lodge DJ. Hippocampal deep brain stimulation reverses physiological and behavioural deficits in a rodent model of schizophrenia. Int J Neuropsychopharmacol 2013; 16:1331–1339

Petherick KJ, Conway OJL, Mpamhanga C, Osborne SA, Kamal A, Saxty B, Ganley IG. Pharmacological Inhibition of ULK1 Kinase Blocks Mammalian Target of Rapamycin (mTOR)-dependent Autophagy. J Biol Chem 2015; 290:11376–11383

Pine J. Recording action potentials from cultured neurons with extracellular microcircuit electrodes. J Neurosci Methods 1980; 2:19–31

Plomin R, Owen M, McGuffin P. The genetic basis of complex human behaviors. Science (80-) 1994; 264:1733–1739

Powell SK, Gregory J, Akbarian S, Brennand KJ. Application of CRISPR/Cas9 to the study of brain development and neuropsychiatric disease. Mol Cell Neurosci 2017; 82:157–166

Prasad KN. DIFFERENTIATION OF NEUROBLASTOMA CELLS: A USEFUL MODEL FOR NEUROBIOLOGY AND CANCER. Biol Rev 1991; 66:431–451

Purcell SM et al. Common polygenic variation contributes to risk of schizophrenia and bipolar disorder. Nature 2009; 460:748–752

Putnam H. Brains in a Vat. Knowl Crit Concepts 1981; 1:192–207

Qian H, Kang X, Hu J, Zhang D, Liang Z, Meng F, Zhang X, Xue Y, Maimon R, Dowdy SF, Devaraj NK, Zhou Z, Mobley WC, Cleveland DW, Fu X-D. Reversing a model of Parkinson’s disease with in situ converted nigral neurons. Nature 2020; 582:550–556

Quiroga RQ, Nadasdy Z, Ben-Shaul Y. Unsupervised Spike Detection and Sorting with Wavelets and Superparamagnetic Clustering. Neural Comput 2004; 16:1661–1687

Rackham OJL, Firas J, Fang H, Oates ME, Holmes ML, Knaupp AS, Suzuki H, Nefzger

CM, Daub CO, Shin JW, Petretto E, Forrest ARR, Hayashizaki Y, Polo JM, Gough J, Consortium TF. A predictive computational framework for direct reprogramming between human cell types. Nat Genet 2016; 48:331–335

Ragusa MJ, Stanley RE, Hurley JH. Architecture of the Atg17 Complex as a Scaffold for Autophagosome Biogenesis. Cell 2012; 151:1501–1512

Ramirez J-M, Tryba AK, Peña F. Pacemaker neurons and neuronal networks: an integrative view. Curr Opin Neurobiol 2004; 14:665–674

Ramon y Cajal S. Degeneration and regeneration of the nervous system. Oxford, England: : Clarendon Press.

Ran FA, Hsu PD, Wright J, Agarwala V, Scott DA, Zhang F. Genome engineering using the CRISPR-Cas9 system. Nat Protoc 2013; 8:2281–2308

Ravenhill BJ, Boyle KB, von Muhlinen N, Ellison CJ, Masson GR, Otten EG, Foeglein A, Williams R, Randow F. The Cargo Receptor NDP52 Initiates Selective Autophagy by Recruiting the ULK Complex to Cytosol-Invading Bacteria. Mol Cell 2019; 74:320-329.e6

Reubinoff BE, Itsykson P, Turetsky T, Pera MF, Reinhartz E, Itzik A, Ben-Hur T. Neural progenitors from human embryonic stem cells. Nat Biotechnol 2001; 19:1134–1140

Rhee HJ, Shaib AH, Rehbach K, Lee C, Seif P, Thomas C, Gideons E, Guenther A, Krutenko T, Hebisch M, Peitz M, Brose N, Brüstle O, Rhee JS. An Autaptic Culture System for Standardized Analyses of iPSC-Derived Human Neurons. Cell Rep 2019a; 27:2212-2228.e7

Rhee HJ, Shaib AH, Rehbach K, Lee CK, Seif P, Thomas C, Gideons E, Guenther A, Krutenko T, Hebisch M, Peitz M, Brose N, Brüstle O, Rhee JS. An Autaptic Culture System for Standardized Analyses of iPSC-Derived Human Neurons. Cell Rep 2019b; 27:2212-2228.e7

Rizzoli SO. Synaptic vesicle recycling: steps and principles. EMBO J 2014; 33:788–822

Rizzoli SO, Betz WJ. Synaptic vesicle pools. Nat Rev Neurosci 2005; 6:57–69

Romero MC, Davare M, Armendariz M, Janssen P. Neural effects of transcranial magnetic stimulation at the single-cell level. Nat Commun 2019; 10:2642

Romo R, Salinas E. Flutter Discrimination: neural codes, perception, memory and

decision making. Nat Rev Neurosci 2003; 4:203–218

Ruaro ME, Bonifazi P, Torre V. Toward the Neurocomputer: Image Processing and Pattern Recognition With Neuronal Cultures. IEEE Trans Biomed Eng 2005; 52:371–383

Sakaba T, Neher E. Calmodulin mediates rapid recruitment of fast-releasing synaptic vesicles at a calyx-type synapse. Neuron 2001; 32:1119–1131

Sakaba T, Neher E. Involvement of Actin Polymerization in Vesicle Recruitment at the Calyx of Held Synapse. J Neurosci 2003; 23:837–846

Sarkisian MR. Overview of the Current Animal Models for Human Seizure and Epileptic Disorders. Epilepsy Behav 2001; 2:201–216

Sasaki T, Suzuki I, Yokoi R, Sato K, Ikegaya Y. Synchronous spike patterns in differently mixed cultures of human iPSC-derived glutamatergic and GABAergic neurons. Biochem Biophys Res Commun 2019; 513:300–305

Sawai T, Sakaguchi H, Thomas E, Takahashi J, Fujita M. The Ethics of Cerebral Organoid Research: Being Conscious of Consciousness. Stem Cell Reports 2019; 13:440–447

Scherberger H. Neural control of motor prostheses. Curr Opin Neurobiol 2009; 19:629–633

Schiavone S, Jaquet V, Trabace L, Krause K-H. Severe Life Stress and Oxidative Stress in the Brain: From Animal Models to Human Pathology. Antioxid Redox Signal 2013; 18:1475–1490

Schlesinger HR, Gerson JM, Moorhead PS, Maguire H, Hummeler K. Establishment and characterization of human neuroblastoma cell lines. Cancer Res 1976; 36:3094–3100

Schobel SA, Chaudhury NH, Khan UA, Paniagua B, Styner MA, Asllani I, Inbar BP, Corcoran CM, Lieberman JA, Moore H, Small SA. Imaging Patients with Psychosis and a Mouse Model Establishes a Spreading Pattern of Hippocampal Dysfunction and Implicates Glutamate as a Driver. Neuron 2013; 78:81–93

Sebat J et al. Strong Association of De Novo Copy Number Mutations with Autism. Science (80-) 2007; 316:445–449

Selemon LD, Kleinman JE, Herman MM, Goldman-Rakic PS. Smaller Frontal Gray Matter Volume in Postmortem Schizophrenic Brains. Am J Psychiatry 2002; 159:1983–1991

Selkoe DJ, Luckenbill-Edds L, Shelanski ML. Effects of Neurotoxic Industrial Solvents on Cultured Neuroblastoma Cells: Methyl n-Butyl Ketone, n-Hexane and Derivatives. J Neuropathol Exp Neurol 1978; 37:768–789

Seong E, Seasholtz AF, Burmeister M. Mouse models for psychiatric disorders. Trends Genet 2002; 18:643–650

Shao Z et al. Dysregulated protocadherin-pathway activity as an intrinsic defect in induced pluripotent stem cell–derived cortical interneurons from subjects with schizophrenia. Nat Neurosci 2019; 22:229–242

Shi X, Chang C, Yokom AL, Jensen LE, Hurley JH. The autophagy adaptor NDP52 and the FIP200 coiled-coil allosterically activate ULK1 complex membrane recruitment. Elife 2020a; 9

Shi X, Yokom AL, Wang C, Young LN, Youle RJ, Hurley JH. ULK complex organization in autophagy by a C-shaped FIP200 N-terminal domain dimer. J Cell Biol 2020b; 219

Shi Y, Kirwan P, Smith J, Robinson HPC, Livesey FJ. Human cerebral cortex development from pluripotent stem cells to functional excitatory synapses. Nat Neurosci 2012; 15:477–486

Shin H, Jeong S, Lee J-H, Sun W, Choi N, Cho I-J. 3D high-density microelectrode array with optical stimulation and drug delivery for investigating neural circuit dynamics. Nat Commun 2021; 12:492

Shin O-H, Lu J, Rhee J-S, Tomchick DR, Pang ZP, Wojcik SM, Camacho-Perez M, Brose N, Machius M, Rizo J, Rosenmund C, Südhof TC. Munc13 C2B domain is an activity-dependent Ca2+ regulator of synaptic exocytosis. Nat Struct Mol Biol 2010; 17:280–288

Shu Y, Duque A, Yu Y, Haider B, McCormick DA. Properties of Action-Potential Initiation in Neocortical Pyramidal Cells: Evidence From Whole Cell Axon Recordings. J Neurophysiol 2007; 97:746–760

Silbereis JC, Pochareddy S, Zhu Y, Li M, Sestan N. The Cellular and Molecular Landscapes of the Developing Human Central Nervous System. Neuron 2016; 89:248–268

Slack-Davis JK, Martin KH, Tilghman RW, Iwanicki M, Ung EJ, Autry C, Luzzio MJ,

Cooper B, Kath JC, Roberts WG, Parsons JT. Cellular Characterization of a Novel Focal Adhesion Kinase Inhibitor*. J Biol Chem 2007; 282:14845–14852

Smucny J, Visani A, Tregellas JR. Could Vagus Nerve Stimulation Target Hippocampal Hyperactivity to Improve Cognition in Schizophrenia? Front Psychiatry 2015; 6

Soldner F et al. Generation of Isogenic Pluripotent Stem Cells Differing Exclusively at Two Early Onset Parkinson Point Mutations. Cell 2011; 146:318–331

Sotthibundhu A, McDonagh K, von Kriegsheim A, Garcia-Munoz A, Klawiter A, Thompson K, Chauhan KD, Krawczyk J, McInerney V, Dockery P, Devine MJ, Kunath T, Barry F, O'Brien T, Shen S. Rapamycin regulates autophagy and cell adhesion in induced pluripotent stem cells. Stem Cell Res Ther 2016; 7:166

Spanu A, Colistra N, Farisello P, Friz A, Arellano N, Rettner CT, Bonfiglio A, Bozano L, Martinoia S. A three-dimensional micro-electrode array for in-vitro neuronal interfacing. J Neural Eng 2020; 17:36033

Staley KJ, Longacher M, Bains JS, Yee A. Presynaptic modulation of CA3 network activity. Nat Neurosci 1998; 1:201–209

Stavoe AKH, Holzbaur ELF. Autophagy in neurons. Annu Rev Cell Dev Biol 2019; 35:477–500

Stephens CL, Toda H, Palmer TD, DeMarse TB, Ormerod BK. Adult neural progenitor cells reactivate superbursting in mature neural networks. Exp Neurol 2012; 234:20–30

Stevens CF, Wesseling JF. Identification of a novel process limiting the rate of synaptic vesicle cycling at hippocampal synapses. Neuron 1999; 24:1017–1028

Stimberg M, Brette R, Goodman DFM. Brian 2, an intuitive and efficient neural simulator. Elife 2019; 8

Stolz A, Ernst A, Dikic I. Cargo recognition and trafficking in selective autophagy. Nat Cell Biol 2014; 16:495–501

Stone JL et al. Rare chromosomal deletions and duplications increase risk of schizophrenia. Nature 2008; 455:237–241

Takahashi K, Yamanaka S. Induction of Pluripotent Stem Cells from Mouse Embryonic and Adult Fibroblast Cultures by Defined Factors. Cell 2006; 126:663–676

Tal D, Jacobson E, Lyakhov V, Marom S. Frequency tuning of input-output relation in a rat cortical neuron in-vitro. Neurosci Lett 2001; 300:21–24

Talamo BR, Rudel R, Kosik KS, Lee VM-Y, Neff S, Adelman L, Kauer JS. Pathological changes in olfactory neurons in patients with Alzheimer's disease. Nature 1989; 337:736–739

Talati P, Rane S, Kose S, Blackford JU, Gore J, Donahue MJ, Heckers S. Increased hippocampal CA1 cerebral blood volume in schizophrenia. NeuroImage Clin 2014; 5:359–364

Talati P, Rane S, Skinner J, Gore J, Heckers S. Increased hippocampal blood volume and normal blood flow in schizophrenia. Psychiatry Res Neuroimaging 2015; 232:219–225

Tan CX, Eroglu C. Cell adhesion molecules regulating astrocyte–neuron interactions. Curr Opin Neurobiol 2021; 69:170–177

Tanabe K, Ang CE, Chanda S, Olmos VH, Haag D, Levinson DF, Südhof TC, Wernig M. Transdifferentiation of human adult peripheral blood T cells into neurons. Proc Natl Acad Sci 2018; 115:6470 LP – 6475

Tang G, Gudsnuk K, Kuo SH, Cotrina ML, Rosoklija G, Sosunov A, Sonders MS, Kanter E, Castagna C, Yamamoto A, Yue Z, Arancio O, Peterson BS, Champagne F, Dwork AJ, Goldman J, Sulzer D. Loss of mTOR-Dependent Macroautophagy Causes Autistic-like Synaptic Pruning Deficits. Neuron 2014; 83:1131–1143

Tao Y, Zhang S-C. Neural Subtype Specification from Human Pluripotent Stem Cells. Cell Stem Cell 2016; 19:573–586

Tessadori J, Chiappalone M. Closed-loop neuro-robotic experiments to test computational properties of neuronal networks. J Vis Exp 2015; 2015:52341

Thijs RD, Surges R, O'Brien TJ, Sander JW. Epilepsy in adults. Lancet 2019; 393:689–701

Thomas CA, Springer PA, Loeb GE, Berwald-Netter Y, Okun LM. A miniature microelectrode array to monitor the bioelectric activity of cultured cells. Exp Cell Res 1972; 74:61–66

Thomson JA, Itskovitz-Eldor J, Shapiro SS, Waknitz MA, Swiergiel JJ, Marshall VS, Jones JM. Embryonic Stem Cell Lines Derived from Human Blastocysts. Science (80-) 1998; 282:1145 LP – 1147

Torper O, Ottosson DR, Pereira M, Lau S, Cardoso T, Grealish S, Parmar M. In Vivo Reprogramming of Striatal NG2 Glia into Functional Neurons that Integrate into Local Host Circuitry. Cell Rep 2015; 12:474–481

Tran Q, Sudasinghe A, Jones B, Xiong K, Cohen RE, Sharlin DS, Hartert KT, Goellner GM. FAM171B is a novel polyglutamine protein widely expressed in the mammalian brain. Brain Res 2021:147540

Trautmann S, Rehm J, Wittchen H-U. The economic costs of mental disorders. EMBO Rep 2016; 17:1245–1249

Tregellas JR, Smucny J, Harris JG, Olincy A, Maharajh K, Kronberg E, Eichman LC, Lyons E, Freedman R. Intrinsic Hippocampal Activity as a Biomarker for Cognition and Symptoms in Schizophrenia. Am J Psychiatry 2014; 171:549–556

Trépanier MO, Hopperton KE, Mizrahi R, Mechawar N, Bazinet RP. Postmortem evidence of cerebral inflammation in schizophrenia: a systematic review. Mol Psychiatry 2016; 21:1009–1026

Trujillo CA, Gao R, Negraes PD, Gu J, Buchanan J, Preissl S, Wang A, Wu W, Haddad GG, Chaim IA, Domissy A, Vandenberghe M, Devor A, Yeo GW, Voytek B, Muotri AR. Complex Oscillatory Waves Emerging from Cortical Organoids Model Early Human Brain Network Development. Cell Stem Cell 2019; 25:558-569.e7

Tsodyks M. Linking Spontaneous Activity of Single Cortical Neurons and the Underlying Functional Architecture. Science (80-) 1999; 286:1943–1946

Tsodyks M, Uziel A, Markram H. Synchrony Generation in Recurrent Networks with Frequency-Dependent Synapses. J Neurosci 2000; 20:RC50–RC50

Turco E, Fracchiolla D, Martens S. Recruitment and Activation of the ULK1/Atg1 Kinase Complex in Selective Autophagy. J Mol Biol 2020; 432:123–134

Turco E, Witt M, Abert C, Bock-Bierbaum T, Su MY, Trapannone R, Sztacho M, Danieli A, Shi X, Zaffagnini G, Gamper A, Schuschnig M, Fracchiolla D, Bernklau D, Romanov J,

Hartl M, Hurley JH, Daumke O, Martens S. FIP200 Claw Domain Binding to p62 Promotes Autophagosome Formation at Ubiquitin Condensates. Mol Cell 2019; 74:330-346.e11

Turrigiano G, LeMasson G, Marder E. Selective regulation of current densities underlies spontaneous changes in the activity of cultured neurons. J Neurosci 1995; 15:3640–3652

Ueda H, Abbi S, Zheng C, Guan J-L. Suppression of Pyk2 kinase and cellular activities by FIP200. J Cell Biol 2000; 149:423–430

Vadodaria KC, Jones JR, Linker S, Gage FH. Modeling brain disorders using induced pluripotent stem cells. Cold Spring Harb Perspect Biol 2020; 12:a035659

Vadodaria KC, Mertens J, Paquola A, Bardy C, Li X, Jappelli R, Fung L, Marchetto MC, Hamm M, Gorris M, Koch P, Gage FH. Generation of functional human serotonergic neurons from fibroblasts. Mol Psychiatry 2016; 21:49–61

Valzania F, Quatrale R, Strafella AP, Bombardi R, Santangelo M, Tassinari CA, De Grandis D. Pattern of motor evoked response to repetitive transcranial magnetic stimulation. Electroencephalogr Clin Neurophysiol Potentials Sect 1994; 93:312–317

Van Gompel JJ, Bower MR, Worrell GA, Stead M, Chang SY, Goerss SJ, Kim I, Bennet KE, Meyer FB, Marsh WR, Blaha CD, Lee KH. Increased cortical extracellular adenosine correlates with seizure termination. Epilepsia 2014; 55:233–244

Van Ooyen A, Van Pelt J, Corner MA. Implications of activity dependent neurite outgrowth for neuronal morphology and network development. J Theor Biol 1995; 172:63–82

Vargas JNS, Wang C, Bunker E, Hao L, Maric D, Schiavo G, Randow F, Youle RJ. Spatiotemporal Control of ULK1 Activation by NDP52 and TBK1 during Selective Autophagy. Mol Cell 2019; 74:347-362.e6

Vico Varela E, Etter G, Williams S. Excitatory-inhibitory imbalance in Alzheimer's disease and therapeutic significance. Neurobiol Dis 2019; 127:605–615

Vierbuchen T, Ostermeier A, Pang ZP, Kokubu Y, Südhof TC, Wernig M. Direct conversion of fibroblasts to functional neurons by defined factors. Nature 2010; 463:1035–1041

Wagenaar DA. Controlling Bursting in Cortical Cultures with Closed-Loop Multi-Electrode Stimulation. J Neurosci 2005; 25:680–688

Wagenaar DA, Nadasdy Z, Potter SM. Persistent dynamic attractors in activity patterns of cultured neuronal networks. Phys Rev E 2006a; 73:051907

Wagenaar DA, Pine J, Potter SM. An extremely rich repertoire of bursting patterns during the development of cortical cultures. BMC Neurosci 2006b; 7:1–18

Wagenaar DA, Pine J, Potter SM. Searching for plasticity in dissociated cortical cultures on multi-electrode arrays. J Negat Results Biomed 2006c; 5:16

Wang C, Liang CC, Bian ZC, Zhu Y, Guan JL. FIP200 is required for maintenance and differentiation of postnatal neural stem cells. Nat Neurosci 2013a; 16:532–542

Wang C, Yeo S, Haas MA, Guan JL. Autophagy gene FIP200 in neural progenitors non-cell autonomously controls differentiation by regulating microglia. J Cell Biol 2017; 216:2581–2596

Wang M, Lu C, Roisen F. Adult human olfactory epithelial-derived progenitors: a potential autologous source for cell-based treatment for Parkinson's disease. Stem Cells Transl Med 2012; 1:492–502

Wang S, Xia P, Ye B, Huang G, Liu J, Fan Z. Transient Activation of Autophagy via Sox2-Mediated Suppression of mTOR Is an Important Early Step in Reprogramming to Pluripotency. Cell Stem Cell 2013b; 13:617–625

Wang X, Ye F, Wen Z, Guo Z, Yu C, Huang W-K, Rojas Ringeling F, Su Y, Zheng W, Zhou G, Christian KM, Song H, Zhang M, Ming G. Structural interaction between DISC1 and ATF4 underlying transcriptional and synaptic dysregulation in an iPSC model of mental disorders. Mol Psychiatry 2021; 26:1346–1360

Wang Y, Song M, Song F. Neuronal autophagy and axon degeneration. Cell Mol Life Sci 2018; 75:2389–2406

Weltha L, Reemmer J, Boison D. The role of adenosine in epilepsy. Brain Res Bull 2019; 151:46–54

Wen J, Yu T, Li Y, Li X. Using electrocorticography for presurgical language mapping in epilepsy patients. J Clin Neurosci 2017a; 44:320–322

Wen J, Yu T, Liu L, Hu Z, Yan J, Li Y, Li X. Evaluating the roles of left middle frontal gyrus in word production using electrocorticography. Neurocase 2017b; 23:263–269

Wen J, Yu T, Wang X, Liu C, Zhou T, Li Y, Li X. Continuous behavioral tracing-based online functional brain mapping with intracranial electroencephalography. J Neural Eng 2018; 15:1–20

Wen Z et al. Synaptic dysregulation in a human iPS cell model of mental disorders. Nature 2014; 515:414–418

Wesseling JF, Lo DC. Limit on the role of activity in controlling the release-ready supply of synaptic vesicles. J Neurosci 2002; 22:9708–9720

Whiteford HA, Degenhardt L, Rehm J, Baxter AJ, Ferrari AJ, Erskine HE, Charlson FJ, Norman RE, Flaxman AD, Johns N, Burstein R, Murray CJL, Vos T. Global burden of disease attributable to mental and substance use disorders: Findings from the Global Burden of Disease Study 2010. Lancet 2013; 382:1575–1586

Wolff AR, Bygrave AM, Sanderson DJ, Boyden ES, Bannerman DM, Kullmann DM, Kätzel D. Optogenetic induction of the schizophrenia-related endophenotype of ventral hippocampal hyperactivity causes rodent correlates of positive and cognitive symptoms. Sci Rep 2018; 8:12871

Wonders CP, Anderson SA. The origin and specification of cortical interneurons. Nat Rev Neurosci 2006; 7:687–696

World Health Organization. Mental Health Gap Action Programme - Scaling up care for mental, neurological, and substance use disorders. World Heal Organ 2008:44

Xu B, Roos JL, Dexheimer P, Boone B, Plummer B, Levy S, Gogos JA, Karayiorgou M. Exome sequencing supports a de novo mutational paradigm for schizophrenia. Nat Genet 2011; 43:864–868

Xu Z, Jiang H, Zhong P, Yan Z, Chen S, Feng J. Direct conversion of human fibroblasts to induced serotonergic neurons. Mol Psychiatry 2016; 21:62–70

Yang N, Chanda S, Marro S, Ng Y-H, Janas JA, Haag D, Ang CE, Tang Y, Flores Q, Mall M, Wapinski O, Li M, Ahlenius H, Rubenstein JL, Chang HY, Buylla AA, Südhof TC, Wernig M. Generation of pure GABAergic neurons by transcription factor programming. Nat Methods 2017; 14:621–628

Yang Y, Coleman M, Zhang L, Zheng X, Yue Z. Autophagy in axonal and dendritic

degeneration. Trends Neurosci 2013; 36:418–428

Yao J, Jia L, Khan N, Lin C, Mitter SK, Boulton ME, Dunaief JL, Klionsky DJ, Guan J-L, Thompson DA, Zacks DN. Deletion of autophagy inducer RB1CC1 results in degeneration of the retinal pigment epithelium. Autophagy 2015; 11:939–953

Yu J, Vodyanik MA, Smuga-Otto K, Antosiewicz-Bourget J, Frane JL, Tian S, Nie J, Jonsdottir GA, Ruotti V, Stewart R, Slukvin II, Thomson JA. Induced Pluripotent Stem Cell Lines Derived from Human Somatic Cells. Science (80-) 2007; 318:1917–1920

Zhan X, Lai PY, Chan CK. Effects of glial release and somatic receptors on bursting in synchronized neuronal networks. Phys Rev E - Stat Nonlinear, Soft Matter Phys 2011; 84:1–11

Zhang S-C, Wernig M, Duncan ID, Brüstle O, Thomson JA. In vitro differentiation of transplantable neural precursors from human embryonic stem cells. Nat Biotechnol 2001; 19:1129–1133

Zhang X, Klueber KM, Guo Z, Cai J, Lu C, Winstead WI, Qiu M, Roisen FJ. Induction of neuronal differentiation of adult human olfactory neuroepithelial-derived progenitors. Brain Res 2006; 1073–1074:109–119

Zhang Y, Pak C, Han Y, Ahlenius H, Zhang Z, Chanda S, Marro S, Patzke C, Acuna C, Covy J, Xu W, Yang N, Danko T, Chen L, Wernig M, Südhof TC. Rapid Single-Step Induction of Functional Neurons from Human Pluripotent Stem Cells. Neuron 2013; 78:785–798

Zhou H et al. Glia-to-Neuron Conversion by CRISPR-CasRx Alleviates Symptoms of Neurological Disease in Mice. Cell 2020; 181:590-603.e16

Zierhut K, Bogerts B, Schott B, Fenker D, Walter M, Albrecht D, Steiner J, Schütze H, Northoff G, Düzel E, Schiltz K. The role of hippocampus dysfunction in deficient memory encoding and positive symptoms in schizophrenia. Psychiatry Res Neuroimaging 2010; 183:187–194

8. Appendices

Supplementary Figure S1. Genotype validation of established RB1CC1^{KO} hPSC lines with Amplicon sequencing

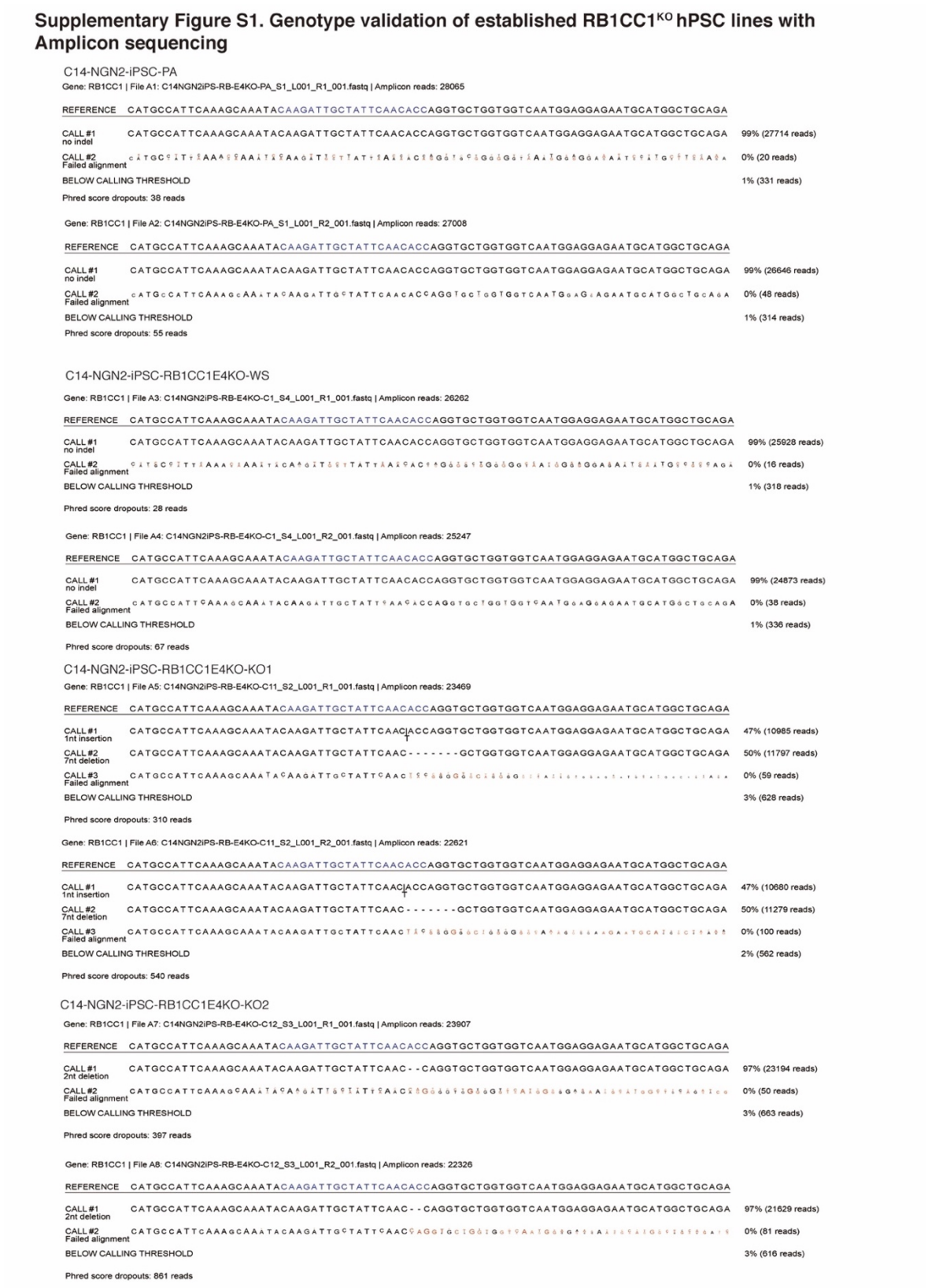

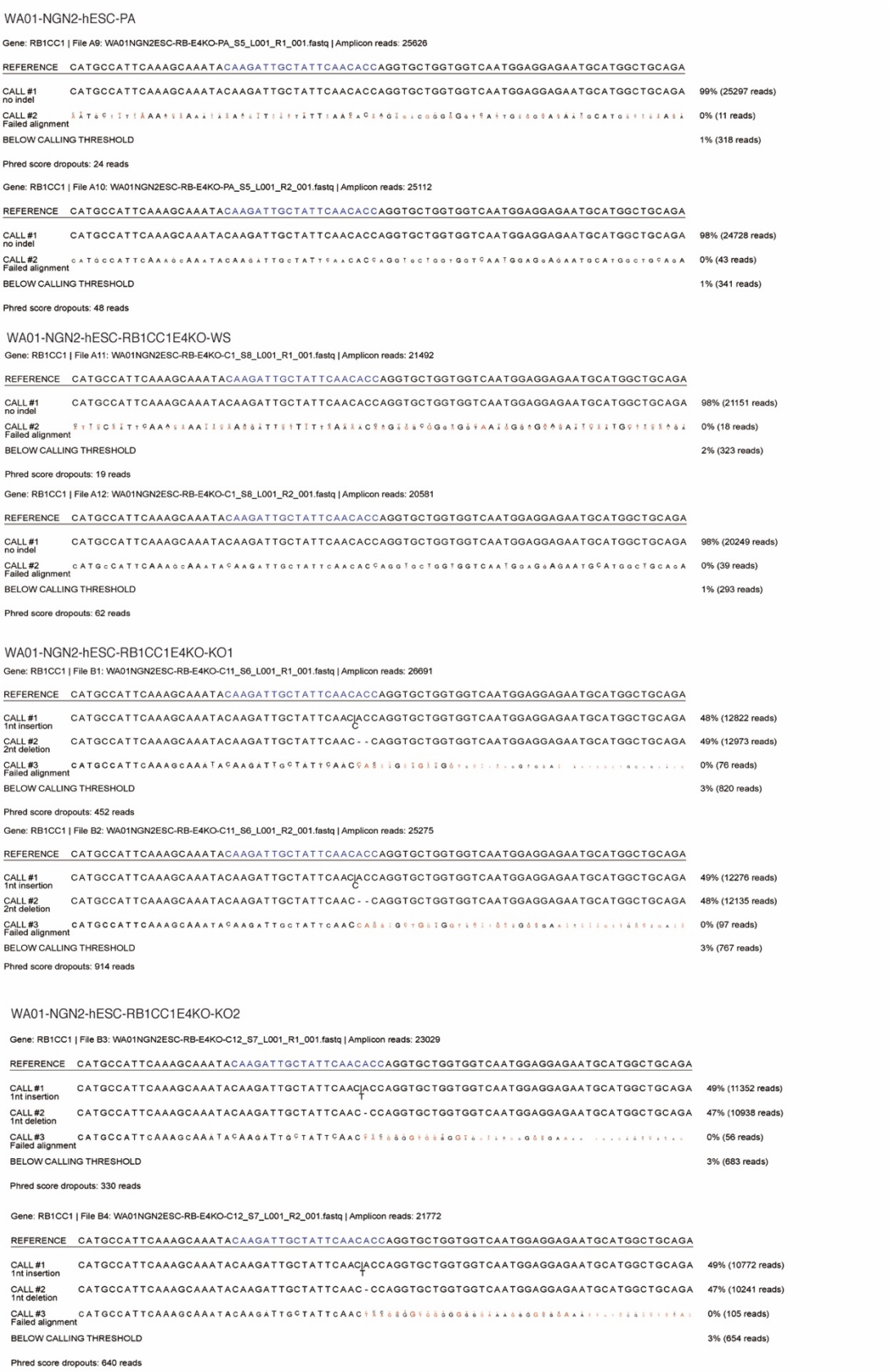
WA01-NGN2-hESC-PA
Gene: RB1CC1 | File A9: WA01NGN2ESC-RB-E4KO-PA_S5_L001_R1_001.fastq | Amplicon reads: 25626
REFERENCE CATGCCATTCAAAGCAAATACAAGATTGCTATTCAACACCAGGTGCTGGTGGTCAATGGAGGAGAATGCATGGCTGCAGA
CALL #1 no indel CATGCCATTCAAAGCAAATACAAGATTGCTATTCAACACCAGGTGCTGGTGGTCAATGGAGGAGAATGCATGGCTGCAGA 99% (25297 reads)
CALL #2 Failed alignment 0% (11 reads)
BELOW CALLING THRESHOLD 1% (318 reads)
Phred score dropouts: 24 reads
Gene: RB1CC1 | File A10: WA01NGN2ESC-RB-E4KO-PA_S5_L001_R2_001.fastq | Amplicon reads: 25112
REFERENCE CATGCCATTCAAAGCAAATACAAGATTGCTATTCAACACCAGGTGCTGGTGGTCAATGGAGGAGAATGCATGGCTGCAGA
CALL #1 no indel CATGCCATTCAAAGCAAATACAAGATTGCTATTCAACACCAGGTGCTGGTGGTCAATGGAGGAGAATGCATGGCTGCAGA 98% (24728 reads)
CALL #2 Failed alignment 0% (43 reads)
BELOW CALLING THRESHOLD 1% (341 reads)
Phred score dropouts: 48 reads
WA01-NGN2-hESC-RB1CC1E4KO-WS
Gene: RB1CC1 | File A11: WA01NGN2ESC-RB-E4KO-C1_S8_L001_R1_001.fastq | Amplicon reads: 21492
REFERENCE CATGCCATTCAAAGCAAATACAAGATTGCTATTCAACACCAGGTGCTGGTGGTCAATGGAGGAGAATGCATGGCTGCAGA
CALL #1 no indel CATGCCATTCAAAGCAAATACAAGATTGCTATTCAACACCAGGTGCTGGTGGTCAATGGAGGAGAATGCATGGCTGCAGA 98% (21151 reads)
CALL #2 Failed alignment 0% (18 reads)
BELOW CALLING THRESHOLD 2% (323 reads)
Phred score dropouts: 19 reads
Gene: RB1CC1 | File A12: WA01NGN2ESC-RB-E4KO-C1_S8_L001_R2_001.fastq | Amplicon reads: 20581
REFERENCE CATGCCATTCAAAGCAAATACAAGATTGCTATTCAACACCAGGTGCTGGTGGTCAATGGAGGAGAATGCATGGCTGCAGA
CALL #1 no indel CATGCCATTCAAAGCAAATACAAGATTGCTATTCAACACCAGGTGCTGGTGGTCAATGGAGGAGAATGCATGGCTGCAGA 98% (20249 reads)
CALL #2 Failed alignment 0% (39 reads)
BELOW CALLING THRESHOLD 1% (293 reads)
Phred score dropouts: 62 reads
WA01-NGN2-hESC-RB1CC1E4KO-KO1
Gene: RB1CC1 | File B1: WA01NGN2ESC-RB-E4KO-C11_S6_L001_R1_001.fastq | Amplicon reads: 26691
REFERENCE CATGCCATTCAAAGCAAATACAAGATTGCTATTCAACACCAGGTGCTGGTGGTCAATGGAGGAGAATGCATGGCTGCAGA
CALL #1 1nt insertion CATGCCATTCAAAGCAAATACAAGATTGCTATTCAAC(C)ACCAGGTGCTGGTGGTCAATGGAGGAGAATGCATGGCTGCAGA 48% (12822 reads)
CALL #2 2nt deletion CATGCCATTCAAAGCAAATACAAGATTGCTATTCAAC--CAGGTGCTGGTGGTCAATGGAGGAGAATGCATGGCTGCAGA 49% (12973 reads)
CALL #3 Failed alignment 0% (76 reads)
BELOW CALLING THRESHOLD 3% (820 reads)
Phred score dropouts: 452 reads
Gene: RB1CC1 | File B2: WA01NGN2ESC-RB-E4KO-C11_S6_L001_R2_001.fastq | Amplicon reads: 25275
REFERENCE CATGCCATTCAAAGCAAATACAAGATTGCTATTCAACACCAGGTGCTGGTGGTCAATGGAGGAGAATGCATGGCTGCAGA
CALL #1 1nt insertion CATGCCATTCAAAGCAAATACAAGATTGCTATTCAAC(C)ACCAGGTGCTGGTGGTCAATGGAGGAGAATGCATGGCTGCAGA 49% (12276 reads)
CALL #2 2nt deletion CATGCCATTCAAAGCAAATACAAGATTGCTATTCAAC--CAGGTGCTGGTGGTCAATGGAGGAGAATGCATGGCTGCAGA 48% (12135 reads)
CALL #3 Failed alignment 0% (97 reads)
BELOW CALLING THRESHOLD 3% (767 reads)
Phred score dropouts: 914 reads
WA01-NGN2-hESC-RB1CC1E4KO-KO2
Gene: RB1CC1 | File B3: WA01NGN2ESC-RB-E4KO-C12_S7_L001_R1_001.fastq | Amplicon reads: 23029
REFERENCE CATGCCATTCAAAGCAAATACAAGATTGCTATTCAACACCAGGTGCTGGTGGTCAATGGAGGAGAATGCATGGCTGCAGA
CALL #1 1nt insertion CATGCCATTCAAAGCAAATACAAGATTGCTATTCAAC(T)ACCAGGTGCTGGTGGTCAATGGAGGAGAATGCATGGCTGCAGA 49% (11352 reads)
CALL #2 1nt deletion CATGCCATTCAAAGCAAATACAAGATTGCTATTCAAC-CCAGGTGCTGGTGGTCAATGGAGGAGAATGCATGGCTGCAGA 47% (10938 reads)
CALL #3 Failed alignment 0% (56 reads)
BELOW CALLING THRESHOLD 3% (683 reads)
Phred score dropouts: 330 reads
Gene: RB1CC1 | File B4: WA01NGN2ESC-RB-E4KO-C12_S7_L001_R2_001.fastq | Amplicon reads: 21772
REFERENCE CATGCCATTCAAAGCAAATACAAGATTGCTATTCAACACCAGGTGCTGGTGGTCAATGGAGGAGAATGCATGGCTGCAGA
CALL #1 1nt insertion CATGCCATTCAAAGCAAATACAAGATTGCTATTCAAC(T)ACCAGGTGCTGGTGGTCAATGGAGGAGAATGCATGGCTGCAGA 49% (10772 reads)
CALL #2 1nt deletion CATGCCATTCAAAGCAAATACAAGATTGCTATTCAAC-CCAGGTGCTGGTGGTCAATGGAGGAGAATGCATGGCTGCAGA 47% (10241 reads)
CALL #3 Failed alignment 0% (105 reads)
BELOW CALLING THRESHOLD 3% (654 reads)
Phred score dropouts: 640 reads

Supplementary Figure S2. Results of single nucleotide polymorphism arrays (SNP-A) based karyotyping of established RB1CC1^{KO} PSC lines

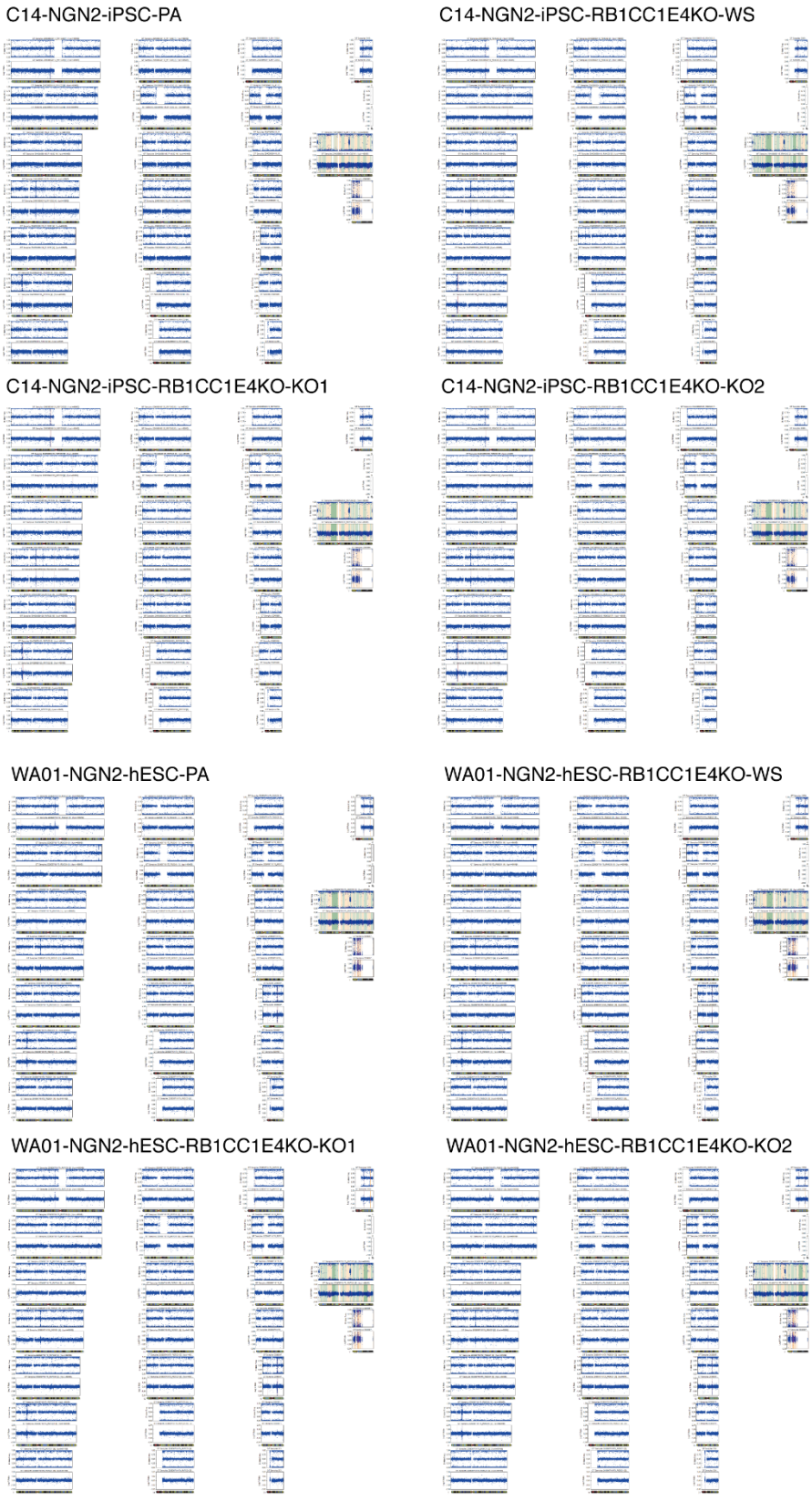

9. Acknowledgements

I would like to thank my supervisors Prof. Oliver Brüstle and Dr. Michael Peitz for their dedicated guidance and support during the past years. Their scientific insights and suggestions were truly critical for this project.

I have to also thank my dear colleagues for their kind assistance on both my work and life: Dr. Kristina Rehbach, Dr. Matthias Hebisch, Dr. Affef Abidi Ostorero, Cornelia Thiele, Melanie Bloschies, Monika Veltel, Tamara Bechler and many others.

Dr. Nils Braun kindly helped me to produce the DCX-hrGFP plasmids. Dr. Nils Gassen and Thomas Bajaj kindly offered me the ptflc3 plasmid and ULK1 inhibitor MRT, as well as many insightful suggestions regarding autophagy. Prof. Raoul-Martin Memmesheimer and Dr. Wilhelm Braun helped me with the *in silico* simulations. Thank you all.

This work was supported by China Scholarship Council (CSC), the IntegraMent Consortium (Integrated Understanding of Causes and Mechanisms in Mental Disorders, sponsored by Federal Ministry of Education and Research, Germany), and the 'Get finished!' scholarship from the University of Bonn.

I would also have to thank my family, who have supported me in their own best ways. And I owe a special thanks to Dr. Jiaqing Li, who one day stupefied me with this poem from the Tang Dynasty of China, which fits well to an ending of this thesis:

前不见古人 / No one to reminisce

后不见来者 / No one to expect

念天地之悠悠 / The solitary in this vast cosmos

独怆然而涕下 / Alone I mourned, alone I wept

Bonn, August 2021